University of Mississippi

eGrove

1-1-2015

Non-invasive drug delivery to the posterior segment of the eye: Development of formulation strategies and evaluation of ocular distribution and pharmacological activity

Goutham Reddy Adelli
University of Mississippi

Follow this and additional works at: https://egrove.olemiss.edu/etd

Part of the Pharmacy and Pharmaceutical Sciences Commons

NON-INVASIVE DRUG DELIVERY TO THE POSTERIOR SEGMENT OF THE EYE:

DEVELOPMENT OF FORMULATION STRATEGIES AND EVALUATION OF OCULAR

DISTRIBUTION AND PHARMACOLOGICAL ACTIVITY

A Dissertation

presented in partial fulfillment of requirements

for the degree of Doctor of Philosophy

in Pharmaceutical Sciences with an emphasis in Pharmaceutics and Drug Delivery

The University of Mississippi

by

GOUTHAM R. ADELLI

May 2016

ABSTRACT

Diseases of the posterior segment of the eye such as diabetic retinopathy, age related macular degeneration and glaucoma are the leading causes for blindness throughout the world. Topical eye drops is the most convenient formulation for daily application. The human eye, however, presents major physiological and dynamic barriers for the topically administered drug/molecule from reaching the retina. Similarly, the blood-retinal and blood-aqueous barriers restricts passage of drug from systemic circulation into the eye. Although intravitreal injections are the gold standards for the treatment of posterior segment ocular diseases, they are associated with pain, inflammation, endopthalmitis and infection. So there is a necessity to develop novel noninvasive drug delivery strategies to treat the posterior segment ocular diseases.

In the present study, we have used melt cast technology to develop a polymeric matrix film system to deliver Hesperetin (HT), a bioflavanoid, to the posterior segment of the eye. The film is 4 mm x 2 mm in dimension and 0.2 to 0.4 mm in thickness. When the HT-film was tested *in vivo* in anesthetized rabbit model, HT levels were maintained above the neuroprotective and anti-inflammatory IC_{50} levels for upto 6 h. We also prepared HT loaded (0.1% w/v) solid lipid nanoparticles (SLN's) using a combination of 85% glyceryl monostereate and 15% compritol ATO 888. The particle size, zeta potential and entrapment efficiency of the HT-SLN's was 225 nm, -21 mV and 85% respectively. Although the dose administered in the animal study was approximately 16-fold lower than the HT-Film, SLN's provided very good HT levels in the anterior segment of the eye. These formulations were tested in the conscious animal model to determine the effect of active lymphatic and tear drainage. Significant elimination of HT was observed in the aqueous

ii

humor due to the turnover rate (1.0% to 1.5% of the anterior chamber volume per minute). But the film formulation was able to maintain 2.3 µg of HT/gm of tissue in the retina choroid and 80 ng of HT/gm of vitreous humor upto 3 h. SLN's were able to deliver 1.9 µg of HT/gm of iris ciliary bodies, but HT levels were below detection limit in the posterior segment of the eye. Thus, polymeric matrix films prove to be a safe and effective platform for the delivery of drugs/drug candidates to the posterior segment of the eye.

Glaucoma is the second leading cause for blindness worldwide. Rise in intraocular pressure (IOP) has been identified as an important risk factor in the pathogenesis of the disease. Δ9-Tetrahydrocannabinol (THC), an active ingredient of the plant cannabis sativa, and an agonist of the cannabinoid receptors, CB1 and CB2, could potentially be such a dual acting anti-glaucoma agent. Delivering therapeutic levels of THC into the inner ocular layers is very challenging due to the extremely lipophilic characteristics of THC. A synthetic amino acid dicarboxylic acid prodrug of THC, Δ^9-Tetrahydrocannabinol valine hemisuccinate (THC-Val-HS) was developed. Micellar and nanoemulsion formulations of THC-Val-HS and THC were prepared. These formulations were evaluated for IOP reduction in an alpha chymotrypsin induced rabbit glaucoma model. With the 0.5%w/v THC emulsion formulation drop in IOP was observed at 30 min, but was very minimal and short acting (60 min). With an increase in dose (0.8% w/v THC) a similar effect was observed with a slight increase in the duration of activity (90 min). With THC-Val-HS (0.6% w/v THC equivalent), drop in IOP was observed at 30 min, but the maximum drop was observed at 90 min, lasting upto 3 h (90% of the baseline). The more gradual drop in IOP can be attributed to the fact that THC-Val-HS has to be enzymatically converted into THC to show activity. Receptor

binding studies revealed that THC-Val-HS has 21.8 and 38 folds less affinity towards CB_1 and CB_2 receptors, respectively, than THC. Thus, the present study demonstrates that a rational combination of prodrug design and formulation strategies can effectively deliver THC to the anterior chamber of the eye. An increased IOP reduction with the prodrug at lower equivalent doses of THC, supports improved ocular penetration of the prodrug. Importantly, with most of the conventionally developed anti-glaucoma drugs having no reported neuroprotective action, THC, an established neuroprotectant, has the potential to become an effective glaucoma medication. Further studies are currently aimed at developing and optimizing various formulations with improved THC delivery to the back-of-the eye.

Since the rate of elimination of drug candidates was relatively rapid in the earlier studies, ion exchange resin - drug complexes were incorporated into the matrix film to improve the sustained release profile. Ion exchange resins (IR) are water insoluble cross linked polymers with ionizable groups that can be exchanged to form complexes. Diclofenac sodium (DFS) was used as a model drug. The goal of this study was to develop polymeric matrix films loaded with a combination of free diclofenac sodium (DFS) and DFS-Ion exchange resin (IR) complexes for immediate and sustained release profiles, respectively. Complexation efficiency of DFS-IR was found to be 99% at 1:1 ratio of DFS:IR. Solution and DFS:IR suspension formulations were not able to maintain therapeutic DFS levels in AH and other ocular tissues. The matrix film, as such, was able to achieve high levels of DFS in the ocular tissues, but was not able to overcome the rapid elimination profile. On the other hand, DFS:IR loaded matrix films were able to maintain DFS levels in the inner ocular tissues fairly constant for upto 8h, probably because of continuous release

iv

of DFS from the IR and retention of the IR complexes on the ocular surface. Thus, drug IR complexes loaded into matrix films could be a potential sustained ocular delivery platform.

DEDICATION

This dissertation is dedicated to my parents Sammi Reddy Adelli and Uma Devi Adelli. I would not have reached this milestone without their constant encouragement, patience, support and love. This dissertation is also dedicated to my brother Vikram Reddy Adelli for being my moral support.

LIST OF ABBREVIATIONS AND SYMBOLS

HD   Hesperidin

HT   Hesperetin

PEO N10   Polyethylene oxide N10

DR   Diabetic retinopathy

AMD   Age related macular degeneration

DME   Diabetic macular edema

PVR   Proliferative vitreo-retinopathy

CNV   Choroidal neovascularization

WHO   World Health Organization

VEGF   Vascular endothelial growth factor

DNA   Deoxyribose nucleic acid

RNA   Ribose nucleic acid

RPE   Retinal pigmented epithelium

ROS   Reactive oxidative species

ERKs   Extracellular-signal-regulated kinases

COX   Cyclooxygenase

TAC   Total Antioxidant Capacity

SLN's   Solid lipid nanoparticles

EE   Entrapment efficiency

PI   Polydispersity index

GMS   Glyceryl monostereate

PGE$_2$ Prostaglandin E$_2$

IPBS   Isotonic phosphate buffered saline

HBSS   Hank's balanced salt solution

DSC   Differential scanning calorimetry

FTIR   Fourier transform infrared spectroscopy

ATR   Attenuated total reflectance

HPLC-UV   High performance liquid chromatography- Ultra violet

mM   Millimolar

µg   Microgram

DMSO   Dimethyl sulfoxide

ACN   Acetonitrile

AH   Aqueous humor

VH   Vitreous humor

IC   Iris ciliary bodies

RC   Retina-choroid

THC Δ^9 Tetrahydrocannabinol

THC-HS Δ^9 Tetrahydrocannabinol hemisuccinate

THC-HG Δ^9 Tetrahydrocannabinol hemiglutarate

THC-Val Δ^9 Tetrahydrocannabinol valine

THC-Val-Val Δ^9 Tetrahydrocannabinol valine valine

THC-Val-HS Δ^9 Tetrahydrocannabinol valine hemisuccinate

CB   Cannabinoid receptor

IOP   Intraocular pressure

CPM   Counts per minute

EDTA   Ethylenediaminetetraacetic acid

BAK   Benzalkonium chloride

Na_2HPO_4 Dibasic sodium phosphate

NaH_2PO_4 Monobasic sodium phosphate

βCD   Beta cyclodextrin

HPβCD   Hydroxy propyl beta cyclodextrin

RMβCD   Randomly methylated beta cyclodextrin

PHCl   Propranolol hydrochloride

CE   Complexation efficiency

ZO   Zone occludens

DFS   Diclofenac sodium

IR   Ion exchange resins

NSAIDs   Nonsteroidal anti-inflammatory drugs

HPMC   Hydroxy propyl methyl cellulose

ACKNOWLEDGMENTS

Obtaining a Ph.D. degree could not be realized without my advisor Dr. Soumyajit Majumdar. His expertise, intellectual support and professional guidance were imperative for this work. I thank him dearly for his encouragement, patience, understanding and support throughout my graduate studies. He was very kind and supportive during my tough times. Words fall short if I start expressing my gratitude for him. I am truly grateful and indebted to him for his help and attention towards my academic and personal growth. Thank you for being my advisor!

I express my heartfelt gratitude to my dissertation committee members Dr. Michael A. Repka, Dr. Dr. S. Narasimha Murthy and Dr. John H. O`Haver for their valuable time, guidance, suggestions and help during the evaluation of this dissertation. I extend my thanks to Dr. Bonnie A. Avery, Dr. Seongbong Jo and Dr. Christy M. Wyandt for making the experience at Ole Miss worthwhile, Ms. Deborah King for her help, patience and affection. I also thank the support and technical help extended by Dr. Harry Fyke and Ms. Penni Bolton during animal experiments.

I thank all graduate students at Department of Pharmaceutics and Drug delivery for their support and for making my stay at Ole Miss memorable. I profusely thank my colleagues and friends, especially Tushar Hingorani, Sai Prachetan and Nagendra Punyamurthula for being such a great support and fun to work with. I also thank them for their help during experimental work and during my stay at Ole Miss. Even though I had spent very little time with Pranjal Taskar and Akshaya Tatke, they have made my last year very joyful and memorable.

My warmest thanks to my Uncle Vijender Adelli for guiding me to Ole Miss in the first place and introducing me to Dr. Majumdar. The support, encouragement and inspiration that he

x

DISSERTATION COMMITTEE

Research Adviser: Dr. Soumyajit Majumdar (Dept. of Pharmaceutics and Drug Delivery)

Committee Members: Dr. Michael A. Repka (Dept. of Pharmaceutics and Drug Delivery)

Dr. Narasimha Murthy (Dept. of Pharmaceutics and Drug Delivery)

Dr. John H. O`Haver (Dept. of Chemical Engineering)

TABLE OF CONTENTS

LIST OF TABLES

LIST OF FIGURES

CHAPTER 1

INTRODUCTION

CHAPTER 1

1.1. INTRODUCTION:

The 'eye' is a specialized sensory organ which responds to light and gives us the visual perception of our surrounding environment. The anatomy of eye and the routes of drug delivery pertaining to eye are shown in the Figure 1.1. Human eye is divided into two major segments: the anterior segment and the posterior segment.

The major parts of anterior segment are cornea, trabecular meshwork and schlemm's canal, anterior uvea (iris, pupil and ciliary
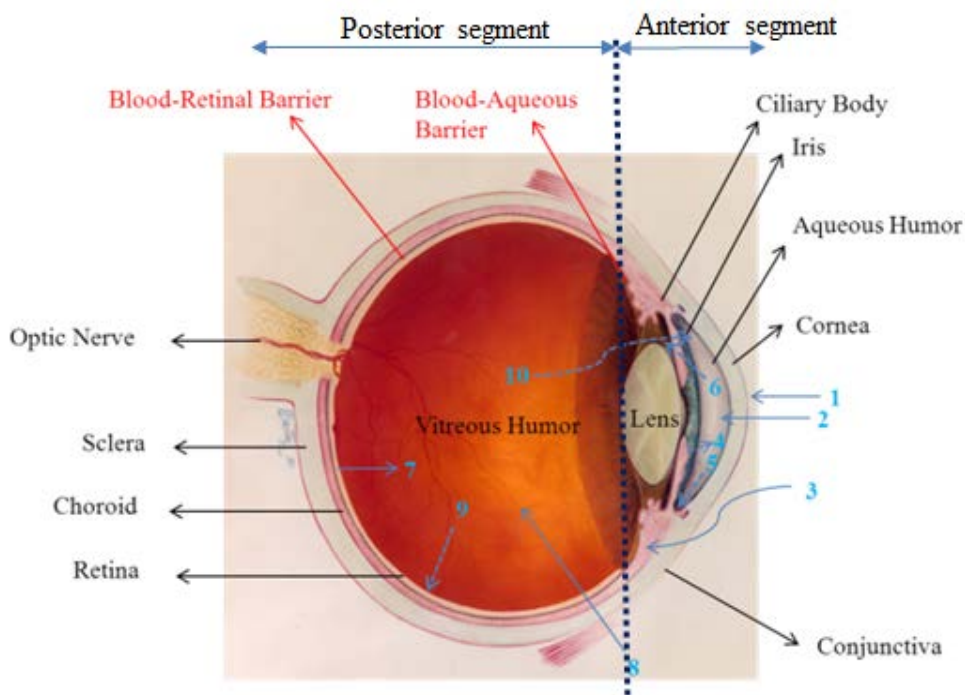
Figure 1.1: Anatomical structure of the human eye.

body), aqueous humor and lens. The posterior segment of the eye consists of sclera, choroid, retina, vitreous humor and optic nerve. It is the retina where the visual information is collected by the rods and cones and passed on to the optic nerve for processing in the central nervous system. Age, disease and injury may cause temporary or permanent damage to the eye. Although, damage to the

anterior segment of the eye may sometimes leads to permanent damage, they can, however be treated by proper medication.

1.1.1. Posterior segment ocular diseases:

A report from the World Health Organization (WHO) in 2011 estimated that approximately 285 million people were suffering from visual impairment worldwide out of which 39 million face blindness while 246 million suffer from moderate to severe vision impairment. With an increase in the average survival age and the percentage of diabetics, diabetes related retinopathies are rapidly gaining in significance. It has been predicted that, without additional steps, these numbers will increase to 75 million blind and 200 million visually impaired by the year 2020 (WHO, 2010). Age seems to be a causative factor in blindness as 90% and 58% of the population with blindness are aged above 45 and 60 years respectively [1].

Oxidative stress, inflammatory mechanisms and decreased antioxidant capacity in the ocular tissues are all thought to play an active role in the development and progression of these ocular diseases. The following sections briefly highlight the etiology of these ocular disorders, followed by discussions on the therapeutic potential of various phytochemicals and challenges encountered in their delivery to the ocular tissues.

Diabetic Retinopathy

Diabetic retinopathy (DR) is the most common diabetes associated eye disease and is the leading cause of blindness in American adults [2, 3]. The WHO estimates that over 360 million worldwide will suffer from diabetes by the year 2030. Currently, 10% of the diabetics suffer from Type I diabetes whereas 90% suffer from Type 2 diabetes. DR in Type 1 diabetics approaches 80 and 90 % prevalence rate after 10 and 20 years of diabetes, respectively. Up to 21% of patients

3

with Type 2 diabetes have recently been found to have retinopathy at the time of first diagnosis of diabetes, and most develop some degree of retinopathy over subsequent decades [4].

DR can be broadly categorized into three stages; background DR, pre-proliferative DR and proliferative DR (PDR) [5-7]. In background DR, hyperglycemia is considered to induce thickening of capillary basement membranes and death of pericytes, which support the vessel wall, and endothelial cells of retinal blood vessels. Microaneurysms and vascular leakage follow, and blockage of retinal capillaries take place. In pre-proliferative DR, loss of vascular patency leads to areas of increasing retinal hypoxia and multiple hemorrhages. Increased areas of tissue non-perfusion stimulate the production of angiogenic factors leading to the proliferation of vessels, which is a typical feature of PDR. The newly formed blood vessels by themselves do not lead to vision loss, but leakage of blood through their weak walls can result in severe vision loss and can ultimately lead to complete loss of sight.

Hyperglycemia and tissue hypoxia, are considered to be principal factors in the DR pathology described above. Multiple studies demonstrate the relationship between high blood glucose, oxidative stress and initiation of DR [7-12]. The retina is highly susceptible to oxidative damage since: a) it has an abundance of the polyunsaturated fatty acids in its membrane bilayers, whose double bonds are prime targets for peroxidation reactions; b) it is periodically subjected to continuous light which, by photoexcitation, can initiate free radical formation and peroxidation reactions and c) the retina is a highly metabolic tissue that requires a high rate of blood flow in order to receive an adequate oxygen supply. Oxidative damage in biological systems occurs when endogenous antioxidant mechanisms are overwhelmed by free oxygen radicals or reactive oxygen species (ROS). These radicals are extremely unstable and can cause cytotoxicity and cellular

damage by reacting with plasma membrane lipids, DNA, RNA and metal-containing compounds [13].

Multiple pathways have been suggested to be activated during hyperglycemia associated oxidative stress, which subsequently leads to damage of retinal blood vessels. These include nitric oxide (NO) synthesis [14, 15], NF-κβ expression, secretion of cytokines such as IL-1β, lipid peroxide generation, activation of retinal caspase-3, protein kinase C (PKC) stimulation and alterations of retinal glutamate levels [13, 16-21].

In advanced stages, i.e. PDR, reduced retinal blood flow induces retinal ischemia which leads to hypoxic conditions in the retina. Hypoxia stimulates production of a variety of local agents including vascular endothelial growth factor (VEGF) [7, 22-26], prostaglandins, cyclooxygenase-2 (COX-2) and nitric oxide (NO), all of which participates in increasing vascular permeability and angiogenesis [7]. The VEGF family plays a key role in the regulation of vascular patency and is involved in both physiological and pathological angiogenesis, stimulating endothelial cells to migrate, proliferate and form tubes [7, 27-30]. VEGF is also a potent vascular bed permeability enhancer [31, 32]. Hypoxia is a stimulant for COX-2 transcription also in various tissues [7, 33-35], including human vascular endothelium [7, 33] and neural cells [36]. NF-kβ, an oxygen sensitive transcription factor [7, 37, 38] mediates the induction of COX-2 in hypoxic conditions. The angiogenic properties of COX-2 are likely to directly involve VEGF, as COX-2 has been shown to up-regulate VEGF synthesis which can be inhibited with selective or non-selective COX inhibitors [7, 39, 40].

In the context of DR, the actions of prostaglandins E2 and I2 are also considered to be important in the development of angiogenesis, breakdown of the blood-retinal barrier and alterations in retinal blood flow [7, 41-46]. These prostaglandins are produced via the COX-2

pathway, [7, 47-49]. Prostaglandins, and in particular PGE2, are also strong inducers of VEGF in cell types such as synovial fibroblasts monocytes and lung and retinal Müller cells. There is evidence that the vascular events prior to angiogenesis may involve the induction of COX-2 followed by VEGF. It has thus been suggested that angiogenesis may be mediated by dual interdependent gene expression pathways that involve COX-2 and VEGF [7, 50].

NO is known to participate in vascular permeability and angiogenesis via interactions with VEGF and COX-2. NO reacts with superoxide anions to form peroxynitrite, a highly reactive oxidant. Excess production of peroxynitrite in diabetes may exhibit cytotoxic effects by increasing DNA damage, stimulating lipid peroxidation and depleting glutathione levels [51-53]. Peroxynitrite alters tyrosine in proteins to form nitrotyrosine and nitration of proteins can inactivate mitochondrial and cytosolic proteins and damage cellular elements leading to nitrative stress [54]. PDR is the most damaging stage of DR as it leads to the generation of abnormally located retinal blood vessels with weak capillary walls. Microvascular leakage from these newly formed blood vessels can lead to total blindness through a variety of mechanisms.

In addition to hyperglycemia associated increased ROS generation, it has recently been demonstrated that the Total Antioxidant Capacity (TAC) of the vitreous humor and aqueous humor is lowered in DR. Mancino et al. determined the antioxidant capacity of blood, aqueous humor and vitreous of controls (non-diabetic) and of patients with non-proliferative DR (NPDR) and with proliferative DR (PDR) [55]. The authors observed that the control group displayed significantly higher TAC levels than the diabetic sub-groups in both the vitreous and aqueous humor. PDR patients had decreased TACs in the vitreous and aqueous humor as compared with control subjects and with the NPDR patient subgroup, pointing to the role of oxidative stress in the progression of

NPDR to PDR [55]. The results strongly support the need for increased antioxidant levels in the retina, aqueous humor and vitreous humor.

Age-Related Macular Degeneration

Age-related macular degeneration (AMD), which can be categorized into dry and wet AMD, is the leading cause of irreversible vision loss in the developed world. As per the statistical data published by the National Eye Institute, AMD affected 1.75 million persons in the United States, in 2004, a number which is expected to rise to nearly 3 million by 2020 due to the aging of the population [56]. Like DR, progression of AMD is linked to the activation of inflammatory and immunological pathways [57]. Presence of excess ROS and decreased antioxidant capacity in the ocular tissues is also considered to play a significant role in the initiation and progression of AMD [58, 59]. Ding et al provides a summary of the molecular pathways involving inflammation, angiogenesis and oxidative stress, considered to play a role in the development of AMD [60].

Cataract

Oxidative stress induced damage to the lens fibers has also been well documented. It is thought that these free radicals accelerate and aggravate cataract development. Additionally, diabetic lenses show an impaired antioxidant capacity that increases their susceptibility to oxidative stress. The loss of antioxidants is exacerbated by glycation and inactivation of lens antioxidant enzymes like superoxide dismutase [61].

Glaucoma

Glaucoma is caused when the aqueous humor builds up in the anterior chamber. This causes increased pressure in the anterior chamber of the eye which is passed on to the posterior

segment of the eye. Elevated intraocular pressure on the retina causes imbalance in adaptive cell response (ant-oxidant system, anti-proteolytic system and adaptive gene expression) and cell death (genetic mutation, chronic and acute oxidative stress, apoptosis and mechanical stress) leading to retinal ganglion cell death and blindness.

1.2. Challenges in drug delivery to the posterior segment of the eye:

The eye is a secluded organ, protected by various physiological barriers that restrict entry of xenobiotics into the ocular tissues from the external environment (topical or periocular) or systemic circulation (**Table 1.1**). The choroidal blood vessels possess many large fenestrations and pinocytic vesicles that allow free exchange of endogenous/exogenous substances between the choroidal stroma and choroidal vasculature.

Thus, systemically administered therapeutic agents can easily diffuse out into the choroidal stroma from the systemic circulation [62]. Bruch's membrane, separating the choroid from the RPE, acts as a barrier to the diffusion of only macromolecules, like proteins and genes, and thus does not pose much of a diffusional barrier to small molecules. The retinal pigmented epithelium (RPE), on the other hand, presents a formidable permeation barrier to small drug molecules in their diffusion into the neural retina and vitreous humor from the choroidal stroma [62-64]. Epithelial cells of the RPE are joined together by tight junctions [65-69] similar to those observed in the blood-brain barrier, severely restricting paracellular diffusion of hydrophilic molecules. The RPE cells also express the efflux proteins P-gp and MRP on the basolateral membrane [70-73]. As a result, trans-retinal permeation of compounds that are substrates of these efflux proteins, from the systemic circulation (choroidal side) into the neural retina/vitreous humor, is strongly modulated by RPE P-gp/MRP mediated efflux. The RPE, thus, presents a major barrier to the exchange of

therapeutic agents between the choroidal stroma and the neural retina / vitreous humor, and is referred to as the outer BRB.

Table 1.1: Route of administration dependent physiological barriers encountered in the diffusion path to the neural retina.

Physiological Barriers	Route of Administration			
	Topical	Peri-ocular	Systemic	Oral
Precorneal loss	√			
Corneal ultrastructure	√			
Corneal efflux proteins	√			
Corneal tight junctions	√			
Conjunctival efflux proteins	√			
Conjunctival tight-junctions	√			
Conjunctival vasculature	√			
Aqueous humor outflow	√			
Anterior chamber metabolism	√			
Scleral vasculature	√	√	√	√
Choroidal vasculature	√	√	√	√
Bruch's membrane	√	√	√	√
Outer BRB				
RPE tight junctions	√	√	√	√
RPE efflux pumps	√	√	√	√
Inner BRB				
Tight-junctions			√	√
Efflux proteins			√	√
Low concentration gradient			√	√
First pass effect				√
Absorption limitations				√
Metabolism in the GIT				√
Systemic metabolism				√

Similar to the RPE, the endothelial cells of the blood vessels perfusing the neural retina express efflux proteins and tight-junction proteins [64, 74]. The efflux proteins are polarized on the apical

membrane of the endothelial cells (facing the lumen of blood vessels) and prevent entry of xenobiotics from the systemic circulation into the neural retina. Like in the outer BRB, tight junction proteins expressed on the inner BRB also severely limits paracellular diffusion of hydrophilic compounds. The barrier properties of the retinal blood vessel endothelial cells are commonly referred to as the inner BRB. Additionally, because of extensive intestinal and heapatic metabolism, the hydrophilic metabolites of the phytochemicals are seen in the systemic circulation and are available for penetration into the ocular tissues. The ambiguity in the results obtained from the limited number of clinical studies that have been carried out with the phytochemicals could be because of the inadequate delivery of the compounds into the tissues of the eye [75].

Periocularly administered agents also encounter the RPE barrier. Thus, the inner and outer BRB acts as a considerable physiological barrier to the ocular delivery of therapeutic agents through the systemic and transcleral routes of administration. Additionally, transcleral permeation is also challenged by the scleral and choroidal blood flow and lymphatics.

Intravitreal and surgical interventions, though very effective, are associated with risks such as retinal detachment and endophthalmitis [76]. Topical administration is the most favored route of administration for ocular disorders. It is thought that following topical application diffusion into the cornea, followed by lateral migration into the sclera and then diffusion across the choroid and RPE into the vitreous, is the major pathway for topically administered agents [77]. Thus, scleral and choroidal vascular and lymphatic systems as well as the RPE present significant barriers in the diffusional path. Additionally, precorneal loss, corneal ultrastructure and efflux proteins expressed on the corneal membrane present additional physiological barriers to topically administered agents. Although significant advances have been made with respect to drug delivery into the front of the eye through the topical route, back-of the eye delivery remains a significant

challenge. Thus there is a necessity in development of novel noninvasive sustained release drug delivery strategies.

The goal of this project is to develop novel formulations of Hesperetin (HT), Tetrahydrocannabinol valine hemisuccinate (THC-Val-HS) and Diclofenac sodium (DFS) and to evaluate *in vivo* ocular distribution and pharmacodynamic response through the non-invasive topical route. Melt-cast films and colloidal systems will be evaluated with respect to ocular distribution and pharmacodynamic response *in vivo*.

1.3. Specific aims:

1. Develop melt-cast films and solid lipid nanoparticles (SLN's) of Hesperetin (HT) and evaluate *in vivo* ocular distribution in male New Zealand albino rabbits.

2. Evaluate intraocular pressure lowering (IOP) efficacy of tetrahydrocannabinol (THC) and THC-Val-HS and compare with marketed formulations in a glaucoma induced rabbit model.

3. Evaluation of the effect of cyclodextrins on morphology and barrier characteristics of isolated rabbit corneas.

4. Development and evaluation of sustained release DFS ion exchange resin complexes loaded into melt cast films and their in vivo ocular distribution.

CHAPTER 2

EVALUATION OF TOPICAL HESPERETIN MATRIX FILM AND SOLID LIPID NANOPARTICLES FOR POSTERIOR SEGMENT OCULAR DELIVERY

CHAPTER 2

INTRODUCTION

Bioflavonoids, a group of plant polyphenols, are reported to exhibit antioxidant, anti-angiogenic and anti-inflammatory properties along with fluid retention reduction and capillary wall strengthening activities [78, 79]. Hesperidin (HD), and its aglycone hesperetin (HT), a plant based flavanone (**Fig. 2.1A & 2.1B**) obtained from *Citrus sinensis*, possess antioxidant [80, 81], and neuroprotectant properties [80], and reduces vascular permeability. HT is recognized to be more potent than HD in scavenging reactive oxidative species (ROS) [82-84]. HT also prevents the cytotoxic effect of peroxynitrites by converting them to non-toxic mono-nitrated products and increasing phosphorylation of extracellular-signal-regulated kinases (ERKs) [85]. Anti-inflammatory activity of HT is thought to be achieved by inhibition of the COX-2 pathway and synthesis of PGE_2 [86], and inhibition of nitric oxide production by blocking nitric oxide synthase [87, 88]. Additionally, HT was observed to increase ocular blood flow and promote recovery of retinal function following ischemic insult of retina [89]. Currently HT is available as an oral dietary supplement to improve blood flow and as a vasoprotectant. Cumulative urinary recovery of HT suggests a bioavailability of less than 25 % after oral administration of HD and HT [90]. Poor oral bioavailability of HT can be attributed to its rapid metabolism into hydrophilic glucuronide metabolites [91] and short half-life (Plasma half-life: 6.7 h and vitreous humor half-life: 110 min) [92, 93].

Treating the posterior segment eye diseases has always been a great challenge because of the unique physiological and anatomical barriers of the eye. Our earlier studies demonstrate that systemic application fails to deliver HT to the ocular tissues [91]. This makes topical or intraocular/periocular application the most effective. Less than 5 -10 % of topically applied drug, however, permeates into the intraocular tissues [94-96]. Various ocular delivery systems are being investigated to increase drug contact time and site specific delivery to the posterior segment of the eye using liposomal formulations and other sustained release and controlled release systems such as ocular inserts, collagen shields, matrix systems, and hydrogel lenses [97-100].

The goal of the present study is to evaluate the effectiveness of topical melt-cast polymeric matrix systems and solid lipid nanoparticles with respect to the delivery of HT to the back-of-the-eye tissues, especially to the retina-choroid (RC) and vitreous humor (VH). The matrix film and the SLN's were evaluated *in vivo* for dose dependent and time dependent drug delivery in anesthetized and conscious animal model.

2.2. Methods:

2.2.1. Chemicals:

PEO (PubChem CID: 5327147) [PolyOx® WSR N-10 (PEO N-10), MW: 100,000 Daltons] was kindly donated by Dow Chemical Company (Midland, MI). HT (PubChem CID: 72281) (Type HP-2, from Helix pomatia) was purchased from Sigma Aldrich (St. Louis, MO). Geleol™ Mono and Diglycerides NF (GMS: PubChem CID: 24699) and Compritol® 888 ATO (PubChem CID: 5362585) were gifted by Gattefossé. All other chemicals were purchased from Fisher Scientific (St. Louis, MO).

2.2.2. Animal tissues:

Whole eye globes of New Zealand albino rabbits were purchased from Pel-Freez Biologicals® (Rogers, AK), shipped overnight in Hanks Balanced Salt Solution (HBSS) over wet ice [32]. Corneas and whole eye globes were used on the day of receipt.

2.2.3. Animals:

Male New Zealand albino rabbits (2.0 - 2.5 Kg) procured from Harlan Laboratories® (Indianapolis, IN) were used in all the studies. All animal experiments conformed to the tenets of the Association for Research in Vision and Ophthalmology statement on the Use of Animals in Ophthalmic and Vision Research and followed the University of Mississippi Institutional Animal Care and Use committee approved protocols (UM protocol # 11-006 and 14-002).

2.2.4. Formulations:

2.2.4.a. Preparation of polymeric matrix film:

Melt-cast method was employed in the preparation of the polymeric matrix film (**Fig 2.2**). PEO N10 was selected as the matrix forming polymer. A physical mixture of HT and PEO N10 was prepared by geometric dilution. Drug load in the film was 10 % or 20 % of the total weight of film. A 13 mm die was placed over a brass plate and heated to 70 °C using a hot plate. The physical mixture of HT and polymer was added in the center of the die and compressed to form a flat matrix surface. The mixture was further heated for 2-3 min. After cooling, 4 mm x 2 mm sections each weighing approximately 8 mg and with a drug load of 0.8 mg or 1.6 mg for the 10 %w/w and 20 %w/w films, respectively, were cut out from the film.
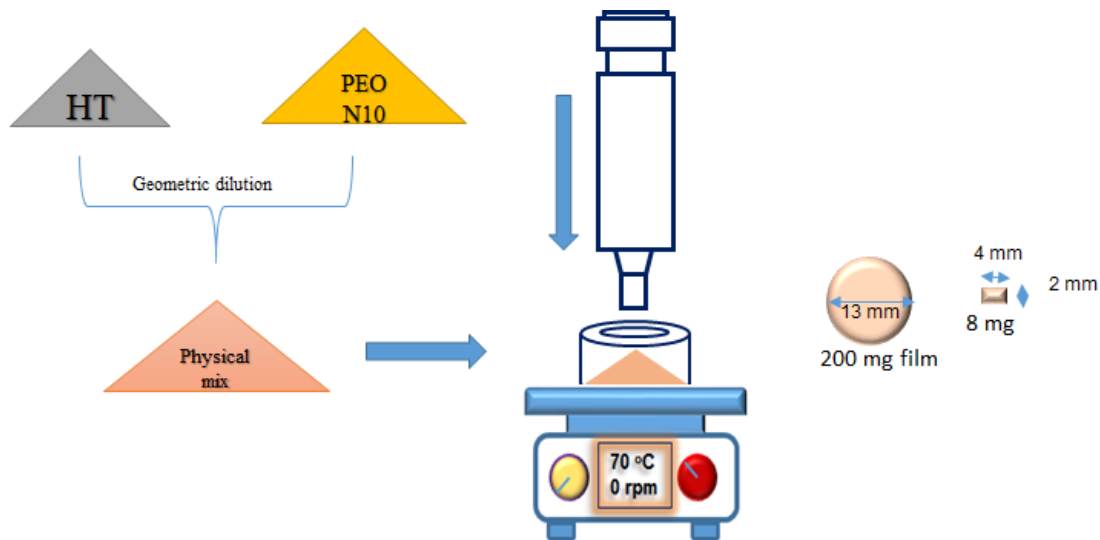
Figure 2.2: Preparation of 10% and 20% w/w HT-Film using melt-cast technology.

2.2.4.b. Preparation of Solid lipid nanoparticles:

HT-SLNs were prepared using a hot homogenization method followed by probe sonication (**Fig.2.3**). Accurately weighed Compritol 888 ATO (60 mg) and Glyceryl monostereate (GMS: 340 mg) was melted, and HT (5% w/w with respect to the lipid) was dissolved therein to obtain a clear lipid phase. Simultaneously, an aqueous phase, containing surfactants (Poloxamer 188 and/or Tween 80) and glycerin (2.25% w/v) in bidistilled water, was heated. The hot aqueous phase was then added to the melted lipid phase under stirring (magnetic stirrer) to form a premix (600 rpm, 1–2 min). The premix was then subjected to emulsification at 16,000 rpm for 6 min using T 25 digital Ultra-Turrax (IKA® Works, Inc.) to form a hot pre-emulsion. This pre-emulsion was further subjected to ultra-sonication using Sonics VibraCell™ at 15 sec pulse rate and 80% amplitude for 5 min. The hot emulsion thus obtained was slowly cooled to room temperature to form HT-SLNs.

14

The final concentrations of the lipid and HT in the formulation were kept constant at 4% w/v and 0.1% w/v, respectively.

Figure 2.3: Preparation of HT-SLN's using hot homogenization method followed by Ultra-probe sonication.
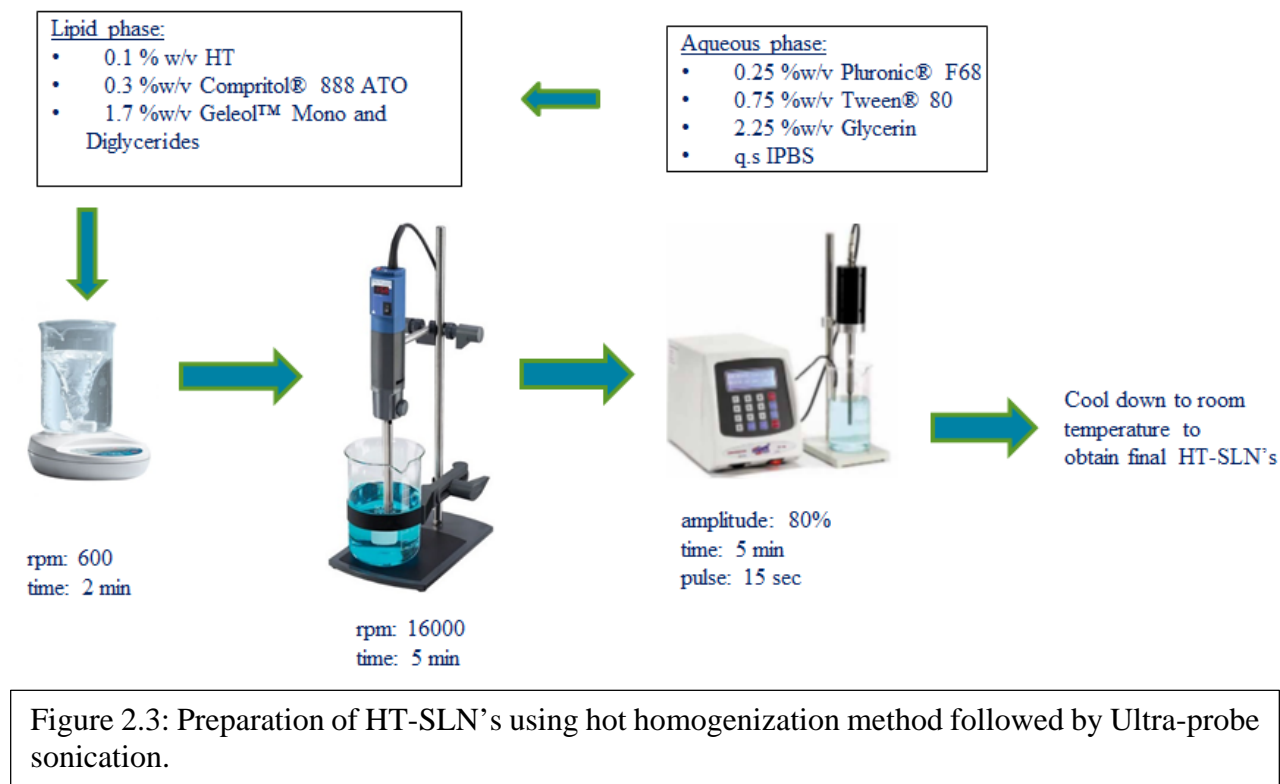
2.2.4.c. HT-Cyclodextrin solution (1% w/v):

Hesperetin cyclodextrin (CD) solution (1% w/v) for topical instillation was prepared by dissolving accurately weighed amount of HT in 100 µL of 1N sodium hydroxide and adding this solution to 10% HPβCD (prepared in IPBS, pH 7.4, containing 0.1% HPMC). Final pH was adjusted to 7.4 using 1N hydrochloric acid.

2.2.5. Physicochemical characterization of the HT-Film and HT-SLN's:

To determine HT content, the film was placed in a mixture of methanol and dimethyl sulfoxide (DMSO) 50:50 and sonicated for 15 min until the film was completely dissolved in the solvent mixture. Content uniformity was determined using four separate sections of 8 mg each,

randomly cut from a single 13 mm film and analyzed as described under analytical procedure using an HPLC-UV method [101].

The lipid in the HT-SLN dispersion was precipitated using 190-proof alcohol, and the drug content in the supernatant after centrifugation (13,000 rpm for 20min), as such or after further dilution with 190-proof alcohol, was measured using an HPLC system.

The percentage of HT entrapped in the SLNs (% EE) was determined by measuring the concentration of free drug in the aqueous phase of an undiluted IN-SLN dispersion. The EE was evaluated by an ultrafiltration technique with a 100-kDa centrifugal filter device composed of a regenerated cellulose membrane (Amicon Ultra). An aliquot (500 mL) of undiluted HT-SLN was added to the sample reservoir and centrifuged at 5,000 rpm for 10 min. The filtrate obtained was further diluted with alcohol (190 proof) and analyzed for drug content using HPLC.

The mean particle size and the polydispersity index (PI) of HT-SLN's were determined by photon correlation spectroscopy using Zetasizer Nano ZS Zen3600 (Malvern Instruments, Inc.) at 25 $^{\circ}$C and 173° backscatter detection in disposable folded capillary clear cells. The measurements were obtained using a helium-neon laser of 633 nm, and the particle size analysis data were evaluated using volume distribution. Zeta-potential measurements were carried out at 25 $^{\circ}$C in folded capillary cells using the same instrument. For measurement of particle size distribution and zeta-potential, SLN samples were diluted (1:500) with water. All measurements were performed in triplicates.

2.2.6. Differential scanning calorimetry (DSC) and Fourier transform infrared spectroscopy (FTIR):

DSC thermograms for HT, excipients, the 10 %w/w film and 0.1% HT-SLN's was collected using a Diamond Differential Scanning Calorimeter (Perkin-Elmer$^{\circledR}$ Life and Analytical

16

Sciences) [102].The samples were weighed and sealed in aluminum pans and were heated from 0 °C to 270 °C at a heating rate of 10 °C/min under nitrogen purge (20 mL/min).

Infrared spectra (IR) for excipients used in both formulations, HT, and the final formulations were obtained using a Cary 660 series FTIR (Agilent Technologies) and MIRacle™ Single Reflection ATR (PIKE Technologies). Further, the IR spectrum of the 13 mm matrix film was collected randomly from different areas of the film, to evaluate distribution uniformity within the polymer matrix.

2.2.7. *In vitro* release and corneal permeability studies:

2.2.7.a. HT-Film:

To study the release profile of HT from the film, *in vitro* release studies were carried out as depicted in **figure 2.4**. Three 20 mL glass vials were taken and a 10 %w/w film (8 mg; Dose:
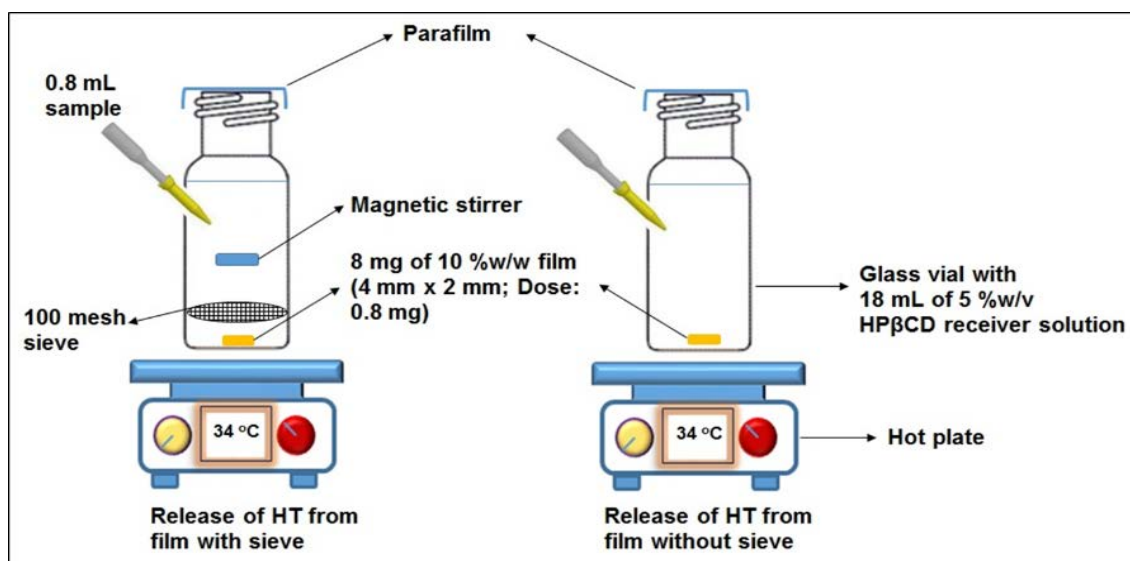
Figure 2.4: Release of HT from film using standard US 100 mesh sieve and without sieve.

0.8 mg) was placed at the bottom of each vial. A standard US 100 mesh sieve was placed over the film and a magnetic bead was placed on the sieve. The glass vials were placed over a magnetic stirrer. Similar set up was employed in 3 more vials but without the sieve and the magnetic stirrer

to evaluate the barrier characteristics of the sieve, if any. In both cases, 18 mL of 5 %w/v HPβCD was used as the release/dissolution medium to ensure sink conditions were maintained (0.6 mg of HT is soluble in 1 mL of 5 %w/v HPβCD). The temperature was maintained at 34 ± 2 °C using hot plates. Aliquots, 0.8 mL, were collected at specific time intervals and replaced with an equal volume of release medium. The release studies were carried out for a period of 2 h. Samples were analyzed using a HPLC-UV method [101].

In vitro corneal permeability of HT from the matrix film was evaluated using a side-by-side diffusion apparatus (PermeGear, Inc., Hellertown, PA) for 3 h (**Fig. 2.5**). The studies were carried out by sandwiching the film (4 mm x 2 mm; 10 %w/w HT; weighing 8 mg approximately; 0.8 mg HT) in between a Spectra/Por® membrane (MWCO: 10,000 Daltons) and isolated rabbit
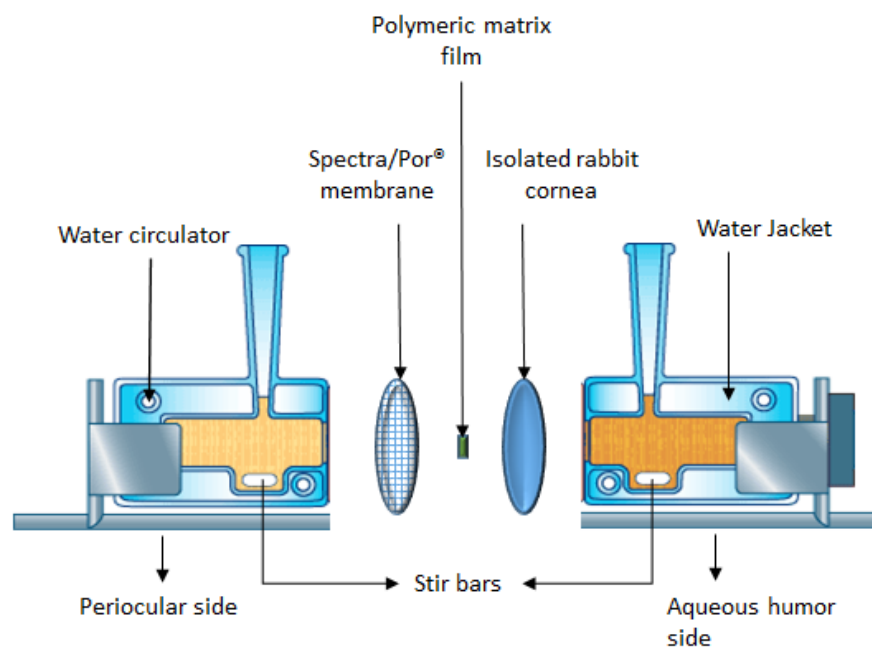
Figure 2.5: Side-by-side diffusion apparatus setup used for in vitro release and transcorneal permeability studies.

cornea (Pel-Freez Biologicals; Rogers, AK). Corneas were excised from whole eye globes, following previously published protocols [103], with approximately 1 mm scleral portions remaining for ease of mounting. The membrane-film-cornea sandwich was then placed in between

18

the side-by-side diffusion cells (the chamber towards the Spectra/Por® membrane representing the periocular surface and the chamber towards the cornea representing the aqueous humor) and samples were collected and analyzed as described above under release study. The side-by-side diffusion cells maintained at 34 °C using a circulating water bath. Five percent HPβCD in isotonic phosphate buffer saline (IPBS) (pH 7.4) was used as the receiver medium. Aliquots (0.6 mL) were drawn at every 30 min interval and replaced with an equal volume of fresh buffer. Samples were analyzed by a HPLC-UV method [101].

2.2.7.b. HT-SLN's:

To determine percentage release and transcorneal permeability of HT from the SLN's, side-by-side diffusion apparatus (PermeGear, Inc., Hellertown, PA), Spectra/Por® membrane and isolated rabbit cornea were used for the release and permeability studies respectively. Three mL of HT-SLN's 0.1% w/v were filled in the donor chamber and 3.2 mL of 5%w/v RMβCD was used as receiver solution. Aliquots of 0.6 mL were collected at predetermined time points and replaced with fresh media. Samples were analyzed using HPLC-UV method.

2.2.8. *Ex vivo* studies:

Whole eye globes obtained from Pel-Freez were placed in 12 well tissue culture plates containing IPBS (pH 7.4) with corneas facing upwards. IPBS was added to the wells and was maintained below the level of corneo-scleral-limbus. The whole set up was maintained at 34 °C using a water bath. The 10 %w/w HT film was placed at the corneo-scleral-limbus and the eye globes were allowed to stand for 3 h. At the end of 3 h the surface of the eye globes were washed thoroughly and aqueous humor (AH), vitreous humor (VH) and retina-choroid (RC) were carefully isolated and analyzed for HT content using HPLC-UV method [101].

2.2.9. *In vivo* bioavailability studies:

Male New Zealand albino rabbits weighing between 2.0 - 2.5 Kg were used to determine *in vivo* bioavailability of HT from the matrix film and SLN's in a time and dose dependent manner. Initially ocular distribution studies were conducted in anesthetized rabbit model. For this study rabbits were anesthetized using a combination of ketamine (35 mg/kg) and xylazine (3.5 mg/kg) injected intramuscularly, and maintained under anesthesia throughout the experiment. In these studies, either the 10 % or the 20 %w/w HT loaded films were placed in the conjunctival sacs of the rabbit eye. Similarly, 100 µL of HT-SLN's 0.1% w/v were administered in the cul-de-sac of the rabbit eye.

To evaluate the effect of active lymphatic and tear drainage on the ocular distribution of HT, studies were conducted in the conscious animal model also. HT-CD solution was used as control formulation for these studies.

At the end of each study, rabbits were euthanized under deep anesthesia with an overdose of pentobarbital injected through the marginal ear vein. The eyes were washed with ice cold IPBS and immediately enucleated and washed again. Ocular tissues were separated, weighed and preserved at -80 °C until further analysis using HPLC-UV method [101]. All experiments were carried out in triplicate. Corneal tissues following 6 h time point were evaluated for morphological changes, if any. Corneas from the contra-lateral eye of the animal were used as controls.

2.2.10. Corneal histology

Corneas exposed to the 20 %w/w HT film (highest dose tested) for 6h (longest duration) *in vivo* were collected and evaluated for histological characteristics. Corneas excised from the contralateral eyes were used as controls. Extracted corneas were fixed in 2 %w/v paraformaldehyde and 2 %v/v gluteraldehyde in IPBS. Histological evaluation was carried out at

Excalibur Pathology Inc. (Oklahoma City, OK) as per previously reported protocols [104]. Corneas embedded in paraffin were sliced into 5µm cross sections using a microtome (American Optical® 820 Rotary Microtome). These sections were placed on a slide and dried overnight in an oven at 68 °C. The slide was washed with xylene to remove paraffin and washed with alcohol and water to hydrate the tissue. This was then stained with nuclear dye Gill III hematoxylin (StatLab medical) for 10 min and rinsed, and then counterstained with eosin. These slides were then washed in reverse manner (running water, alcohol, and xylene), cover slipped and examined under microscope (Chromavision ACIS II).

2.2.11. Analytical procedure for *in vitro* Samples

Waters HPLC system with 600 E pump controller, 717 plus auto sampler and 2487 UV detector was used. Data handling was carried out using an Agilent 3395 integrator. HT stock solution was prepared in acetonitrile (ACN). A 50:50 mixture of 20 mM phosphate buffer (pH 2.5) and ACN was used as mobile phase with Phenomenex *Luna*® 5 µm C_{18} 100 Å, *250* x 4.6 mm column at a flow rate of 1 mL/min and 284 nm.

2.2.12. Bio-analytical method

2.2.12.a. Standard solution preparation:

To 100 µL of aqueous humor (AH) or 500 µL of vitreous humor (VH) and to a weighed amount of the cornea, sclera, iris ciliary bodies (IC) and retina-choroid (RC), 20 µL of HT stock solution in ACN (0.5, 1, 2.5, 5, 7.5, and 10 µg/mL) was added and allowed to stand for 5 min. To precipitate the proteins, ice cold ACN was added to the AH and VH standards in 1:1 ratio and 1 mL to the cornea, sclera, IC and RC standards. Final concentrations of the standard solutions prepared were in the range of 10 - 200 ng/mL for AH; 10 - 100 ng/mL for VH; 20 - 200 ng/mL: cornea & sclera and 10 - 200 ng/mL: IC & RC. All samples were centrifuged at 13,000 rpm and 4

°C for 30 min and analyzed using HPLC-UV. All the standard curves generated an R^2 value greater than 0.95. Average recovery values were determined in AH (93.5 %), VH (94.7 %), IC (92.1 %), RC (97.3 %), cornea (89.6 %) and sclera (88.7 %).

2.2.12.b. Sample preparation:

Approximately 0.1 mL of AH and 0.5 mL of VH was collected from each test eye into individual centrifugal tubes. All other tissues, RC, IC, cornea & sclera, from each test eye were individually cut into very small pieces and placed into individual vials. Protein precipitation was carried out similar to the standard solution preparation and analyzed using HPLC-UV method. A mixture of 20 mM phosphate buffer (pH 2.5) and ACN in a ratio of 65:35 was used as the mobile phase and Phenomenex *Luna*® 5 µm C_{18} 100 Å, *250* x 4.6 mm column at a flow rate of 1 mL/min and 284 nm.

2.2.13. Data analysis

All experiments were carried out at least in triplicate.

The entrapment efficiency (EE) of HT in the SLN's was estimated using Equation (1):

$$EE\ (\%) = [(W_i - W_f)/(W_i)] \times 100 \qquad Eq\ (1)$$

Where,

W_i = total drug content,

W_f = amount of free drug in aqueous phase.

HT release data was fitted to zero order, first order and Higuchi models (Equations 2, 3 & 4).

$$C_t = C_0 + K_0 t \qquad Eq\ (2)$$

$$LogC_t = LogC_0 + Kt/2.303 \qquad Eq\ (3)$$

$$C_t = K_H t^{1/2} \qquad Eq\ (4)$$

Where,

C_0 & C_t = concentration at time 0 min and t min,

K_0, K & K_H = kinetic constants for zero order, first order and Higuchi models.

Drug diffusion parameters across cornea such as cumulative amount (M_n) , rate (R) and flux (J) were calculated using previously described method [105].

Cumulative amount of HT released from the film was calculated using equation 5

$$M_n = V_r\,C_{r(n)} + \sum_{x=1}^{x=n} V_{s(x-1)}\,C_{r(x-1)} \qquad \text{Eq (5)}$$

Where,

 n = sampling time point (n=1, 2, 3 and 4… corresponding to 15, 30, 45 and 60..min respectively),

V_r = volume of the medium in the receiver chamber (mL),

V_S = volume of the sample withdrawn at the nth time point (mL),

$C_{r(n)}$ = concentration of the drug in the receiver chamber medium at n^{th} time point ($\mu g/mL$).

Steady state flux was determined using equation 6

$$\text{Flux (J)} = \frac{(dM/dt)}{A} \qquad \text{Eq (6)}$$

Where,

M = cumulative amount of HT (μg),

t = time (min),

A= surface area of cornea (0.636 cm^2).

Statistical analysis was carried out using ANOVA to compare between different groups and Tukey's post-hoc HSD was used to compare differences between two groups. A 'p' value less than 0.05 was considered to denote statistically significant difference.

2.3. Results:

2.3.1. Physicochemical characterization:

HT content in all the films was observed to be approximately between 90 – 93 % of the theoretical values and was found to be uniformly distributed within the matrix (RSD<2.3 %). HT content in the SLN's was found to be 92 - 97% of the theoretical value. Entrapment efficiency, particle size, polydispersity index and zeta potential were found to be 86.4 ±0.7 %, 225.5 ± 21 nm, 0.379 and -21 ± 9 mV respectively.

2.3.2. DSC and FTIR studies:

2.3.2.a. HT-Film:

DSC thermograms of PEO N10, drug and polymeric film are presented in **Figure 2.6**. HT exhibited an endotherm at 234 $^{\circ}$C corresponding to its melting point. PEO N10 exhibited a melting point temperature of 65 $^{\circ}$C. PEO N10 demonstrated an endothermic peak shift from 65 to 63 and 60 $^{\circ}$C with the 10 %w/w and 20 %w/w films, respectively. HT peak at 245 $^{\circ}$C was absent in the melt-cast films.

FTIR spectra of HT showed aromatic stretching from 1650 to 1500 cm^{-1}, and –OH phenolic stretching was observed at 1200 cm^{-1}. PEO revealed -CH stretching at 2890 cm^{-1}. Scissoring and wagging movement of -CH$_2$ were observed at 1450 and 1350 cm^{-1}. Aromatic stretch bands corresponding to HT and -CH stretch bands corresponding to PEO N10 were observed with the 10 %w/w film. Similar spectral bands were observed with the 20 %w/w film (**Figure 2.7**).
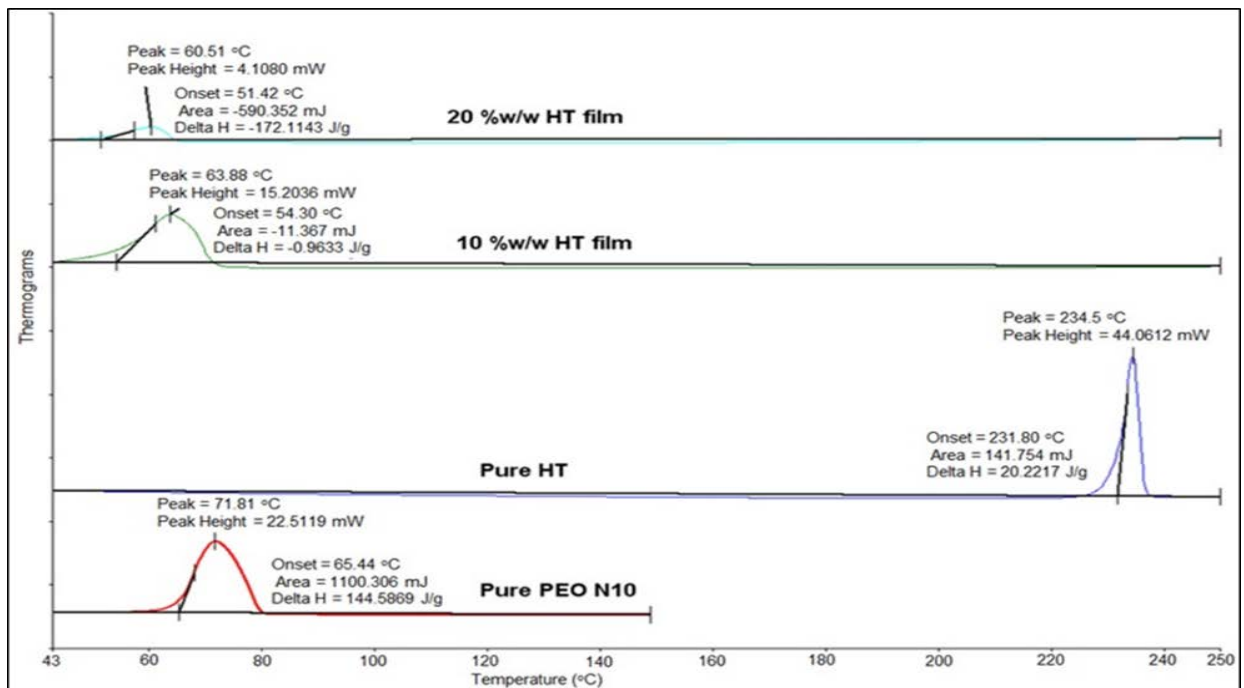
Figure 2.6: Differential scanning calorimetry thermograms of hesperetin (HT) polymeric matrix film, PEO N10 and HT.
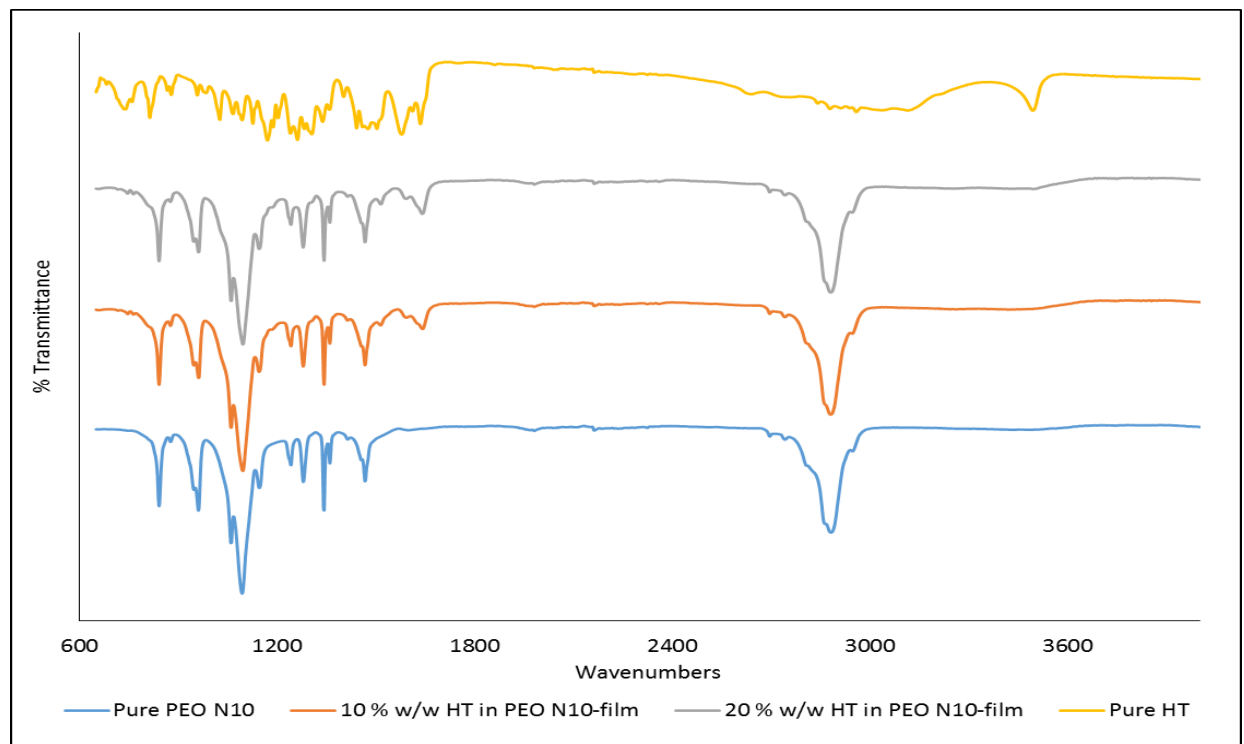
Figure 2.7: FTIR spectral images of PEO N10, hesperetin (HT), 10 %w/w HT polymeric matrix film and 20 %w/w HT polymeric matrix film.

25

2.3.2.b. HT-SLN:

DSC thermograms of HT, GMS, Compritol 888 ATO, lyophilized HT-SLNs, and other excipients used in the formulation are presented in **Figure 2.8**. HT had similar endothermic peak at 234 $^{\circ}$C as seen in the thermograms with the matrix film. All other excipients had corresponding
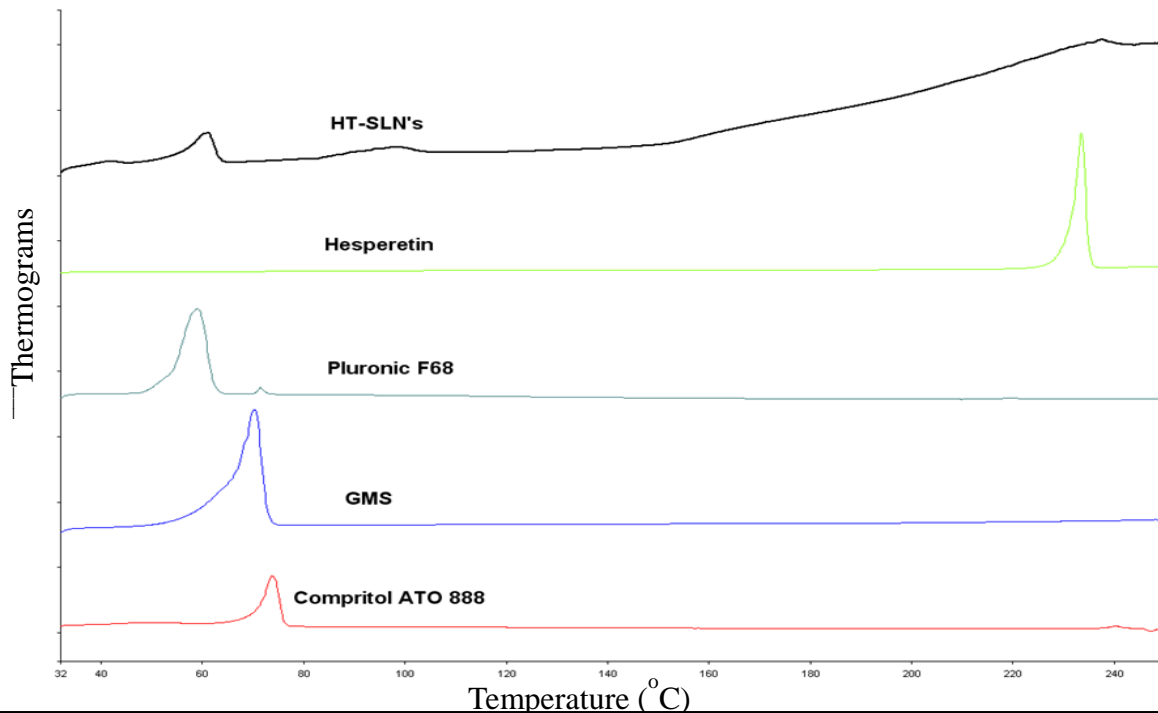
Figure 2.8: DSC thermograms of A) Compritol® ATO 888, B) GMS, C) Pluronic® F-68, D) HT and E) HT-SLN's.

endothermic peaks between 45 and 60 $^{\circ}$C. The thermal curve of the bulk Compritol 888 ATO and GMS exhibited an endothermic peak at 70-75 $^{\circ}$C. Additionally, an endotherm at 50-55 $^{\circ}$C corresponding to the melting point of Pluronic F68 was also observed in HT-SLNs. The endothermic peak of HT was not observed in the SLN formulation.
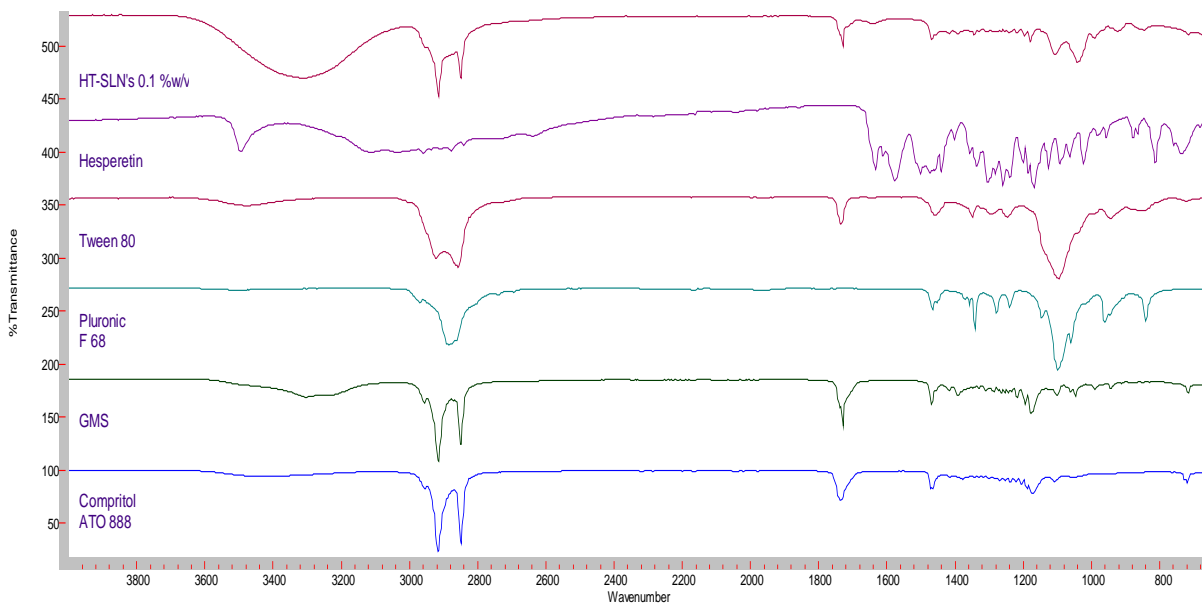
Figure 2.9: FTIR spectra of HT-SLN's and different excipients used in the preparation of HT-SLN's.

FTIR spectra of IR spectra of compritol and GMS show typical bands at 2820 cm^{-1}, due to C-H stretching, and 1705 cm^{-1} due to C = O (carbonyl) stretching (**Fig.2.9**). Pluronic F68 exhibits characteristic peaks at 2886 and 1112 cm^{-1} due to stretching vibrations of C–H, and C–O groups. Tween 80 exhibits broad peak between 3400 and 3600 corresponding to OH stercthing. While the peak at 2880 corresponds to CH stretching. The spectral peak corresponding to OH group in HT was absent in the SLN formulation. Instead a broad peak was observed.

2.3.3. *In vitro* release and corneal permeability studies:

Release of HT from the matrix films was 95.3 ± 1.3 % (with sieve) and 89.3 ± 11.9 (without sieve and no stirring) within 120 minutes (**Fig.2.10**). Rate and flux across the corneal and Spectra/Por® membranes were found to be 0.37 ± 0.03 μg/min and 0.58 ± 0.05 μg/min/cm^2 and 0.57 ± 0.05 μg/min and 0.89 ± 0.06 μg/min/cm^2, respectively (**Fig.2.11**). Under the settings employed release towards the periocular surface (representing the precorneal loss) of HT from the film was found to be 16.1 ± 4.5 % in 3 h. Cumulative precorneal loss of HT was 1.7-folds higher

than that observed across the cornea. Cumulative amount of HT permeating across the isolated rabbit cornea in 3 h was determined to be 59.9 ± 5.2 µg.
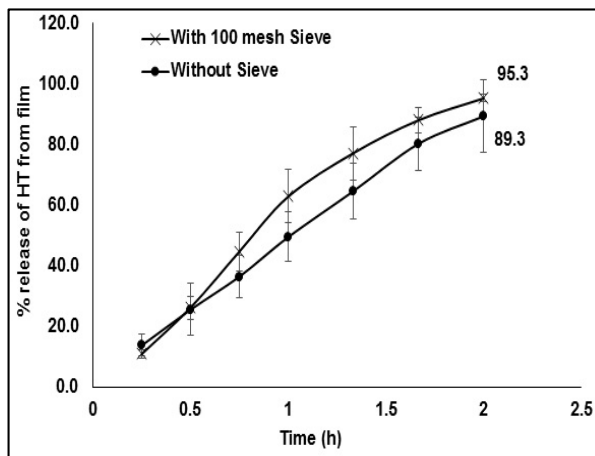
| Figure 2.10: Percentage release of HT from 10 %w/w film across the standard US 100 mesh and without sieve. | Figure 2.11: *In vitro* transcorneal permeability of HT from 10 %w/w matrix film across isolated rabbit cornea. |
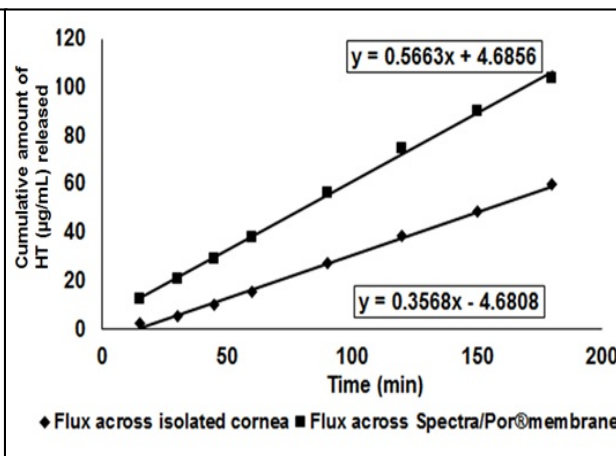
HT release from the SLN's was found to be $60.7 \pm 6.03\%$ in 3 h. Rate, flux and permeability coefficient of HT from the SLN's were found to be 1.4 ± 0.2 µg/min, 2.2 ± 0.24 µg/min/cm^2 and 28.7 ± 3.1 x 10^{-6} cm/sec respectively.

2.3.4. *Ex vivo* studies:

HT content in the AH, VH and RC were found to be 5.8 ± 0.2 µg/gm of tissue, 5.6 ± 1.4 µg/gm of tissue, and 14.2 ± 3.8 µg/gm of tissue, respectively. Amount of HT in RC was found to be 2.5-fold higher compared to that in the AH or VH.

2.3.5. *In vivo* studies:

Initially, ocular tissue concentrations obtained with 10 %w/w HT loaded matrix film was evaluated *in vivo* 1h after topical application of the film in anesthetized animal model. AH, VH, IC, RC, cornea and sclera were analyzed for HT content. Significant levels of HT were detected in the IC, cornea and sclera tissues. HT levels were also observed in the back-of-the-eye tissues:

28
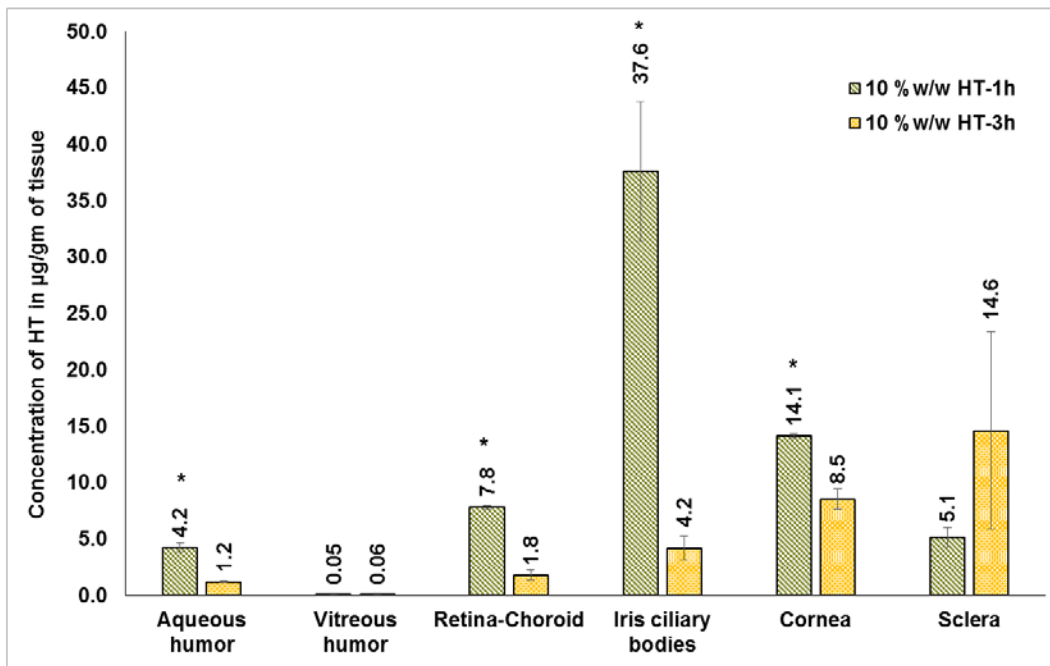
Figure 2.12 A: Ocular tissue hesperetin (HT) concentrations (µg/g of tissue) obtained from 10%w/w film 1h and 3h following topical application. * - Significantly different from 10%w/w HT-3 h. Anesthetized animal model.

VH (0.05 ± 0.03 µg/gm of tissue) and RC (7.8 ± 0.2 µg/gm of tissue). When, HT load in the film was doubled (Dose: 1.6 mg per 4 mm x 2 mm; 8 mg of film) HT levels in the AH, IC, and cornea were 2-fold higher than that of the 10 %w/w HT film. With the 20 %w/w film, amount of HT in the posterior segment ocular tissues was found to be 1.4 ± 0.5 µg/gm of tissue (VH) and 23.5 ± 6.9 µg/gm of tissue (RC). It was observed that doubling the dose of HT in the matrix resulted in an approximately 10- and 28-folds increase in scleral and VH HT concentrations, respectively. The results are presented in **Figure 2.12 A&B**.

Ocular tissue concentrations, 3 h post topical instillation of the 10 %w/w and the 20 %w/w HT film *in vivo,* were also evaluated. Expectedly, HT concentrations at the end of 3h were relatively low compared to the 1 h time point. Results from the 3 h study are presented in **Figure 2.12 A&B**.
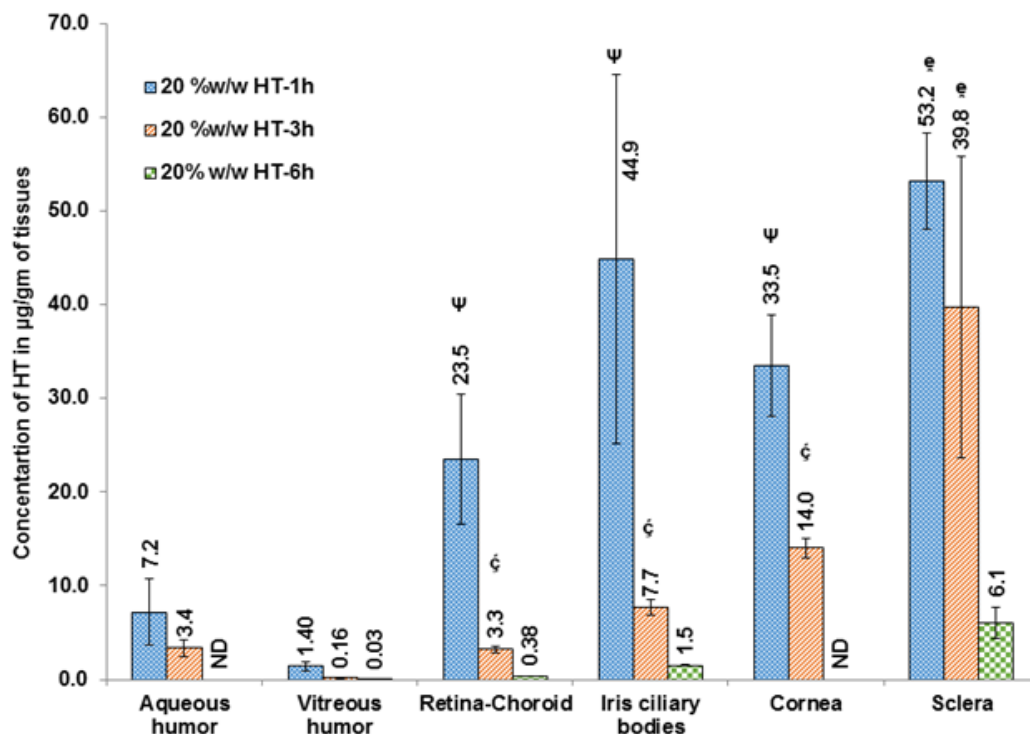
Figure 2.12 B: Ocular tissue hesperetin (HT) concentrations (µg/g of tissue) obtained from 20%w/w film 1h, 3h and 6h following topical application. ND – not determined. Ψ - Significantly different from 10%w/w HT-3h and 6h, ȼ - Significantly different from 10%w/w HT- 1h and 6h and ȩ- Significantly different from 10%w/w HT- 1h and 3h. Anesthetized animal model.

Ocular tissue HT concentrations obtained with the 20 %w/w film was also tested 6 h post topical application. HT was detected in VH (0.03 ± 0.02 µg/gm of tissue), RC (0.4 ± 0.02 µg/gm of tissue), IC (1.5 ± 0.1 µg/gm of tissue) and sclera (6.1 ± 1.6 µg/gm of tissue) (Figure 2.8 B). Only the posterior segment ocular tissue concentrations were determined in the 6h study as the cornea was carefully isolated and taken for histology studies. Thus, both cornea and AH HT concentrations were not determined in the 6h study.

Ocular distribution of HT from the SLN's are presented in **figure 2.13**. Anterior chamber of the eye exhibited high HT levels with the HT-SLN's 1 h post topical application. While the posterior segment of the eye had very little concentration of HT.

Ocular distribution of HT in the conscious animal model with active lymphatic and tear drainage, HT-Film, HT-SLN's and HT-CD solution were evaluated after 3 h of topical application. Results were presented in the **figure 2.14**.
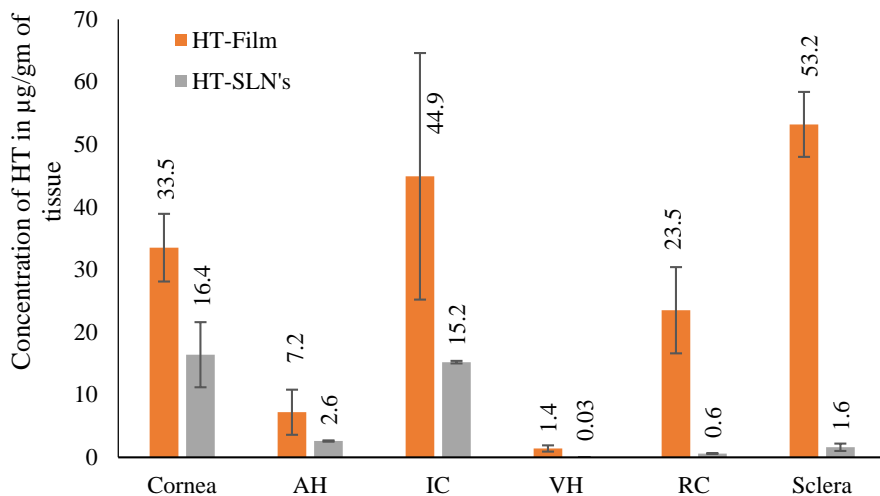
Figure 2.13: Ocular tissue concentrations of HT obtained from HT-CD, HT-SLN's and HT-Films 1 h post topical administration in anesthetized animal model. AH- Aqueous humor, VH- Vitreous humor, IC-Iris ciliary bodies and RC- Retina choroid. Anesthetized animal model.
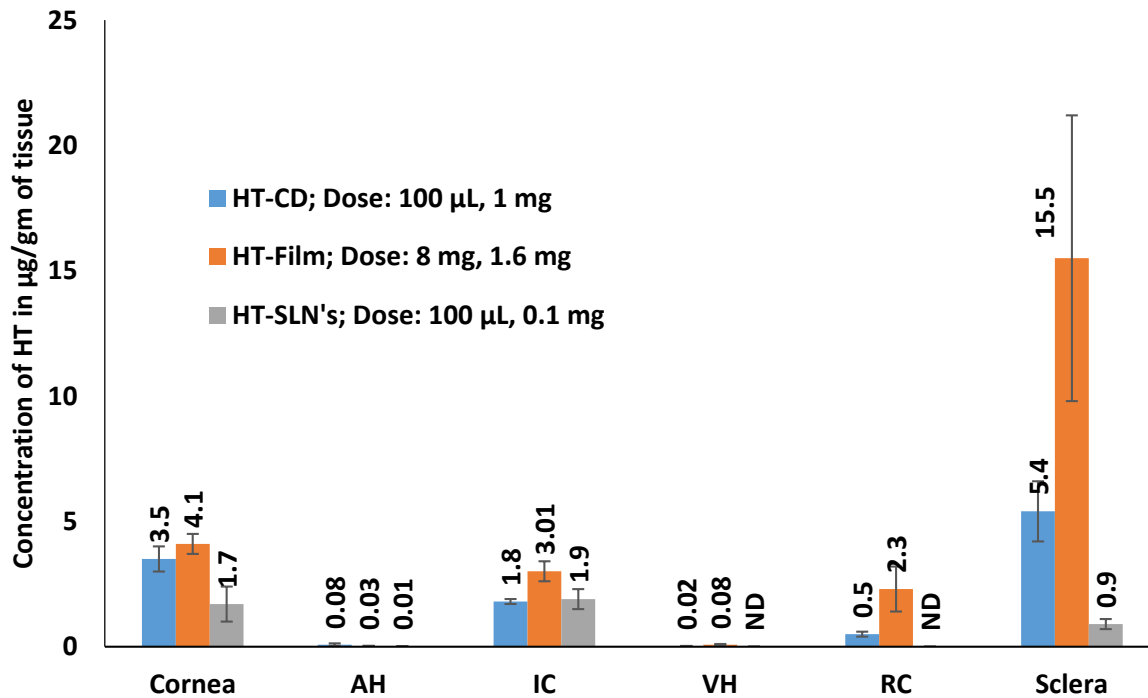
Figure 2.14: Ocular tissue hesperetin (HT) concentrations (µg/g of tissue) obtained from 1% w/v HT-10% w/v HPβCD, 20%w/w film and 0.1% HT-SLN's at the end of 3h following topical application. ND – below detection limit. AH-aqueous humor, IC-Iris ciliary bodies, VH-Vitreous humor and RC-Retina choroid. Conscious animal model.

Table 2.1: Compiled ocular tissue hesperetin (HT) concentrations (µg/g of tissue) obtained from 1% w/v HT+10% w/v HPβCD, 10% w/w and 20%w/w film and 0.1% HT-SLN's at the end of 1h, 3h, and 6h following topical application. ND – below detection limit. AH-aqueous humor, IC-Iris ciliary bodies, VH-Vitreous humor and RC-Retina choroid. A-Anesthetized animal model and C-Conscious animal model.

Formulations	Volume; Dose (mg)	Time (h)	Model	Tissue concentrations (µg/gm of tissue)					
				Cornea	AH	IC	VH	RC	Sclera
Solution (1 % w/v HPβCD)	100 µL; 1 mg	3	C	3.5 ± 0.5	0.08 ± 0.05	1.8 ± 0.1	0.02 ± 0.01	0.52 ± 0.1	5.4 ± 1.2
Film (10% w/w)	4 mm x 2 mm x 0.2 mm; 0.8 mg	1	A	14.1 ± 0.2	4.2 ± 0.4	37.6 ± 6.2	0.05 ± 0.03	7.8 ± 0.2	5.02 ± 0.9
Film (10% w/w)	4 mm x 2 mm x 0.2 mm; 0.8 mg	3	A	8.5±0.9	1.2±0.1	4.2± 1.1	0.06 ±0.02	1.8±0.5	14.6 ±8.8
Film (20% w/w)	4 mm x 2 mm x 0.2 mm; 1.6 mg	1	A	33.5 ± 5.4	7.2 ± 3.6	44.9 ± 19.7	1.4 ± 0.51	23.5 ± 6.9	53.2 ± 5.2
Film (20% w/w)	4 mm x 2 mm x 0.2 mm; 1.6 mg	3	A	14±1.1	3.4±0.9	7.7± 0.8	0.16 ±0.07	3.3±0.4	39.8 ±16.1
Film (20% w/w)	4 mm x 2 mm x 0.2 mm; 1.6 mg	3	C	4.1 ± 0.4	0.03 ± 0.01	3.01 ± 0.4	0.08 ± 0.03	2.3 ± 0.96	15.5 ± 5.7
Film (20% w/w)	4 mm x 2 mm x 0.2 mm; 1.6 mg	6	A	NA	NA	1.5±.1	0.03 ±0.02	0.38± 0.02	6.1± 1.6
SLN (0.1% w/v)	100 µL; 0.1 mg	1	A	16.4 ± 5.2	2.6 ± 0.1	15.2 ± 0.2	0.03 ± 0.01	0.59 ± 0.02	1.6 ± 0.6
SLN (0.1% w/v)	100 µL; 0.1 mg	3	C	1.7 ± 0.7	0.01 ± 0.001	1.9 ± 0.36	ND	ND	0.9 ± 0.2

Corneas exposed to the 20 %w/w HT film for 6 h did not show any substantial damage when compared to the control. Extracellular swelling of the corneal epithelium or stromal lamellae
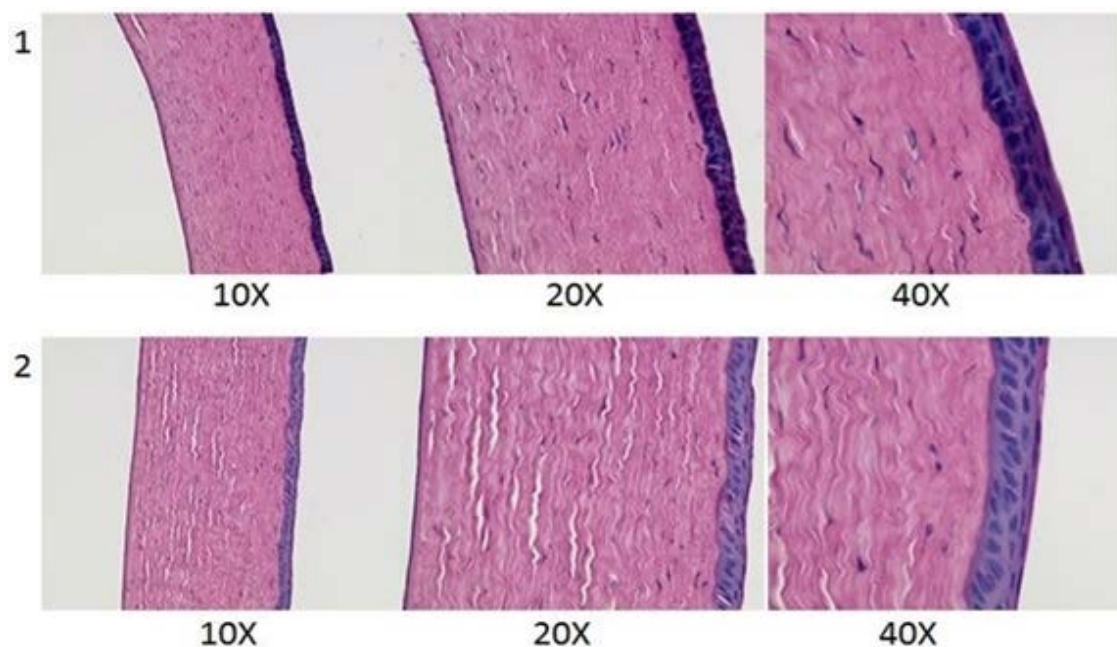
Figure 2.15: Histological images of rabbit corneas exposed to 1) IPBS & 2) 20 %w/w HT film for 6h.

was observed in the control and the corneas exposed to the film representing the minor artifacts that were introduced during the fixating process (**Fig. 2.15**).

2.4. Discussion:

In this study HT was incorporated into a polymeric matrix system utilizing a melt-cast method. In this method, the active compound is embedded in a carrier matrix comprised of one or more meltable substances and other functional excipients. Once the formulation comes into contact with the release media (*in vitro*) or tear fluid (*in vivo*) it quickly transforms into a gel and releases the drug slowly over prolonged periods of time, depending on the matrix composition. Moreover, high drug loads (20 - 40 %w/w) can be easily incorporated without the need for any organic solvent. Importantly, both hydrophilic and hydrophobic moieties can be incorporated into the polymeric matrix without any difficulty. Considering the low volumes that can be administered

topically (35 - 50 µL in general) and the fact that a large number of new drug candidates are poorly water soluble, most of the current dosage forms require surfactants or other solubilization approaches. The melt-cast technology converts the compounds into its amorphous state, or disperses them at a molecular level in the polymer matrix, because of which the solubility of the compound is increased. Increased solubility could improve transcorneal permeability of the therapeutic agent several folds. By altering the type of matrix polymer, this process technology can be employed to design sustained release dosage forms.

In this study we also evaluated solid lipid nanoparticles (SLN's) as a secondary approach to deliver HT to the intraocular tissues. Nanotechnology offers many advantages in drug delivery from controlled release to targeted drug delivery. SLNs have been used in the field of ocular drug delivery for decades. They have shown enhanced corneal absorption and improved ocular bioavailability of both hydrophilic and hydrophobic drugs. In this study, we have prepared HT-SLN using a mixture of 15% Compritol and 85% GMS. Particle size of HT-SLN's was 225 nm approximately. This helps improve corneal absorption and at the same time keeps them from getting eliminated easily from the ocular surface and tissues. With Zeta potential at -21 mV, a stable SLN's were achieved. Although the polydispersity index of the SLN's was slightly higher than the ideal requirement (approximately ≤0.2), further optimization of the process technique can be helpful.

We prepared the melt cast films with 10 %w/w and 20 %w/w HT loads such that the total amount of HT per unit dosage of 4 mm x 2 mm film was maintained at 0.8 mg and 1.6 mg, respectively. The thickness of the films was maintained between 0.2 mm - 0.4 mm. PEO N10 was selected as the matrix forming material because of its good aqueous solubility, low viscosity and low toxicity [106]. Since the polymer is water soluble, it can easily transform into a gel and be

37

slowly washed away by the tear fluid. PEO N10 has a low melting point and an excellent film forming ability. This property helps in achieving smooth flexible films at low temperatures and can thus be employed to develop matrix films for thermo-sensitive compounds. Surface of the film was flat and smooth avoiding any discomfort *in vivo*. Uniform distribution of HT was achieved within the polymeric matrix by continuous geometric dilution as confirmed by both FTIR and HPLC analysis. PEO N10 has been reported to form simple binary eutectic mixtures due to its low entropy of fusion thereby improving drug release from the matrix [107, 108]. Endothermic peak shifts observed in the DSC thermograms could be because of this eutectic mixture formation.

Side-by-side diffusion apparatus was employed to determine flux across the cornea. A modified protocol was used to represent periocular loss of HT from the film. To the best of our knowledge, this is the first time an *in vitro* model has been used to study transcorneal permeation in the presence of precorneal/periocular loss. In this study, flux across the Spectra/Por® membrane, used on the precorneal side, was 1.7-fold greater than the corneal tissue. The ratio of precorneal loss to corneal penetration was thus 1.7:1 under the conditions tested. By changing the experimental parameters (e.g. use of different backing membranes, vertical apparatus, sandwiched cassettes, continuous dilution of the donor chamber solution) periocular/precorneal loss can be increased to mimic precorneal loss *in vivo* and to develop *in vitro in vivo correlations*. The apparatus/set-up can be easily modified to accommodate various types of ophthalmic formulations.

Release of HT from the film, with or without sieve, followed the Higuchi model with coefficient of determination (R^2) 0.9899 and 0.9873, respectively. The results demonstrate that the sieve did not act as a barrier to HT release and diffusion in the release medium. Flux across the membranes exhibited zero-order kinetics. *In vitro* transcorneal flux was several folds greater than

that obtained with other formulations reported in the literature [109], even in the presence of a precorneal loss. This demonstrates the value of the melt-cast topical HT dosage form.

The whole eye globes obtained from Pel-Freez Biologicals served as a good *ex vivo* model. HT film required approximately 30 min to transform into a gel in the absence of any tear fluid. The concentrations observed in the RC were 3-fold higher when compared to the levels in the AH and VH. The results suggest that the film was preferentially delivering HT to the posterior segment of eye through conjunctival-scleral pathway. Considering the data, from the subsequent *in vivo* studies, ocular tissue concentrations of HT in AH, VH and RPE were found to be overestimated in the *ex vivo* model due to lack of vascular and lymphatic drainage systems.

As expected, and unlike the *ex vivo* studies, HT films transformed into a gel in less than 5 min following topical application. This was much quicker when compared to the *ex vivo* study due to the presence of tear fluids. Allergic reactions such as inflammation or redness or excessive tearing were not observed throughout the duration of the study. Results from the topical HT films indicate that significant levels of HT can be delivered to the posterior segment of the eye with these matrix film formulations. With the 10 %w/w HT film significant amounts of HT was detected in both VH and RC. On doubling the amount of HT in the matrix, VH and RC levels markedly increased by 28- and 3-folds, respectively. Thus, a dose dependent concentration profile was observed from the matrix system. Significant HT levels were detected in the cornea, sclera, IC and AH 1 h post topical application of the matrix. The concentration profile, higher HT concentrations in the RC when compared to the VH, was consistent with scleral absorption pathway, as also suggested by the *ex vivo* studies. High drug concentration in the PEO matrix in close contact with the ocular tissues could favor direct partitioning from the matrix into the ocular tissues. This might

be one of the possible reasons for achieving significant intraocular tissue concentrations from the matrix film.

With SLN's, the dose administered was 8 and 16-folds lower than the 10% w/w and 20% w/w film. Even at such low doses HT-SLN's were able to deliver significant levels to the anterior segment of the eye (Table 2.1). When compared with the solution formulation, which has a 10 fold higher dose than the SLN formulation, SLN's were able to deliver much higher concentration to the anterior segment tissues. This shows improved ocular absorption of the nanoparticle through corneal route of absorption.

Ramesh *et al,* have previously evaluated ocular bioavailability of HT through intravenous and topical routes of application [110]. In these studies, 1 %w/v HT solution (Dose: 1 mg) for topical instillation was prepared using 10 %w/v HPβCD and 10 %w/v RMβCD. HT concentrations in the AH, VH, RC and IC achieved with the 1 %w/v HT-CD solution (dose: 1 mg; 100 µL instilled volume) were approximately 3-5 folds lower than the levels obtained with the 10 %w/w HT film (Dose: 0.8 mg) in the current study. Concentrations in the sclera and cornea were similar in both the cases. When benzalkonium chloride (BAK) was included in the HT-CD solution formulation [110], the ocular tissue concentrations achieved were 2-fold higher than that obtained with the 10 %w/w film, which did not contain any BAK, at the 1 h time point [110]. The 20 %w/w HT film, however, was able to deliver significantly higher HT levels in all cases. Thus, although the melt-cast film did not have any preservatives or solubilizers, the intraocular tissue concentrations achieved with this dosage form were very high.

HT is rapidly eliminated from the ocular tissues due to choroidal and lymphatic drainage. HT levels in all ocular tissues declined rapidly after application of both 10 % and 20 %w/w film (**Fig.2.12A & B**). Less than 50% of the concentration determined at the 1 h time point remained

in the VH, RC and IC 3 h post topical application, suggesting a vitreal half-life of less than 2 h. The results are consistent with vitreal half-life of 110 minutes reported in earlier studies [110]. Matrix films containing 20% HT, however, maintained significant levels in all the ocular tissues at the end of 3 h. In fact, with the 20 %w/v HT films a significant amount of HT was maintained in the VH and RC and other ocular tissues, even after 6 h post application.

Smith et al. reported that at 0.1-0.3 µM (30.2 - 90.7 ng/mL) concentrations, HT demonstrates neuroprotective activity when mouse primary cortical neurons were subjected to a pro-apoptotic insult by exposing them to staurosporine [111]. All studies determining IC_{50} values report solution concentrations and not actual tissue concentrations. Thus, the AH and VH concentrations, which are in equilibrium with the anterior and posterior segment ocular tissues, serve as good therapeutic response indicators for IC and RC sites. Considering that the VH is on the receiving side with the scleral side being the dosing side (topical application) it can be expected that the HT concentrations in the RC or IC will be well within the therapeutic range at least for as long as the VH and AH concentrations are within the IC_{50} range. In the current study we observe that even at the 6h time point, the levels of HT in VH (30 ng/mL), are within this range. Although the AH was not analyzed at the 6h time point, since the AH concentrations were typically several folds greater than the VH concentrations at all time-points, following topical application, it can be concluded that the AH concentrations would also be within the neuroprotective concentration range at the 6h time point. Thus, with the 20% matrix films, ocular tissue HT concentrations were maintained within and above levels required for neuroprotectant activity for at least 6h post topical application.

With respect to anti-oxidant activity, HT levels at the end of 1 h in the AH (4.2 µg/mL) was greater than the IC_{50} values for peroxynitrites (IC_{50}: 4.67 µM; 1.4 µg/mL) and superoxide

inhibition (IC_{50}: 7.47 µM; 2.3 µg/mL) [82]. With the 20 %w/w film, at the end of 1h, HT levels in both AH and VH were above these IC_{50} values. Levels of HT in AH (3.4 µg/mL) were maintained above the IC_{50} values for peroxynitrites and superoxide inhibition even at the end of 3h, following topical application of the 20 %w/w film.

In terms of anti-inflammatory activity, Yang et al. reported that at 1-10 µM (0.3 – 3.02 µg/mL) HT concentrations, cellular levels of COX-2 and PEG2 are markedly attenuated [112]. With both the 10% and 20 %w/w films, HT levels in the AH (1.2 and 3.4 µg/mL, respectively) were maintained within the concentration range required for COX-2 and PEG2 inhibition, even at the end of 3h.

When the 1%w/v HT+10%w/v CD solution, 0.1%w/v HT-SLN's and 20%w/w HT-Film formulations were tested for intraocular distribution in the conscious animal model, 3 h post topical application, HT concentrations in all the tissues dropped significantly compared to the anesthetized model. This was expected and can be attributed to the active lymphatic and tear drainage in conscious animals. Aqueous humor outflow is presumed to be the one of the major routes of elimination from the intra ocular tissues [113]. As a result, AH concentrations in all conscious animal model were significantly lower compared the same formulations in anesthetized model (**Table 2.1**). When these concentrations were compared against the IC_{50} values, films were able to maintain neuroprotective HT levels in all the tissues. Anti-oxidant and anti-inflammatory levels were maintained in IC and RC. Although SLN's were administered at much lower doses, were able to deliver significant levels of HT to the anterior segment of the eye. But we were not able to achieve and maintain the levels in posterior segment of the eye.

Thus, the polymeric matrix film was successfully able to deliver and maintain levels of HT required for neuroprotectant, anti-oxidant and anti-inflammatory activity in the ocular tissues. As

mentioned earlier, the AH and VH concentrations represent the innermost ocular tissues (receiver solutions) in the anterior and posterior segments, respectively, for a topical route of application. Thus, the concentrations in the retina, choroid, cornea or iris-ciliary bodies would be significantly higher compared to what would be achieved if the AH or VH concentrations were to represent donor concentrations (e.g. intravitreal injection).

2.5. Conclusion:

In conclusion, appreciable ocular tissue concentrations were achieved using non-invasive topical melt-cast films. A 2-fold increase in HT content in the matrix film led to several fold increase in the HT concentration in the ocular tissues. With the 20 %w/w HT film high concentrations of HT were maintained in the posterior segment ocular tissues even at 3 h post topical application. Quantifiable levels of HT was still retained in the VH and RC even after 6 h. While matrix films were able to deliver HT to the posterior and anterior segment of the eye, SLN's can be a promising platform to deliver drug to the anterior segment of the eye. Corneal histology studies indicate that the formulations did not produce any damage to the ocular tissues. Thus, the melt-cast matrix films appear to be a promising approach for drug delivery to the back-of-the-eye.

CHAPTER 3

EVALUATION OF PHARMACODYNAMIC RESPONSE OF Δ^9-TETRAHYDROCANNABINOL AND TETRAHYDROCANNABINOL VALINE HEMISUCCINATE

CHAPTER 3

3.1. INTRODUCTION

Glaucoma is an ocular neuropathy characterized by progressive and irreversible loss of vision. It affects nearly 60 million people worldwide and is the second leading cause of blindness [114]. Intraocular pressure (IOP) has been identified as an important risk factor in the pathogenesis of the disease [115]. Elevated IOP leads to damage to the retinal ganglion cell (RGC) axons leading to progressive and irreversible vision loss [116]. Current therapy targets a reduction in IOP to prevent progression of the disease. This, however, is often not enough to prevent or arrest the development of glaucoma related optic neuropathy [117-119]. A number of hypotheses exist, but the complete mechanism of RGC cell death has not yet been elucidated [120-122]. New classes of agents that can reduce IOP as well as prevent or slow the loss of RGC are direly needed.

Δ^9-Tetrahydrocannabinol (THC; **Fig.3.1A**), an active ingredient of the plant *cannabis sativa*, and an agonist of the cannabinoid receptors, CB1 and CB2, could potentially be such a dual acting anti-glaucoma agent [123-125]. The presence of cannabinoid receptors in the ocular tissues have been recently identified [126] lending support to a localized IOP reducing mechanism, rather than central nervous system involvement. What makes THC especially attractive is that in addition to its IOP lowering activity, THC has also demonstrated independent neuroprotective potential [79].

In terms of the route of delivery, since glaucoma is a chronic disease, non-invasive topical application would be the most preferred means of drug delivery. The anatomy and physiology of the eye, however, presents a formidable barrier to intraocular delivery of drugs, especially to the back-of-the eye which is needed for neuroprotectant activity, through the topical route. The combination of precorneal and corneal barriers, and other physiological barriers, results in only about 5-10% of the topically applied drug reaching the inner ocular tissues [94, 95, 127]. Development of THC as an eye drop is especially challenging due to its poor aqueous solubility (1-2 µg/mL) and high logP (6.42) [128]. In view of the challenges in topical delivery of THC it is not surprising that disparity exists in the literature with respect to the efficacy of THC administered through the topical route [129-131]. Some reports showed IOP lowering activity of THC in normotensive rabbits [130], ocular hypertensive human subjects [132], rabbit glaucoma model [133], normotensive dogs [134] and normotensive cats [135], while several other studies showed no IOP lowering activity in normal human subjects [129, 136], glaucoma models [137]. In fact, based on the earlier data a study panel constituted by the National Eye Institute of the National Institutes of Health had concluded that there was insufficient evidence to conclude that THC could be useful in the treatment of glaucoma [138].

Review of the literature revealed that in most of these earlier studies evaluating the efficacy of THC through the topical route, researchers used mineral oil or surfactant based solutions or emulsions as the formulation platform. While these formulations improved solubility of THC they would not alter its membrane permeation characteristics. Taking into consideration the formulations used and the associated preclinical data, we hypothesized that THC, because of its lipophilic characteristics, would rapidly partition into the lipophilic corneal epithelia but would remain trapped there – failing to efficiently partition out into the more hydrophilic stromal layers

- and not reach the intraocular tissues [139]. Thus, we started evaluating various THC prodrugs to enhance ocular tissue permeation characteristics of THC.

We previously synthesized and studied dicarboxylic acid prodrugs, the hemisuccinate (THC-HS) and the hemiglutarate (THC-HG) esters, to improve ocular bioavailability [79]. A significant improvement in aqueous solubility was observed due to the ionization of the molecules at physiological pH. Transcorneal permeability, however, remained low at physiological pH. Use of ion-pairs, which shielded the negative charge of THC-HG at physiological pH, significantly improved permeability at pH 7.4. Topical administration of THC-HG in rabbits using these ion-pair formulations delivered THC to the front of the eye tissues, such as aqueous humor and the iris-ciliary bodies. THC levels were below detection levels in the retina and vitreous humor [139].

In contrast to the dicarboxylic acid prodrugs, the amino acid THC prodrugs has shown greater stability, especially the valine ester, but low aqueous solubility at physiological pH [140].
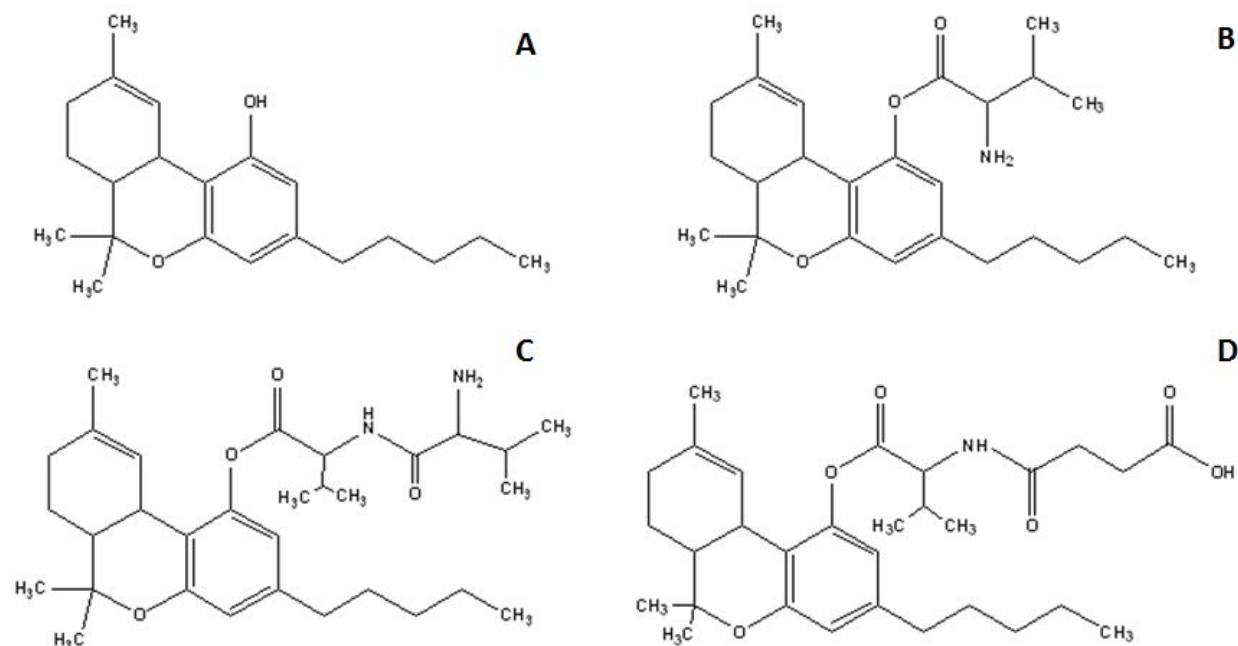
Figure 3.1: Chemical structures of A) Δ^9-Tetrahydrocannabinol (THC), B) Δ^9-Tetrahydrocannabinol Valine (THC-Val), C) Δ^9-Tetrahydrocannabinol Valine Valine (THC-Val-Val) and D) Δ^9-Tetrahydrocannabinol Valine Hemisuccinate (THC-Val-HS).

Thus, THC-Val (**Fig.3.1B**) and THC-Val-Val (**Fig.3.1C**) were included in this study. Their ocular

penetration and solubility in the presence of surfactants and cyclodextrins have been evaluated.

However, due to poor aqueous solubility, Val and Val-Val were not evaluated further.

Additionally, to overcome the drawbacks observed with the dicarboxylic acid esters and the

solubility limitations of the amino acid prodrugs, a new amino acid-dicarboxylic acid prodrug,

THC-Val-HS (**Fig.3.1D**), was designed.

The preformulation characteristics and ocular tissue homogenate stability and IOP

lowering activity of the most promising compound was tested in alpha-chymotrypsin induced

rabbit glaucoma model. Therapeutic activity was compared to that of the controls - THC, timolol

maleate and pilocaprine eye drops (the latter two being marketed ophthalmic formulations).

3.2. MATERIALS AND METHODS

3.2.1. Materials

Hydroxypropyl methyl cellulose (HPMC, 4000 cps), 2-Hydroxypropyl-β-cyclodextrin

(HPβCD), randomly-methylated-beta-cyclodextrin (RMβCD), Tyloxapol and alpha-chymotryspin

(Type II, lyophilized powder, ≥40 units/mg protein) were purchased from Sigma-Aldrich (St.

Louis, MO). Super Refined™ Tween 80™ was received as a gift sample from Croda Inc. (Mill

Hall, PA). Pluronic® F 68 (Poloxomer 188), Pluronic® F 127 (Poloxomer 407) and Cremophor®

RH 40 were received as a gift sample from BASF (Florham Park, NJ). Tocrisolve™100 was

purchased from Tocris Biosciences (Minneapolis, MN). Timolol maleate eye drops (0.25 % w/v)

and Pilocarpine HCl eye drops (2 %w/v) were marketed eye drops. All other chemicals and

solvents were purchased from Fisher Scientific (St. Louis, MO).

Buffer reagents used in the cannabinoid receptor binding studies were purchased from

Sigma-Aldrich (St. Louis, MO). All radioligands and MicroScint™ were purchased from

PerkinElmer (Waltham, MA). Non-labeled controls were purchased from Tocris Bioscience (Minneapolis, MN). Membrane preparation was made using a Tris-HCl buffer (50 nM Tris-HCl), pH 7.4. Dilutions of membrane, radioligand and control/test compounds were made in a Tris-EDTA buffer (50mM Tris-HCl, 20mM EDTA, 154mM NaCl and 0.2% fatty-acid BSA), pH 7.4. *In vitro* transcorneal permeability studies were carried out using corneas of New Zealand albino rabbits (isolated from whole eye globes) delivered overnight on wet ice in Hanks Balanced Salt Solution from Pel-Freez Biologicals® (Rogers, AK). The tissues were used on the day of receipt [139].

3.2.2. Animals

Male New Zealand albino Rabbits (2-2.5 kg) were procured from Harlan laboratories® (Indianapolis, IN). All animal experiments conformed to the tenets of the Association for Research in Vision and Ophthalmology statement on the Use of Animals in Ophthalmic and Vision Research and followed the University of Mississippi Institutional Animal Care and Use Committee approved protocols.

3.2.3. Synthesis and characterization of Δ^9-Tetrahydrocannabinol Prodrugs

THC-Val, THC-Val-Val and THC-Val-HS were synthesized as per previously established protocols [140]. The final product was purified using column chromatography and characterized by mass spectroscopy in the positive ionization mode. Identity and purity of the synthesized prodrugs was established by spectral means including 1H-NMR, 13C-NMR and 2D-NMR such as correlation spectroscopy (COSY), Heteronuclear single-quantum correlation spectroscopy (HMQC), Heteronuclear multiple-bond correlation spectroscopy (HMBC), as well as other spectroscopic means as reported earlier [140].

3.2.4. Stability of THC-Val-HS in Ocular Tissue Homogenates

3.2.4.a. Tissue Preparation

Aqueous humor and vitreous humor was used as such. Retina choroid and iris ciliary bodies used in this study were homogenized in ice cold IPBS, on an ice bath, using TISSUEMISER (Fisher Scientific, St Louis, USA). The homogenate was then centrifuged at 13000 rpm at 4 °C for 15 min. Protein content in the supernatant was determined according to the method of Bradford [103] and were standardized to 1 mg/mL approximately.

3.2.4.b. Hydrolysis Procedure

The tissue homogenates were equilibrated for 30 min at 37 °C to activate the enzymes. To 1.9 mL of the supernatant, 100 µL of THC-Val-HS (2 mg/mL) in ethanol was added and mixed. Hundred microliters of samples were withdrawn at specific time intervals up to 6 h post initiation. An equal volume of ice cold acetonitrile was added to the samples, to arrest the reaction, and centrifuged at 13,000 rpm for 15 min. The supernatant was collected and analyzed using HPLC-UV method described under section Analytical Method for *In vitro* Studies.

3.2.5. Formulations

An accurately weighed amount of THC and/or the prodrug was dissolved in light mineral oil, NF, to prepare the mineral oil based formulation. Emulsion-1 (THC) formulations were prepared according to previously published protocols [141]. Tocrisolve™ emulsion formulations were prepared by dispersing known amount of THC or prodrug in the emulsion and sonicating for 30 sec followed by stirring for 2 min. Micellar solutions were prepared by dissolving the drug/prodrug in HPβCD solution in IPBS (pH; 7.4) for 24 h and adding Cremophor® RH 40 in it and mixing for 2 min. Weighed amounts of BAK and EDTA were also added and the final volume

was made up with IPBS (pH: 7.4). All the formulations used for the IOP efficacy studies are listed

under **table 3.1.**

Table 3.1: THC, THC-Val-HS, Timolol maleate and pilocarpine HCl formulations used for *in vivo* efficacy studies in alpha chymotrypsin induced rabbit glaucoma model.

Ingredients	THC	THC-Val-HS		Timolol maleate	Pilocarpine HCl
(%w/v)	Tocrisolve Emulsion	Tocrisolve Emulsion	Micellar solution	Aqueous solution	Aqueous solution
Drug/Drug canditate	0.37 (THC)	0.6 (THC equivalent)	0.55 (THC equivalent)	0.25	2
Soyabean oil	14	14	-	-	-
Oleic acid	6	6	-	-	-
Glycerine	2.25	2.25	-	-	-
Poloxamer 188	2	2	-	-	-
Lipoid E 80	1	1	-	-	-
α-tocopherol	0.02	0.02	-	-	-
Cremophor® RH 40	-	-	0.25	-	-
HBβCD	-	-	15	-	-
HPMC	-	-	0.5	-	X
BAK	-	-	0.02	0.01	-
EDTA	-	-	0.1	-	X
NaH$_2$PO$_4$	-	-	-	X	X
Na$_2$HPO$_4$	-	-	-	X	X

HPβCD: (2-Hydroxypropyl)-β-cyclodextrin, HPMC: Hydroxypropyl methyl cellulose, BAK: Benzalkonium chloride, EDTA: Ethylenediamine tetra acetic acid, Na$_2$HPO$_4$: Dibasic sodium phosphate and NaH$_2$PO$_4$: Monobasic sodium phosphate.

3.2.6. Efficacy studies

Open angle glaucoma was induced in New Zealand white rabbits (weighing about 2-2.5 kg). Rabbits were anesthetized by intramuscular injection of Xylazine (3.5 mg/ kg), and Ketamine (35 mg/kg). Chronic open ocular glaucoma was induced by a single posterior injection of alpha-chymotrypsin (20 mg/mL, 50 µL) into the vitreal cavity [142, 143]. Care was taken to avoid the

contact of alpha-chymotrypsin with the surface of the eye. Daily ocular examination was conducted for a few days. Following the intravitreal injection, one drop each of ciprofloxacin, dexamethasone and diclofenac sodium ophthalmic solutions were instilled for about 5 days to prevent topical inflammation. When the elevating IOP was stabilized to 30 ± 3 mmHg (approximately 14 days post-intravitreal injection of alpha-chymotrypsin) for three successive days, the IOP lowering efficacy studies were initiated.

For IOP lowering studies, about 50 µL of each formulation was instilled into the lower *cul de sac* of the left eye of the rabbits (n = 3), while the right eye served as control. Immediately after instillation the eye lid was closed for 10 seconds in order to avoid spillage of the preparation. IOP was measured before instillation (baseline IOP) and every 30 min post instillation till the IOP returned to 90% of baseline IOP using Tonovet® tonometer (Reichert Inc.). As a result of alpha chymotrypsin, corneal surface of the eye was very flaccid compared to the normal eye. So the during the IOP measurement in the glaucomatous eye, tonometer applied with slight pressure. Each value is an average of five concurrent measurements, in triplicates, at each time point for each animal. Same measurement steps were followed during each time point of the study. The IOP determined at each point is reported as the percent baseline IOP ($\pm$ SEM) i.e. (measured IOP/baseline IOP) x 100.

3.2.7. Cannabinoid Receptor Binding Assay

Cannabinoid receptor binding studies were carried out as per previously reported methods [110, 144] with suitable modifications in order to determine the affinity of the designed prodrug in comparison with CP-55,940, a full agonist of CB1/CB2 receptors and THC, the parent molecule.

3.2.7.1. Cell Culture

HEK293 cells (ATCC, Manassas, VA) were stably transfected via electroporation with full-length human recombinant cDNA (OriGene, Rockville, MD) for cannabinoid receptor subtypes 1 and 2. These cells were maintained at 37°C and 5% CO_2 in a Dulbecco's Modified Eagles' Medium (DMEM) and F-12 HAM nutrient mixture (50/50), supplemented with 2 mM L-glutamine, 10% fetal bovine serum, 1% penicillin− streptomycin, and G418 antibiotic solutions.

3.2.7.2. Membrane Preparation

Membranes were made by washing the cells with cold IPBS. The cells were lysed and scraped in cold Tris-HCl, pH 7.4 and then centrifuged at 5,200 x g for 10 min at 4°C. The supernatant was discarded and the pellet was resuspended in the same buffer and homogenized via Sonic Dismembrator Model 100 (Fisher Scientific, Pittsburgh, PA) for 30 seconds and then centrifuged at 1,000 x g for 10 min at 4°C. The supernatant was saved and the pellet underwent the suspension and homogenization process 2 more times with the same conditions. The supernatants were combined and centrifuged at 23,300 x g for 40 minutes at 4°C. The pellet was re-suspended in cold Tris-HCl buffer, aliquoted into 2mL vials and stored at -80°C. The total protein concentration was determined using a Pierce BCA Protein Assay Kit (Thermo Scientific, Rockford, IL) using to manufactures instructions.

3.2.7.3. Method for Cannabinoid Receptor Binding Assay

For each assay, non-specific binding was determined using 10μM of CP-55,940 as a positive control and total binding was ascertained with 0.1% DMSO in Tris-EDTA buffer. Each test well contained 50μL of radioligand ([3H]-CP-55,940), 50μL of compounds, control or vehicle and 100μL cell membrane. The assays were incubated for 90 minutes at 37°C with gentle agitation. The reaction was terminated via rapid filtration with cold Tris-HCl with 0.1% BSA through a

UniFilter GF/C 96-well plate pre-soaked with 0.5% PEI. When the filters were dry, 25μL MicroScint-20 was applied to each filter and the plates were read on a TopCount NXT HTS Microplate Scintillation Counter (PerkinElmer, Waltham, MA) where the counts per minute (CPM) were recorded.

The K_d for the radioligand for each receptor was established through a membrane evaluation and saturation binding experiment. For the membrane evaluation experiment 1-10 μg of membrane was incubated with 1 nM of [3H]-CP-55,940. For the saturation assay, the optimal membrane concentration and 0-10 nM of [3H]-CP-55,940 was incubated with 10 μM of a non-labeled CP-55,940 or 0.1% DMSO in buffer. Data was analyzed by a non-linear curve fit model using GraphPad Prism 5.04 software (GraphPad, La Jolla, CA) and the K_d value was calculated. The competitive binding assay was performed using the optimal concentration of membrane with a radioligand concentration equal to the K_d, and concentrations of each compound ranging from 0.00032-100 μM. Each compound was tested in triplicate. The assays were performed as stated above. The IC_{50} and K_i values were calculated by a non-linear curve fit model using GraphPad Prism 5.0 software.

3.2.8. Data Analysis

Difference in variance between the groups was checked with Levenes test before carrying out ANOVA. Statistical significant difference among multiple groups was checked using one way ANOVA. Tukey's Honestly Significant test was carried out to differentiate between the groups. A p value less than 0.05 was considered to be statistically significant.

3.3. RESULTS

3.3.1. Preformulation studies

The predicted physicochemical properties of THC-Val-HS, THC-Val and THC-Val-Val,

Table 3.2: Comparison of the predicted physicochemical properties of the dicarboxylic acid ester and Amino Acid-dicarboxylic acid ester THC Prodrugs, using ACD/I-Lab 2.0.

Prodrug	ACD I-Lab 2.0 Predicted Values				
	Molecular Weight	pKa	logP	logD (pH 7.4)	Polar Surface Area
THC	314.2	9.6 ± 0.6	7.68 ± 0.4	7.07	29.46
THC-HG	428.26	4.6	7.77	4.66	72.3
THC-Val	413.6	7.5 ± 0.3	6.7 ± 0.4	6.3	61.6
THC-Val-Val	512.7	8.2 ± 0.3 / 13.4 ± 0.5	7.4 ± 0.6	5.9	90.7
THC-Val-HS	513.6	4.53 ± 0.1 / 13.3 ± 0.5	7.65 ± 0.5	3.97	101.13

as well as THC and THC-HG have been depicted in **Table 3.2**. Considering the critical physicochemical properties, THC-Val-HS was expected to be relatively more hydrophilic with improved $LogD_{pH\ 7.4}$ and higher polar surface area, compared to the other prodrugs.

3.3.2. Stability of THC-Val-HS in Ocular Tissue Homogenates

Apparent first order degradation rate constants and half-life of THC-Val-HS in aqueous humor, vitreous humor iris ciliary bodies and retina-choroid homogenates have been depicted in **Table 3.3**. THC-Val-HS was rapidly converted to THC in the ocular tissues ($t_{1/2}$: 46.4 ± 3.1 and 39.2 ± 10.3 min, respectively).

Table 3.3: Apparent first order rate constants (k*) and half-lives (t1/2) of THC-Val-HS in ocular tissue homogenates. Results are depicted as mean ± SD.

Tissue	Protein concentration (mg/mL)	k (min^{-1})	$t_{1/2}$ (min)
Aqueous humor	1.0 (diluted)	0.0105 ± 0.0005	66.2 ± 3.2
Vitreous humor	1.05 (undiluted)	0.015 ± 0.001	46.4 ± 3.1
Iris ciliary bodies	1.02	0.019 ± 0.005	39.2 ± 10.3
Retina-choroid	0.8	0.009 ± 0.003	86.2 ± 26.9

3.3.3. Efficacy studies

THC lowered IOP in the glaucoma model, but not in the normotensive rabbits, in a dose dependent manner **(Fig.3.2)**. The maximum percent drop in the IOP from the baseline IOP (ΔIOP_{max}) and time for peak IOP reduction (T_{max}), both varied depending on the THC dose. With a 0.5% w/v THC
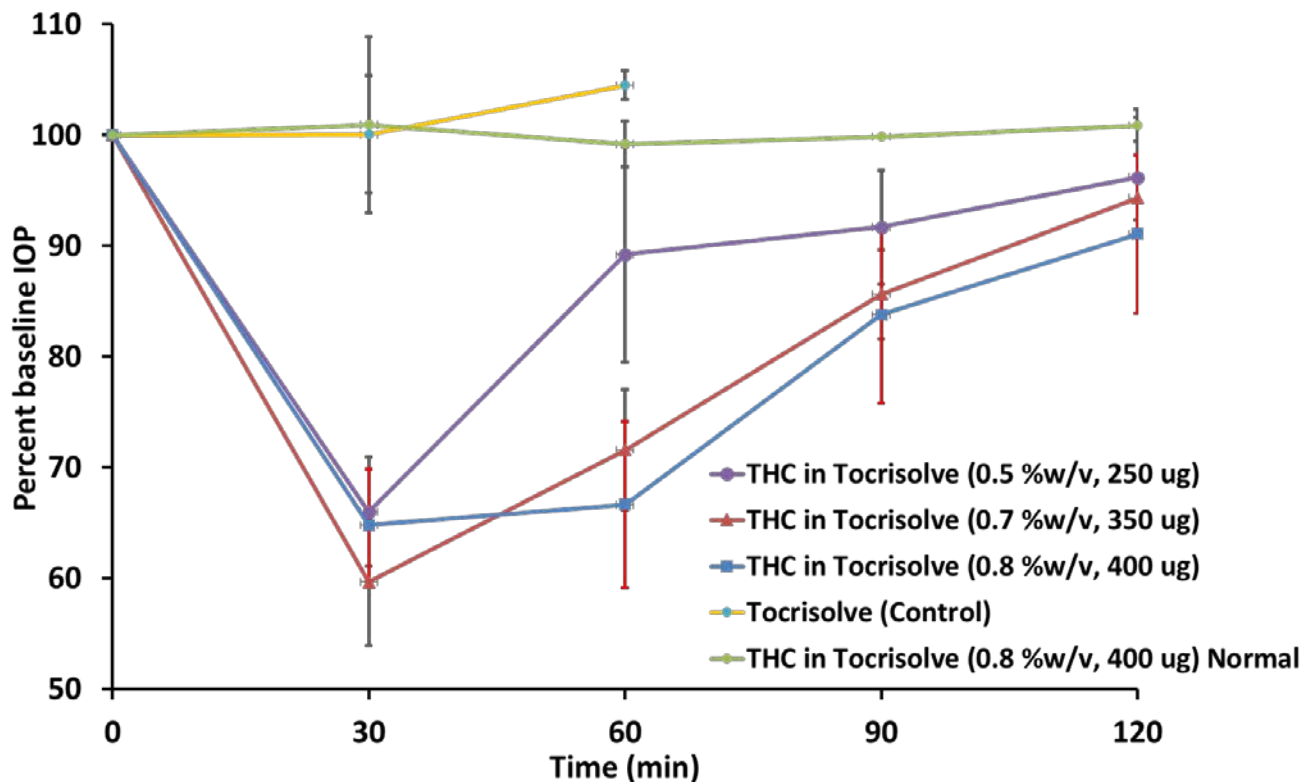
Figure 3.2: IOP-Time profile for THC in normotensive and α-chymotrypsin induced rabbit glaucoma model. Data represents Mean ± SEM. Numbers in brackets represent concentration and dose of THC.

in Tocrisolve™ formulation, IOP was 66.0 % of the baseline (at 30 min) and rapidly started

returning back to baseline IOP, reaching 89.2 % (at 60 min). The short duration of action observed with THC could be due to poor penetration and rapid elimination of THC from the eye. With a 0.7% THC concentration, a slightly prolonged duration in IOP lowering activity was observed. THC (0.8 %w/v), demonstrated further improvement in IOP reduction. The percent baseline IOP was 64.8% at 30 min and 66.6% at 60 min. IOP started reverting back to baseline after 60 min, reaching 83.7% and 91.0% at 90 min and 120 min, respectively. Tocrisolve™ did not show any effect on IOP.
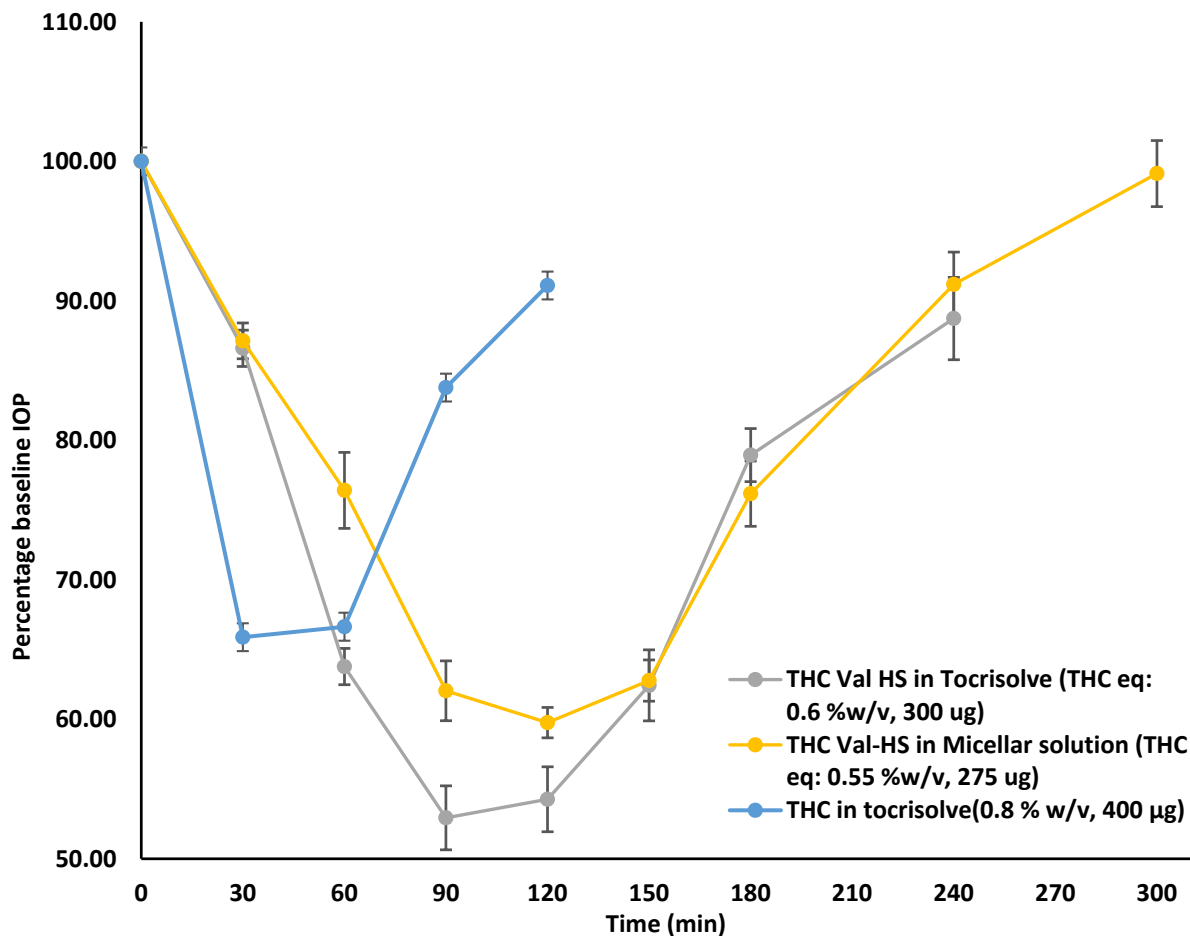
Figure 3.3: IOP-Time profile for THC-Val-HS in comparison with THC in rabbit glaucoma model. Data represents Mean ± SEM. Numbers in brackets represent concentration and dose of THC.

With THC-Val-HS emulsion and micellar solution formulations, an improved IOP lowering activity was observed **(Fig.3.3).** At a THC equivalent dose of 0.6 % w/v (THC-Val-HS: 0.99 %w/v) improved IOP lowering activity, compared to THC, was seen. Though the onset of action was delayed, due to slower bioconversion of the prodrug into THC, the duration of action was prolonged. The maximum percent change in IOP from the baseline was observed to be at 90 min and was maintained till the 120 min time point and reverted back to the baseline IOP by the end of 240 min. The overall IOP lowering profile was more profound compared to THC, even at a lower THC dose. THC-Val-HS formulated in the cyclodextrin + surfactant solution, also showed improved IOP lowering activity (THC equivalent dose: 0.55 % w/v). Although the duration of activity was slightly shorter compared to the emulsion formulation the overall profile remained the same.

Timolol maleate eye drops showed a prolonged IOP lowering activity lasting for about 6h, with a maximum percent IOP change from baseline of 59% (120 min). IOP returned to baseline more slowly showing a longer duration of action. THC-Val-HS was slightly better in IOP lowering compared to Timolol, though the former showed a shorter duration of action. When compared to another marketed anti-glaucoma product, Pilocarpine eye drops, THC-Val-HS showed much improved IOP lowering activity **(Fig.3.4).**
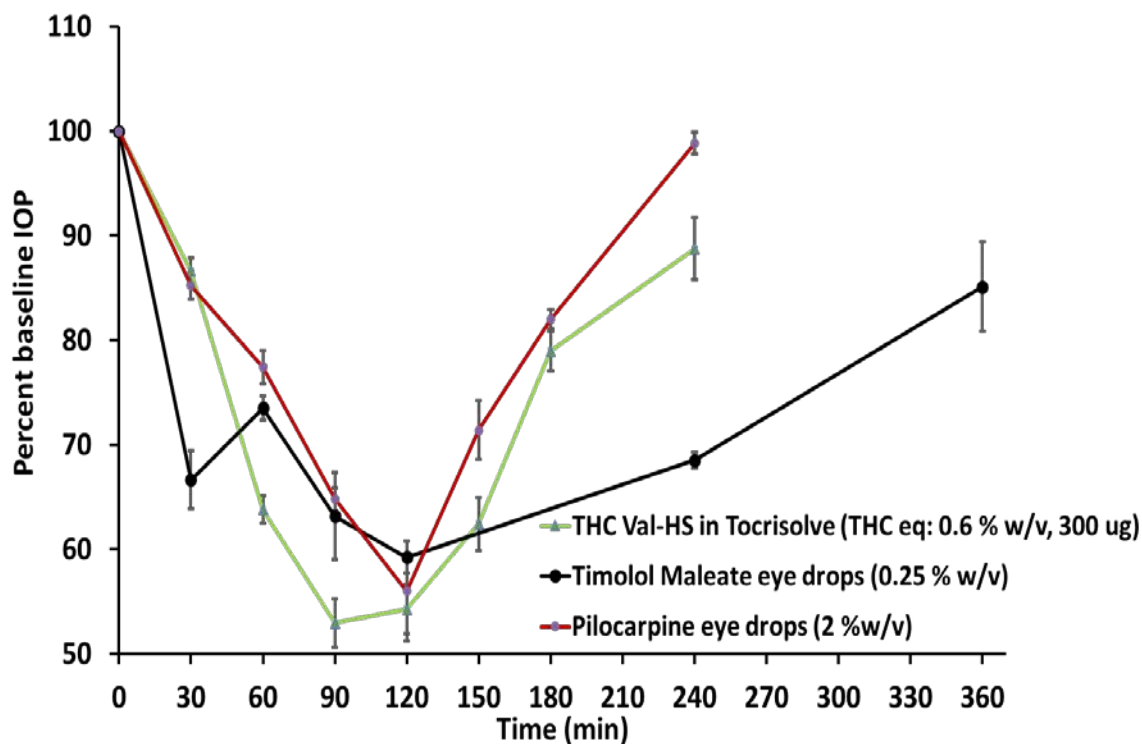
Figure 3.4: IOP-Time profile for THC-Val-HS in comparison with Timolol maleate and Pilocarpine eye drops (marketed) in rabbit glaucoma model. Data represents Mean ± SEM. Numbers in brackets represent concentration and dose.

3.3.4. Receptor binding studies

The receptor binding studies showed that the IC_{50} and K_i for THC-Val-HS was much higher than CP-55,940 and THC for both CB_1 and CB_2 receptors **(Fig.3.5).** The Ki of CB_1 receptors for THC-Val-HS (0.960 ± 0.174 µM) compared to that of CP-55,940 (0.003 ± 0.0 µM) and THC (0.044 ± 0.005) was found to be 320 and 21.8 folds higher respectively, while K_i for CB_2 receptors for THC-Val-HS ($1.2154 \pm 0.0.082$ µM) compared to that of CP-55,940 (0.002 µM) and THC (0.032 ± 0.001) was about 607.5 and 38 folds higher respectively. The IC_{50} values for CB_1 receptors for THC-Val-HS (1.593 ± 0.289 µM) compared to that of CP-55,940 (0.005 ± 0.001 µM) and THC (0.077 ± 0.008) were found to be 318.6 and 20.6 folds higher respectively, while K_i for CB_2 receptors for THC-Val-HS (2.430 ± 0.164 µM) compared to that of CP-55,940 (0.004 ± 0.0

μM) and THC (0.047 ± 0.002) were about 607.5 and 51.7 folds higher respectively. The results suggested that the prodrug (THC-Val-HS) has much lower affinity for the cannabinoid receptors and the pharmacologically inactive *as is*.
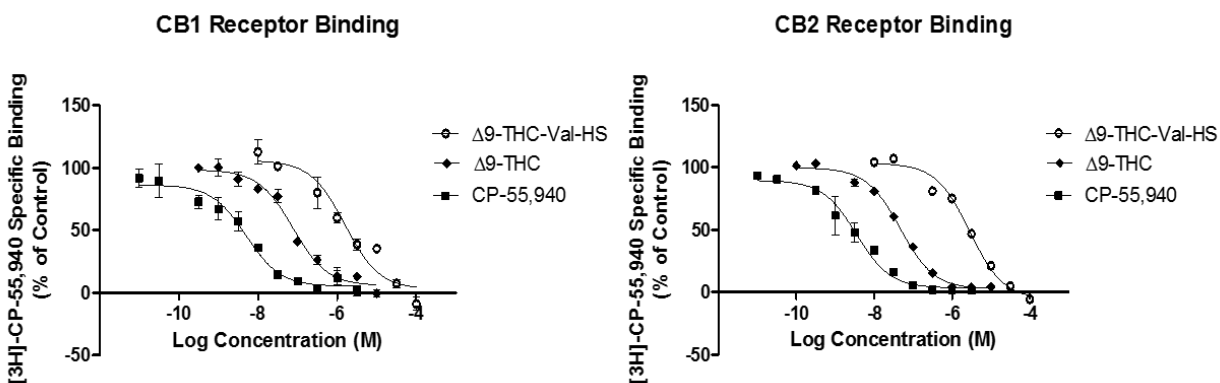
Compound	CB1		CB2	
	IC-50 (μM)	Ki (μM)	IC-50 (μM)	Ki (μM)
Δ9-THC-VAL-HS	1.593 ± 0.289	0.960 ± 0.174	2.430 ± 0.164	1.215 ± 0.082
Δ9-THC	0.077 ± 0.008	0.044 ± 0.005	0.047 ± 0.002	0.032 ± 0.001
CP-55,940	0.005 ± 0.001	0.003 ± 0.000	0.004 ± 0.000	0.002 ± 0.000

Figure 3.5: Cannabinoid receptor (CB1 and CB2) binding studies of THC-Val-HS, THC and CP-55,940.

3.4. DISCUSSION

We previously reported that 1 hour post topical instillation of THC eye drops, formulated in light mineral oil, nanoemulsion or micellar solutions, THC levels in the deeper ocular tissues such as the aqueous humor, iris-ciliary bodies, vitreous humor and retina choroid of anesthetized rabbits, could not be detected by the analytical method used [79]. A hydrophilic THC ester prodrug, THC-HG, formulated as an ion-pair, significantly increased ocular tissue concentrations in anesthetized rabbits. THC-HG, however, was not very stable in the formulations tested [141]. Initial studies with several amino acid ester prodrugs suggested that the valine ester prodrug was significantly more stable. This is consistent with previous literature reports [145, 146]. It had also

been suggested that addition of an amide linkage to the ester link enhances the stability of the ester bond [147]. The combination prodrug THC-Val-HS was thus conceived with the expectation that the valine ester would be the most stable and the stability of the ester bond would be enhanced by the amide linkage with the hemisuccinate. The hemisuccinate moiety was selected based on the fact that it would have the minimum chain length while providing enhanced solubility by virtue of ionization at physiological pH. Thus, the overall objective of this study was to evaluate THC-Val-HS, as well as THC-Val and THC-Val-Val, in terms of its *in vivo* IOP lowering activity.

The alpha-chymotrypsin induced rabbit glaucoma model was used to evaluate the *in vivo* IOP lowering activity of THC-Val-HS [142, 143, 148-151]. This model has been widely used to study effect of drug and drug candidates on IOP. In an attempt to increase THC loading, compared to that achieved with the formulations used for the bioavailability studies (**Table 3.1**), Tocrisolve™, a commercially available optimized emulsion, was used which allowed a 0.8 %w/v THC loading. With the THC- Tocrisolve™ emulsion formulation, a dose dependent decrease in IOP was observed. The IOP lowering effect duration was, however, short and IOP returned to the baseline value within 2h. This is consistent with the ocular distribution data obtained with the lower THC doses, showing poor penetration into the intraocular tissues and/or rapid clearance. The results however are different from that reported in an earlier study evaluating the effect of Δ^8-THC on IOP [133]. The authors reported that, 50 µL of a submicron emulsion formulation of 0.4 %w/v Δ^8-THC produced a drop of 10.83 ± 2.04 mm of Hg reduction in IOP in an alpha-chymotrypsin induced rabbit model of ocular hypertension. Moreover, the drop in IOP lasted upto 8 h in the animal model.

THC did not show any effect on IOP in normotensive rabbits, suggesting an unique mode of action and requires further investigation [152]. Muchtar et al also reported that the drop in IOP

in normotensive rabbits with the submicron emulsion formulation was not significant to that observed in hypertensive model [133]. Crandall et al, reported that even systemic administration of THC (5 mg/kg body weight) did not show any drop in normotensive control eye compared to hypertensive eye (approximately 6 mm of Hg drop) [123].

For THC-Val-HS also the formulations employed in the ocular disposition could dissolve only upto 0.25 %w/v THC, which was significantly lower than the THC dose in Tocrisolve™. Thus, a new formulation was prepared combining HPβCD (15 %w/v) and Cremophor® RH 40 (0.25 %w/v) as the solubilizers, which increased the drug loading to 0.55 %w/v THC equivalent (THC-Val-HS: 0.9 %w/v). Tocrisolve™ emulsion could load 0.6 % w/v THC equivalent (THC-Val-HS: 0.99 %w/v). Both formulations were used to evaluate the effect of THC-Val-HS on IOP.

THC-Val-HS, administered topically to the alpha-chymotrypsin induced high IOP rabbits, displayed a gradual onset of IOP lowering effect and a longer time to achieve maximum effect, in comparison to THC. THC-Val-HS exhibited a much longer duration of activity, up to 4h, even at a lower THC equivalent dose. The significantly increased duration observed with THC-Val-HS could be due to increased penetration of the prodrug into the inner ocular tissues (as seen in the ocular distribution studies) and, thus, availability of higher amounts of THC at the target tissues. The more gradual achievement of peak IOP reduction could be because of the need for regeneration of THC, from the prodrug, in the ocular tissues (**Table 3.3**). Though both Tocrisolve™ emulsion and micellar solution-2 were similar in IOP reduction profile, the former was slightly more efficacious than the latter.

When compared to Pilocarpine HCl and Timolol maleate marketed eye drops, the IOP lowering action of THC-Val-HS was equivalent to that of Pilocarpine with equal intensity (if not more) and duration of action. Timolol maleate eye drops exhibited a prolonged IOP lowering

activity compared to THC-Val-HS emulsions; however, the latter was more intense in terms of maximum IOP reduction. The IOP lowering profiles observed for pilocarpine and timolol was similar to that reported in earlier studies [153, 154].

The receptor binding studies demonstrated that the THC Val-HS did not have significant affinity for both CB1 and CB2 receptors. This indicates that the cannabinoid receptor mediated action is solely dependent THC and that THC-Val-HS does not act as a THC analog. This is consistent with the gradual IOP lowering profile and the delayed maximum drop in IOP seen with THC-Val-HS as a result of dependence on THC regeneration.

Thus, the present study demonstrates that a rational combination of prodrug design and formulation strategy can effectively deliver THC to the anterior chamber of the eye. An increased IOP reduction with the prodrug at lower equivalent doses of THC, supports improved ocular penetration of the prodrug. Importantly, with most of the conventionally developed anti-glaucoma drugs having no reported neuroprotective action, THC, an established neuroprotectant, has the potential to become an effective glaucoma medication. Further studies are currently aimed at developing and optimizing various formulations with improved THC delivery to the back-of-the eye.

CHAPTER 4

EFFECT OF CYCLODEXTRINS ON MORPHOLOGY AND BARRIER

CHARACTERISTICS OF ISOLATED RABBIT CORNEAS

CHAPTER 4

4.1. INTRODUCTION:

Cyclodextrins (CD's) are a group of cyclic oligosaccharides with a hydrophobic inner core and a hydrophilic outer surface. Based on the number of glucopyranose units in the structure, they are classified into alpha (α), beta (β) and gamma (γ) CD's (6, 7 and 8 units respectively). Over the last few decades, CD's have emerged as an important pharmaceutical excipient for solubility enhancement of lipophilic drugs and permeability improvement across biological membranes [155]. CD's act as penetration enhancers by increasing the availability of drug molecules at the surface of the biological membrane barrier. Because of their aqueous solubility improving characteristics, suitable cavity size and drug complexation efficiency [155], beta-cyclodextrins (βCD's; **Fig.4.1A**) such as hydroxypropyl beta cyclodextrin (HPβCD; **Fig.4.1B**) and randomly methylated beta cyclodextrin (RMβCD; **Fig.4.1C**) are widely used in the field of formulation and drug delivery.

It is only recently that the mechanism of permeability enhancement across biological membranes, such as skin, buccal mucosa and cornea, have been discussed. CD's interact with cholesterol present in the phospholipid monolayers of the cell membranes, thus exchanging them with the drugs/drug candidates held in the hydrophobic CD core (**Fig.4.5**). In addition to their utility as transcorneal permeability enhancers, by virtue of their ability to extract lipophilic components like cholesterol and phospholipids from the corneal membrane [156], CD's are often added to the receiver solutions to maintain sink conditions during *in vitro* transcorneal permeability

65

studies of lipophilic molecules [157]. Unknowingly damaging the cornea (epithelium, stroma lamellae or endothelium), however, may lead to altered permeability of the drug/drug candidates as a result of the receiver solution characteristics rather than formulation or drug/prodrug candidate properties. This can lead to misinterpretation of the results and overestimation of the permeability enhancement of the formulation/drug candidate if
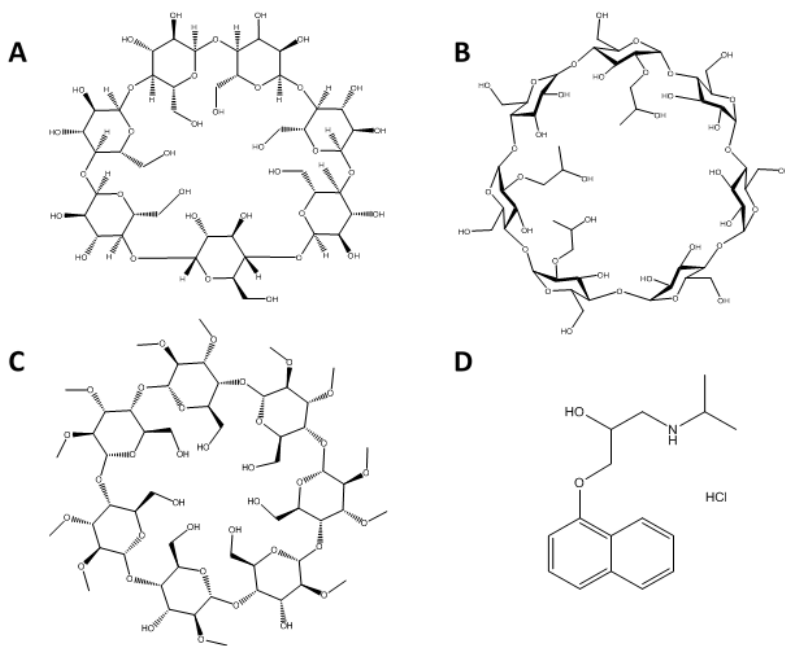
Figure 4.1: Chemical structure of A) General structure of beta cyclodextrin (β-CD), B) Hydroxypropyl-βeta-cyclodextrin (HPβCD), C) Randomly methylated-βeta-cyclodextrin (RMβCD) and D) Propranolol (PHCl).

adequate controls were not included in the experiment design. Thus, an understanding of the effect of CDs on the corneal permeability characteristics, when added as a solubilizer in the receiver solution, is very important and has not been analyzed as yet. The aim of the present study is to evaluate the effect of CD concentration, duration and type on the morphological characteristics and barrier properties, using propranolol hydrochloride (PHCl; **Fig.4.1D**) as a paracellular diffusion marker, of isolated rabbit cornea *in vitro*.

4.2. Methods:

4.2.1. Phase solubility studies:

Complexation of PHCl with HPβCD and RMβCD was evaluated using phase-solubility studies according to the method of Higuchi and Connors [158]. Excess amount of PHCl was added

to 1 mL IPBS, containing increasing concentrations of CDs. The concentrations ranged from 2.5 -

10 %w/v. The resulting suspensions were shaken at 25°C for 24 h in a reciprocating water bath.

Following equilibration, the suspensions were centrifuged at 13,000 rpm for 20 min at 25°C and

the supernatant thus obtained was analyzed using an HPLC-UV method [159].

Phase-solubility profile was obtained by plotting the solubility of PHCl against the

concentration of CD's used. The binding constants ($K_{1:1}$) and complexation efficiencies (CE) for

the PHCl-CD complex were calculated from the linear region of the solubility curves using

Equation 1 & 2:

$$K_{1:1} = \frac{Slope}{S_o(1-Slope)} \quad \text{Eq (1)}$$

$$CE = K_{1:1} \: x \: S_o = \frac{Slope}{(1-Slope)} \quad \text{Eq (2)}$$

Where $K_{1:1}$ is the binding constant, S_o is the saturation concentration of PHCl in water, and slope

denotes the slope of the straight line.

4.2.2. *In vitro* transcorneal permeability:

A series of *in vitro* transcorneal permeability studies were carried out using 9 mm side-by-

side diffusion apparatus (PermeGear Inc., Hellertown, PA). Freshly excised rabbit whole eye

globes received from Pel-Freez Biologicals® were used for these studies. Briefly, corneas were

excised by making a brief incision, about 2 mm from the corneal-scleral junction and cutting

radially along the sclera. The excised corneas were immediately mounted between the diffusion

cells. The half-cell facing the epithelial layer was termed as the donor compartment and the other

half towards the endothelium was termed as receiver chamber. The nomenclature is based on the

addition of PHCl to the epithelial side half-cell. A circulating water bath was used to maintain the

temperature at 34 °C during the transport studies.

In vitro transcorneal permeability studies were carried out with 2.5 and 5 %w/v HPβCD and RMβCD in IPBS (pH 7.4) for 1 or 3h at 34 °C. PHCl (1 mg/mL) was used as the paracellular marker (PHCl; pKa = 9.4). PHCl solution was always added on the donor side. Permeation studies were performed with IPBS as control; with CD's on donor side only, CD's on receiver side only and CD's on both donor and receiver sides as represented in **Table 4.1**. Aliquots, 600 µL, were withdrawn at predetermined time points for 1 or 3 h and replaced with an equal volume of the receiver solution. Samples were analyzed by HPLC-UV system [159].

4.2.3. Corneal Histology:

Histological evaluation was carried out at Excalibur Pathology Inc. (Oklahoma City, OK). At the end of each study, corneas were fixed in 2 %w/v paraformaldehyde and 2 %v/v gluteraldehyde in IPBS. Corneas embedded in paraffin were sliced into 5 µm cross sections using a microtome (American Optical® 820 Rotary Microtome). These sections were mounted on a slide and dried overnight in an oven. The slide was washed with xylene to remove paraffin and washed with alcohol and water to hydrate the tissue. This was then stained with nuclear dye Gill III hematoxylin (StatLab medical) for 10 min and rinsed, and then counterstained with eosin. These slides were then washed in reverse manner (running water, alcohol, and xylene), cover slipped and examined under microscope (Chromavision ACIS II).

4.3. Results:

4.3.1. Phase solubility studies:

Binding constants of PHCl with HPβCD and RMβCD were very low (278.1 and 326.4 µM⁻¹ respectively). Complexation efficiency of PHCl with HPβCD and RMβCD were 0.94 and 1.1 respectively. RMβCD was observed to have slightly higher CE with PHCl than HPβCD. Low

binding constant values demonstrate that only a low fraction of PHCl was bound to either of the CDs and that there was more free concentrations of CDs and PHCl in the solution.

4.3.2. CDs on receiver side:

With 5 %w/v HPβCD and RMβCD on the receiver side permeability coefficient of PHCl at the end of 1 h was found to be 40.8 ± 5.7 x 10^{-6} cm/sec and 52.1 ± 8.4 x 10^{-6} cm/sec respectively (1.5-fold and 1.9-fold higher than the control) (**Table 4.1** and **Fig.4.2**). Similar results were

Table 4.1: *In vitro* transcorneal permeability coefficients of PHCl at different concentrations of CD's. I) IPBS without CD's (control; 1), II) CD's in donor solution (3 & 6), III) CD's in receiver solution (2 & 5) and IV) CD's in both donor and receiver solutions (4 & 7). Experiments were carried out for 1 h or 3 h. * - Experiments were carried out for 1 h and 3 h. Permeability coefficients were calculated only for 1 h experiment.

S. No	DONOR	RECIEVER
	3ml	3.2ml
1	IPBS	IPBS
2	IPBS	HPβCD
3	HPβCD	IPBS
4*	HPβCD	HPβCD
5	IPBS	RMβCD
6	RMβCD	IPBS
7*	RMβCD	RMβCD

encountered with the use of 2.5% w/v HPβCD and RMβCD on the receiver side at the end of 1h (32.2 ± 4.9 x 10^{-6} cm/sec and 41.3 ± 6.6 x 10^{-6} cm/sec respectively).

Histological studies at the end of 1 h, revealed damage to both endothelium and epithelium in case of 5 %w/v HPβCD on the receiver side. Stroma lamellae were found to be disrupted at several points on the cornea. When 5% w/v RMβCD was used on the receiver side less damage was caused to the epithelium, and little or no damage to the endothelium was observed. HPβCD at 2.5% w/v caused significant rupture of the corneal epithelium, but the endothelium was found to

be intact. At the same concentration, RMβCD showed little damage to the epithelium and none to the endothelium. These studies revealed that more damage was caused when HPβCD is used in the receiver solution in comparison to RMβCD (both 5% w/v and 2.5% w/v) (**Fig.4.3 & 4.4**).
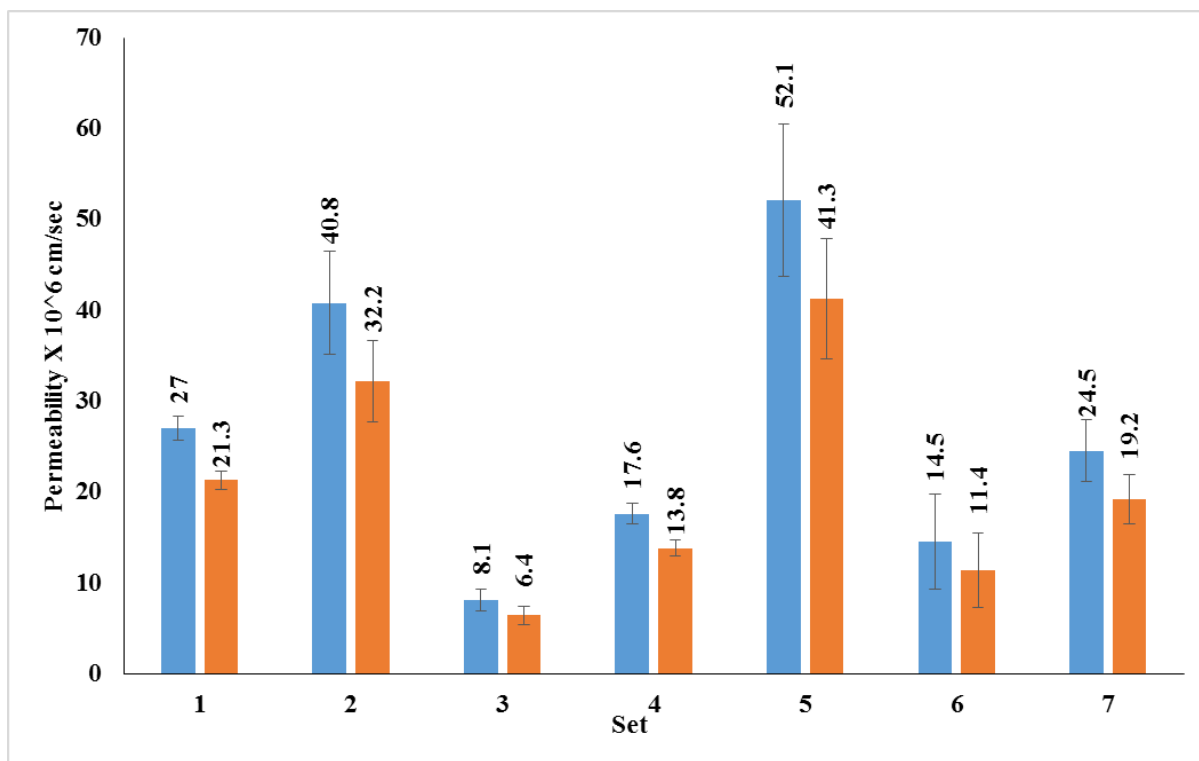
Figure 4.2: *In vitro* transcorneal permeability coefficients of PHCl at different concentrations of CD's. I) IPBS without CD's (control; 1), II) CD's in donor solution (3 & 6), III) CD's in receiver solution (2 & 5) and IV) CD's in both donor and receiver solutions (4 & 7).

4.3.3. CDs on donor side:

The permeability coefficients of PHCl at the end of 1 h with 5 %w/v HPβCD and RMβCD were found to be 8.1 ± 1.2 x 10^{-6} cm/sec and 14.5 ± 5.2 x 10^{-6} cm/sec. Permeability coefficient of PHCl in IPBS (control) was found to be 27.02 ± 1.2 x 10^{-6} cm/sec. Permeability coefficients of PHCl were also observed to be lower than the control in case of 2.5% w/v HPβCD and RMβCD (**Table 4.1** and **Fig.4.2**).

Histological studies revealed rupture of the corneal epithelium with the use of 5% w/v and 2.5% w/v HPβCD in the donor solution. With 5% w/v and 2.5% w/v RMβCD on the donor side little or no damage was caused to the corneal epithelium. In case of control group, corneal morphology was found to be intact. In all the studies HPβCD and RMβCD in the donor chamber, at the concentrations used, did not cause any damage to the endothelium (**Fig.4.3 & 4.4**).
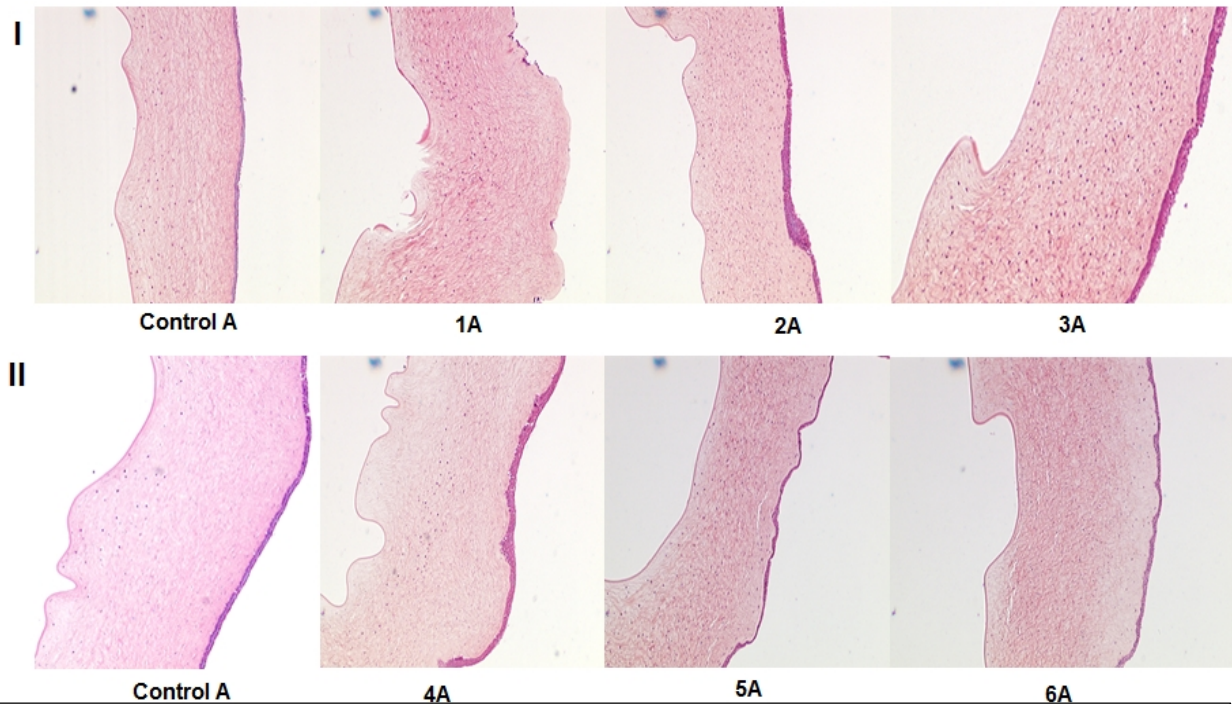
Figure 4.3: Hematoxylin-eosin stained corneal cross-sections 1 h post exposure to 1) IPBS: control A, 1A) 5% w/v HPβCD in receiver solution, 2A) 5% w/v HPβCD in donor solution, 3A) 5% w/v HPβCD in receiver and donor solutions, 4A) 5% w/v RMβCD in receiver solution, 5A) 5% w/v RMβCD in donor solution and 6A) 5% w/v RMβCD in receiver and donor solutions.
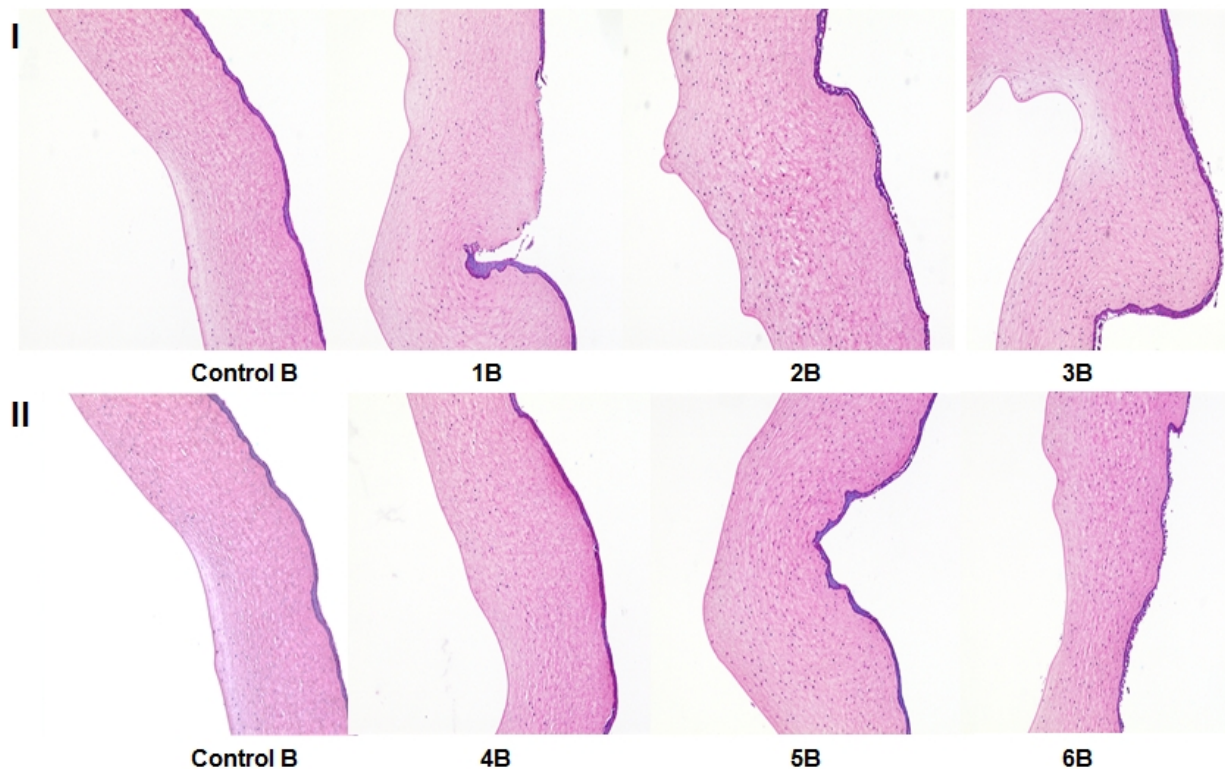
Figure 4.4: Hematoxylin-eosin stained corneal cross-sections 1 h post exposure to 1) IPBS: Control B, 1B) 2.5% w/v HPβCD in receiver solution, 2B) 2.5% w/v HPβCD in donor solution, 3B) 2.5% w/v HPβCD in receiver and donor solutions, 4B) 2.5% w/v RMβCD in receiver solution, 5B) 2.5% w/v RMβCD in donor solution and 6B) 2.5% w/v RMβCD in receiver and donor solutions.

4.3.4. CDs in both donor and receiver chamber:

Surprisingly, use of 5 %w/v and 2.5 %w/v RMβCD in both donor and receiver chambers simultaneously, did not show significant difference compared to the control. Permeability coefficients of PHCl in control, 5 %w/v HPβCD and 5 %w/v RMβCD solutions on the donor and the receiver sides were observed to be $27.0 \pm 1.3 \times 10^{-6}$ cm/sec, $17.6 \pm 1.1 \times 10^{-6}$ cm/sec and $24.5 \pm 3.4 \times 10^{-6}$ cm/sec respectively. Permeability coefficients of PHCl in control, 2.5 %w/v HPβCD and 2.5 %w/v RMβCD solutions on the donor and the receiver sides were observed to be $21.3 \pm$

1.03×10^{-6} cm/sec, $13.8 \pm 0.9 \times 10^{-6}$ cm/sec and $19.2 \pm 2.7 \times 10^{-6}$ cm/sec respectively. On an average, a 20% drop in the permeability was observed as a function of 50% drop in CD concentrations.

No damage was observed to the corneal epithelia with 5% w/v and 2.5% w/v RMβCD. At the end of 1h, when 5% w/v and 2.5% w/v HPβCD solution was used in both donor and receiver chambers, the corneal epithelia were found to be damaged. In all cases endothelia was found to be intact without any significant damage compared to the control (**Fig.4.3 & 4.4**). When corneas were exposed to 2.5% w/v HPβCD on both sides for 3h, complete erosion of the epithelium was observed, exposing the stroma. But no significant damage to the endothelium was noted (**Fig.4.5**).
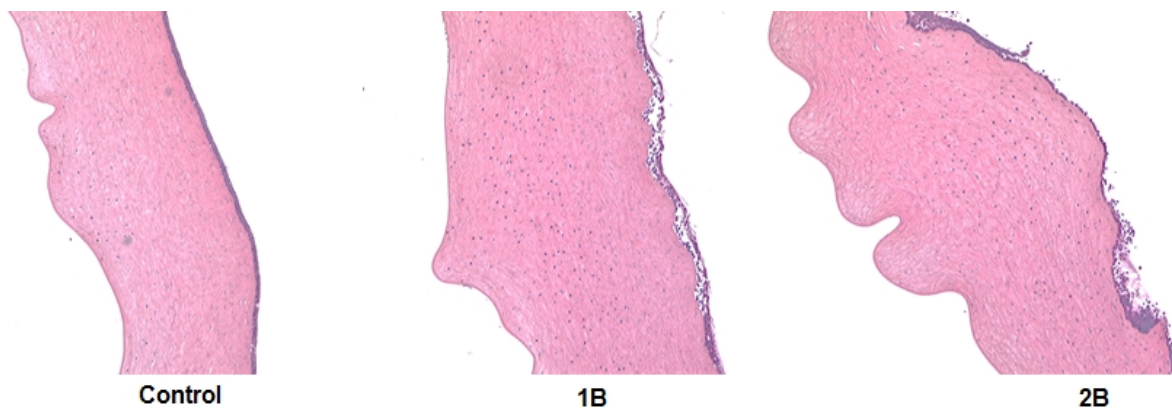
Figure 4.5: Hematoxylin-eosin stained corneal cross-sections 3 h post exposure to 1) IPBS: control, 1B) 2.5% w/v HPβCD in receiver and donor solutions and 2B) 2.5% w/v RMβCD in receiver and donor solutions.

4.4. Discussion:

CDs have become important pharmaceutical excipients due to their ability to improve solubility of lipophilic molecules and to enhance permeability across biological membranes. It is considered that CD's increase permeability across biological membranes through their surface activity, membrane partitioning and cholesterol extraction characteristics [160, 161].

In the present study, we used rabbit corneas because of their similarities to human corneal ultra-structure [162] and common use in *in vitro* studies evaluating corneal drug penetration. We selected HPβCD and RMβCD because of their widespread use in the ocular formulations and permeability studies. Permeability coefficients of PHCl were in the order of CD's on receiver side > control > CD's on both sides > CD's on donor side. Corneal histology revealed the damage to
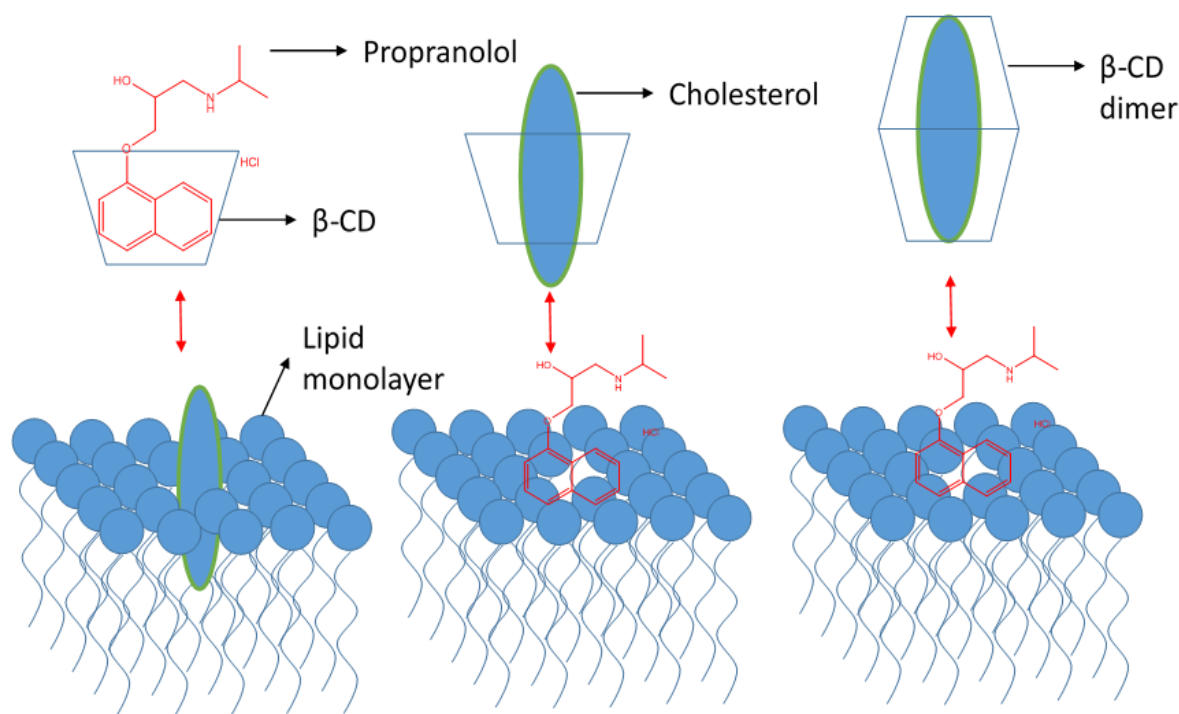
Figure 4.6: Extraction of cholesterol and the exchange of active moiety by cyclodextrins from the phospholipid cell membrane.

the membranes in the order of CD's on receiver side > CD's on donor side > CD's on both sides > control. CD's after forming inclusion complexes are known to improve permeability of compounds across the biological membranes. Thus, we observed higher permeability coefficients with the RMβCD-PHCl complex which could be because of the higher CE of PHCl with RMβCD compared to HPβCD.

RMβCD produced less corneal damage than HPβCD. This is in agreement with previous literature reports. Savolainen et al. studied toxicity/irritation caused by CD's on human corneal epithelial cell lines and observed that the cytotoxic effect were in the order of αCD > Dimethyl-βCD >SBEβCD = HPβCD > γCD [163]. In another study, Lopez et al. performed a computational simulation of CD's interacting with cholesterol (**Fig.4.6**) [164]. It was reported that within 10 ns of the initial interaction, CD's orient in a perpendicular direction to the surface of the phospholipid monolayer and the hydroxyl groups of membrane cholesterol penetrate into the inner core of the CD. On an average, rate of extraction of 1 cholesterol molecule per CD was found to be 0.5 µs. Based on the stoichiometric ratios, it was observed that one HPβCD is required to extract one molecule of cholesterol or membrane lipid forming a 1:1 soluble complex [165]. In some cases, two molecules of CD interact with one another in a head-head, head-tail or tail-tail fashion to form a dimer [166]. Both head-tail and tail-tail interactions are less stable than head-head interactions due to their spontaneous dissociation in water. Tsamaloukas et al. reported that extraction of one molecule of cholesterol/membrane lipid requires two molecules of RMβCD stoichiometrically (cholesterol: RMβCD::1:2), since the formation of 1:1 complex is not a spontaneous process [167]. These reports suggest that at a given concentration, number of cholesterol molecules extracted per

RMβCD are less compared to HPβCD. This could probably explain why RMβCD caused less damage to the corneal membranes.

Besides the type of CDs used, the duration of contact and concentration used are other important parameters. Duckner et al. studied the effect of HPβCD concentration on porcine corneal endothelium [168]. It was observed that use of 10 %w/v HPβCD caused high grade of endothelial damage followed by minimal damage with 1 %w/v HPβCD and none with 0.1 %w/v HPβCD within 3 h of the study. Similar observations were recorded in our studies also. In the current report, use of 5 %w/v HPβCD caused severe damage to the corneal epithelium and endothelium layers within 3 h of exposure. Disruptions in the stromal lamellae were also observed when CD's were employed in the receiver media. Damage to the corneal layers was observed to be minimum with the use of 2.5 %w/v CD's. In our study, we observed that 2.5 %w/v RMβCD causes minimal damage compared to HPβCD, but only after 3h of exposure.

In the current study, permeability coefficients of PHCl were found to be higher when CD's were taken on the receiver side rather than on donor side. This was attributed to the fact that corneal endothelium is more permeable when compared to the epithelium [169]. Due to the concentration gradient, CD's incorporated in the receiver side, probably cross the endothelium and stroma and interacts with basal cells and tight junctions of the corneal epithelium; thus causing more damage to the epithelia and endothelia. In contrast, CD's on the donor side are unable to pass through the non-keratinized squamous cells of the epithelia; thus causing less damage to the cornea. When CD's were employed on both donor and receiver side, due to the absence of net concentration gradient, little or no change was observed in the corneal integrity. But prolonged exposure (3 h) to

CD solutions leads to the loss of the ZO-1 initiating significant damage and complete erosion of corneal epithelium. As a result, we observed severe damage of the corneal epithelia after 3 h exposure of the cornea to both HPβCD and RMβCD.

Several studies in the literature, including some from our own laboratory, have used CDs in the receiver solution during *in vitro* transcorneal permeability evaluation [94, 156, 170-173]. In view of the findings from this study, it is apparent that use of CDs as solubilizers in the receiver solution could significantly impact transcorneal flux. Thus, it is very important to understand and use proper controls and experimental design during *in vitro* transcorneal permeability studies using CDs.

4.5.   Conclusion:

The effect of CD's on corneal membrane *in vitro* was observed to be dependent on factors such as type of CD's employed, type of inclusion complex formed, CD concentration and the duration of exposure to the biological membrane. Thus, the use of CD's in *in vitro* transcorneal permeation experiments as solubilizers in the receiving medium, especially when used only on one side of the tissue, needs to be carefully considered to avoid confounding effects in the permeability data obtained due to damage to the corneal ultra-structure.

CHAPTER 5

DICLOFENAC SODIUM AND ION EXCHANGE RESIN COMPLEX LOADED MELT CAST FILMS FOR SUSTAINED RELEASE OCULAR DELIVERY

CHAPTER 5

5.1. INTRODUCTION:

Ion exchange resins (IR) are water insoluble cross linked polymers with ionizable groups that can be exchanged to form complexes [174]. They are differentiated into anionic and cationic exchange resins based on the charge of the exchangeable ionic group [175]. The strong cation exchangers such as Amberlite^{TM} IRP69 contain sulfonic acid functional groups, while the weak cation exchange resins such as Amberlite^{TM} IRP64 and IRP88 contain carboxylic acid functional groups. Similarly anion exchange resins are also divided into strong exchange resins with quaternary ammonium groups attached to the matrix such as Duolite^{TM} AP 143/1083 (**Fig.5.1**) and Amberlite® IRA-410. Weak anion exchangers such as Dowex® WGR-2, Amberlite® IRA-67 have tertiary amine substitutes.

In the past, IR's were used primarily in the field of agriculture and for the purification of water [176]. Application of IR's as excipients in the field of medicine started when synthetic ion-exchange resins were used as taste masking and as stabilizing agents in oral dosage forms [177-180]. Drug-IR complexes show a modified release profiles when compared to the release with the drug [181]. Saunders and Srivatsava studied the complexation efficiencies and release kinetics of alkaloids from IR's and suggested that IR's can be used as suitable carriers for the development of sustained-release formulations [182]. Sriwongjanya and Bodmeier have studied the complexation of propranolol hydrochloride and diclofenac sodium (DFS; **Fig.5.1**) by Amberlite® IRP 69 and

79

Duolite® ATP-143, respectively. These drug IR complexes were loaded in hydroxyl propyl methyl cellulose (HPMC) matrix tablets to slow their release and achieve a sustained release profile [175].

The use of IR's in the field of ophthalmic formulations, however, has been given little interest. In the present study, we are using drug-IR complexes loaded into polymeric melt cast films to deliver DFS into the eye for prolonged periods of time. DFS belongs to the class of drugs known as nonsteroidal anti-inflammatory drugs (NSAIDs) and are used to treat swelling (anterior inflammation) of the eye after cataract surgery [183]. DFS is also used after corneal refractive surgery [184] to temporarily relieve pain and photophobia (sensitivity to light). One drop of the current DFS ophthalmic solution formulation is applied to the affected eye, 4 times daily beginning 24 hours after cataract surgery and continued throughout the first 2 weeks of the postoperative period [185].

Drug delivery to the eye has always been a challenging task due to various ocular physiological and dynamic barriers [99, 186]. Topical ophthalmic solutions have been the most accepted and conventional drug delivery system for treating ocular diseases [186]. However, they present major challenges when it comes to treating chronic issues such as chronic inflammation, dry eye, uveitis, age related macular degeneration, glaucoma and diabetic retinopathy [78, 187]. These diseases require long term therapy and frequent administration of eye drops. Conventional drops only deliver 5-10% of the applied dose into the anterior segment of the eye because of precorneal drainage and other ocular barriers [95, 99]. As a result, the frequency of administration of the eye drops is usually 4-6 times based on the severity of the pathological condition of the anterior segment of the eye. For posterior segment diseases, although intravitreal injections are very successful, they are associated with complications such as pain, infection, endopthalmitis and retinal detachment [187].

Thus, there is an unmet need for novel and efficient delivery strategies to prolong the duration of action of the drug or drug candidates to the eye. Some of these delivery systems include surface functionalized nanoparticles [188, 189], liposomes [190, 191] and matrix films [192-194]. Of all these formulation strategies matrix films are easy to prepare and are also free of any solvents or other additives that might cause unwanted reactions at the site of application.

Thus, the objective of the present study is to develop a sustained release DFS-IR complex (**Fig.5.1**) loaded polymeric matrix film for once or twice a day application based on the severity of the inflammation. Matrix films loaded with free DFS (uncomplexed) or DFS-IR complex or a combination of free and complexed DFS (DFS-IR) in various ratios were examined with respect to their release profiles.
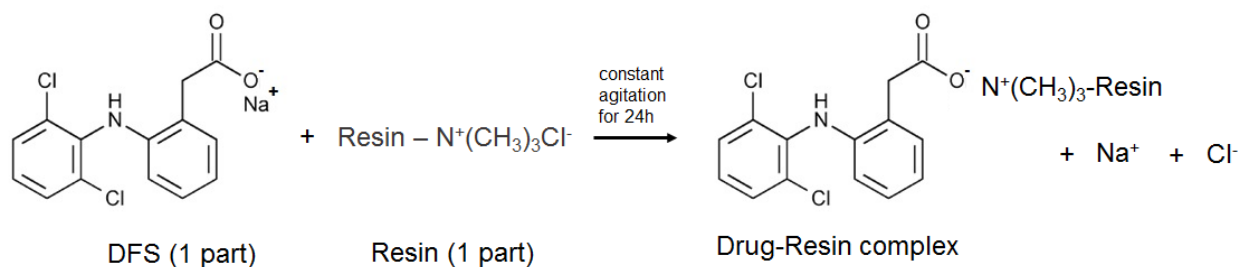
Figure 5.1: Interaction of Diclofenac sodium (DFS) 1 part in solution with 1 part of Duolite[TM] AP 143/1083 (resin). Chloride ion from the resin is exchanged for negatively charged diclofenac in solution to form DFS-IR complex.

5.2. Methods:

5.2.1. Chemicals:

PEO [PolyOx® WSR N-10 (PEO N-10), MW: 100,000 Daltons; PubChem CID: 5327147] and Duolite[TM] AP 143/1083 (Cholestyramine Resin USP; PubChem CID: 70695641) was kindly donated by Dow Chemical Company (Midland, MI). DFS (PubChem CID: 5018304) was purchased from Sigma Aldrich (St. Louis, MO). Pearlitol® 160 C was obtained from Roquette Pharma as gift sample. DFS 0.1% w/v ophthalmic solution was purchased from Akorn

pharmaceuticals Lake Forest, IL. All other chemicals were purchased from Fisher Scientific (St. Louis, MO).

5.2.2. Animal tissues:

Whole eye globes of New Zealand albino rabbits were purchased from Pel-Freez Biologicals® (Rogers, AK), shipped overnight in Hanks Balanced Salt Solution over wet ice [139] and used on the same day of receipt.

5.2.3. Animals:

Male New Zealand albino rabbits (2.0 - 2.5 Kg) procured from Harlan Laboratories® (Indianapolis, IN; now known as Envigo) were used in all the studies. All animal experiments confirmed to the tenets of the Association for Research in Vision and Ophthalmology statement on the Use of Animals in Ophthalmic and Vision Research and followed the University of Mississippi Institutional Animal Care and Use committee approved protocols (UM Protocol # 14-022).

5.2.4 Preparation of DFS-IR complex:

Prior to the complex formation IR's were washed thoroughly with deionized water. To activate the resin, they are washed with chloride and hydroxide forms and rinsed with water again. The drug-resin complexes were formed by batch process [195]. A concentrated aqueous solution of DFS (20 mg/mL) was prepared. To this, accurately weighed amount of resin in three different ratios (DFS:IR = 1:2, 1:1 and 2:1) was added and agitated for 24h. DFS-IR complexes, thus formed were separated by centrifugation, washed with deionized water to remove unbound drug and dried in a desiccator overnight.

Percentage of drug bound was calculated by analyzing the amount of drug remaining in the supernatant liquid using the equation 1:

$$\text{Percentage of bound drug} = \frac{A_1 - A_2}{A_3} \text{x}100 \qquad \text{Eq (1)}$$

Where A_1= amount of DFS in initial aqueous solution (mg)

A_2= amount of DFS in supernatant solution (mg)

A_3= amount of IR in the solution (mg)

To confirm the complexation of DFS with IR, Fourier transmission infrared (FTIR) spectra for IR, DFS and DFS-IR complex were obtained using a Cary 660 series FTIR (Agilent Technologies) and MIRacle™ Single Reflection ATR (PIKE Technologies).

5.2.5. Preparation of polymeric matrix film and IR suspension:

Melt-cast technology was employed in the preparation of the polymeric matrix film. A previously published protocol was used to prepare the films [192]. All matrix films were prepared with 20% w/w drug load. Briefly, DFS and/or DFS-IR complex was mixed with PEO N10 in geometric dilutions to obtain a uniform physical mixture. A 13 mm die was placed over a brass plate and heated to 70 °C using a hot plate. The physical mixture (200 mg) was added in the center of the die and compressed. The mixture was further heated for 2-3 min. After cooling, 4 mm x 2 mm sections, each weighing approximately 8 mg and with a drug load of 1.6 mg, was cut out from the film.

IR suspension was prepared by first dissolving the free DFS part into water (pH 7.2). Then accurately weighed amount of DFS-IR was added to the solution. Mannitol 4.5% w/v (Pearlitol® 160 C) was added as tonicity agent. To this 0.5% HPMC (4000 cps) was added as suspending

agent and kept for stirring until all the HPMC got dissolved. To adjust the pH of the formulation to 7.3, 0.1 N hydrochloric acid or sodium hydroxide was used.

5.2.6. Assay and content uniformity:

To determine the assay and content uniformity of DFS in the film a static assay method was used [195]. A 50:50 mixture of isotonic phosphate buffer saline at pH 7.4 and dimethyl sulfoxide was used. Each film segment of 8 mg was placed in sufficiently large enough quantity of medium (50 mL) to allow for the API to unload from the resin and sonicated for 15 min. This cloudy suspension was kept under constant stirring for 2 h, to allow complete release of the complexed drug, and centrifuged at 13000 rpm for 15 min. The supernatant was filtered through 0.2 μ filter and analyzed for free drug using HPLC-UV method.

5.2.7. *In vitro* release and corneal permeability studies

To study the release profile of DFS from the various formulations Side-A-Lyzer dialysis cassettes (10000 Dalton MWCO) were used. A 20 mL glass vial was filled with 18 mL of release media (IPBS pH 7.34) and a magnetic stirrer was added to maintain equilibrium. Films (20 %w/w loading; Dose: 1.0 mg) loaded with 100% complexed DFS (1:1::DFS:IR) or with 50% un-complexed (free) DFS and 50% complexed DFS (1+1:1) were placed in each dialysis cassette. Hundred microliters of IPBS was added in the dialysis cassette to wet the film. Similarly in three more sets (n=3), 1 mL of 0.1%w/v DFS ophthalmic solution (marketed formulation), 1:1::DFS:IR suspension and 1+1:1::DFS:IR complex in suspension (Dose: 1 mg) was added, to evaluate the effect of the matrix on the release profile. The glass vials were placed over a magnetic plate. The temperature was maintained at 34 ± 2 ºC using calibrated hot plates. Aliquots, 0.8 mL, were collected at specific time intervals and replaced with an equal volume of release media. Studies

were carried out for a period of 24 h. Samples were analyzed using a HPLC-UV method. The results from the studies were fit into Zero order, first order and Huguchi models.

In vitro corneal flux and permeability of DFS from the IR loaded film formulation was evaluated using a side-by-side diffusion apparatus (PermeGear, Inc., Hellertown, PA) for a period of 6 h. The studies were carried out by sandwiching the film (4 mm x 2 mm; 20 %w/w DFS; weighing 8 mg approximately; Dose: 1.6 mg) in between a Spectra/Por® membrane (MWCO: 10,000 Daltons) and isolated rabbit cornea (Pel-Freez Biologicals; Rogers, AK). Corneas were excised from whole eye globes, following previously published protocols [103, 139]. The membrane-film-cornea sandwich was then placed in between the side-by-side diffusion cells (the chamber towards the Spectra/Por® membrane representing the periocular surface and the chamber towards the cornea representing the aqueous humor). In another set up wherein the cornea was mounted in between the two half-cells (membrane was not used in this case), 3 mL of DFS control solution and 1:1::DFS:IR complex suspension was added to the donor chamber. Phosphate buffer was used as receiver media (3.2 mL). The side-by-side diffusion cells maintained at 34 °C using a circulating water bath. Six hundred microliters of sample was collected at specific intervals of time and analyzed using HPLC method.

5.2.9. *In vivo* bioavailability studies

Male New Zealand albino rabbits weighing between 2.0 - 2.5 Kg were used to determine *in vivo* ocular bioavailability of DFS from the topically instilled formulations. Rabbits were kept conscious throughout duration of the study. In these studies, 20 %w/w DFS or DFS-IR loaded films were placed in the conjunctival sac of the rabbit eye (weight 8 mg; dose: 1.6 mg), while 1.6 %w/v DFS-IR suspension (volume: 0.1 mL and dose: 1.6 mg) were administered in the eye. Hundred microliters of the 0.1% w/v DFS commercially marketed ophthalmic solution was

administered twice with half an hour gap between the two applications (at -30 and 0 min; total dose: 200 µg). Initially studies were carried out with 0.1% w/v DFS ophthalmic solution, 3+1:1::DFS:IR film (3 parts DFS in uncomplexed form and 1 part in complexed form) and with uncomplexed DFS film for 4 h. Marketed ophthalmic solution (0.1% w/v 0.1% w/v Diclofenac sodium solutions from Akorn Pharmaceuticals, Lake Forest, Illinois) was used just to get an estimate of ocular bioavailability of DFS with the solution, but not as control formulation.

Based on the 4h data obtained, and to determine time dependent ocular tissue concentrations of DFS, another set of *in vivo* studies were carried out for 8h exposure using the following formulations: 3+1:1::DFS:IR (3 parts DFS free and one part DFS bound to the IER) suspension, matrix films containing 3+1:1::DFS:IR, and uncomplexed DFS loaded films. Matrix films containing uncomplexed DFS served as the control for the DFS:IR loaded films The compositions of all the formulations used for the *in vivo* studies are reported in **table 5.1**.

Table 5.1: Composition of various formulations of Diclofenac sodium (DFS) used for ocular disposition studies.

Formulations	Formulation #1	Formulation #2	Formulation #3	Formulation #4
Ingredients	0.1% DFS ophthalmic solution	3+1:1::DFS:IR in suspension	Pure DFS film	3+1:1::DFS:IR in film
Diclofenac sodium	10 mg	120 mg	1.6 mg	1.2 mg
DFS-IR::1:1 complex	-	80 mg	-	0.8 mg
Boric acid	√	-	-	-
Edetate Disodium	10 mg	-	-	-
Polyxyl 35 Castor Oil	√	-	-	-
Sorbic acid	20 mg	-	-	-
Tromethamine	√	-	-	-
Mannitol	-	450 mg	-	-
HPMC	-	10 mg	-	-
PEO N10	-	-	6.4 mg	6 mg
Water	10 mL	10 mL	-	-

At the end of 4h and 8h post topical application (post last application in case of multiple applications), the rabbits were euthanized under deep anesthesia with an overdose of pentobarbital injected through the marginal ear vein. The eyes were washed with ice cold IPBS and immediately enucleated and washed again. Ocular tissues were separated, weighed and preserved at -80 °C until further analysis.

5.2.11. Analytical procedure for *in vitro* Samples

Waters HPLC system with 600 E pump controller, 717 plus auto sampler and 2487 UV detector was used. Data handling was carried out using an Agilent 3395 integrator. A 40:60 mixture of water (pH 3.5-4.0) and ACN was used as mobile phase with Phenomenex *Luna*® 5 µm C_{18} 100 Å, 250 x 4.6 mm column at a flow rate of 1.5 mL/min and 276 nm. DFS stock solution was prepared in mobile phase.

5.2.12. Bio-analytical method

5.2.12.1. Standard solution preparation:

To 100 µL of aqueous humor (AH) or 500 µL of vitreous humor (VH) and to a weighed amount of the cornea, sclera, iris ciliary bodies (IC) and retina-choroid (RC), 20 µL of DFS stock solution prepared in mobile phase (0.5, 1, 2.5, 5, 7.5, and 10 µg/mL) was added, vortexed and allowed to stand for 5 min. To precipitate the proteins, ice cold ACN was added to the AH and VH standards in 1:1 ratio and 1 mL to the cornea, sclera, IC and RC standards. Final concentrations of the standard solutions were in the range of 10 - 200 ng/mL for AH; 10 - 100 ng/mL for VH; 20 - 200 ng/mL: cornea & sclera and 10 - 200 ng/mL: IC & RC. Similarly, blank samples were prepared for all the tissues by adding 20 µL of mobile phase instead of standard stock solutions. All samples

were centrifuged at 13,000 rpm and 4 °C for 30 min and the supernatant was analyzed using HPLC-UV. All the standard curves generated an R^2 value greater than 0.99.

5.2.12.2. Sample preparation:

Approximately 0.1 mL of AH and 0.5 mL of VH was collected from each test eye into individual centrifugal tubes. All other tissues, RC, IC, cornea & sclera, from each test eye were collected and weighed. Tissues were cut into very small pieces and placed into individual vials. Protein precipitation was carried out similar to the standard solution preparation procedure and the supernatant analyzed using HPLC-UV method.

A mixture of water (pH 3.5) and ACN in a ratio of 65:35 was used as the mobile phase and Phenomenex *Luna*® 5 µm C_{18} 100 Å, 250 *x* 4.6 mm column at a flow rate of 1 mL/min and 284 nm.

5.2.13. Data analysis

All experiments were carried out at least in triplicate. DFS release data was fitted to zero order, first order and Higuchi models (Equations 2, 3 & 4).

$$C_t = C_0 + K_0 t \qquad\qquad \text{Eq (2)}$$

$$LogC_t = LogC_0 + Kt/2.303 \qquad\qquad \text{Eq (3)}$$

$$C_t = K_H t^{1/2} \qquad\qquad \text{Eq (4)}$$

Where,

C_0 & C_t = concentration at time 0 min and t min,

K_0, K & K_H = kinetic constants for zero order, first order and Higuchi models.

Drug diffusion parameters across cornea such as cumulative amount (M_n) , rate (R) and flux (J) were calculated using previously described method [105].

Cumulative amount of DFS released from the film was calculated using equation 5

$$M_n = V_r\, C_{r(n)} + \sum_{x=1}^{x=n} V_{s(x-1)}\, C_{r(x-1)} \qquad \text{Eq (5)}$$

Where,

n = sampling time point (n=1, 2, 3 and 4... corresponding to 15, 30, 45 and 60...min respectively),

V_r = volume of the medium in the receiver chamber (mL),

V_S = volume of the sample withdrawn at the nth time point (mL),

$C_{r(n)}$ = concentration of the drug in the receiver chamber medium at n^{th} time point ($\mu g/mL$).

Steady state flux was determined using equation 6

$$\text{Flux (J)} = \frac{(dM/dt)}{A} \qquad \text{Eq (6)}$$

Where,

M = cumulative amount of DFS (μg),

t = time (min),

A = surface area of cornea (0.636 cm^2).

Rate of elimination of DFS from ocular tissues for the formulations was calculated from the slopes of the concentration obtained at the end of 4h and 8h time points.

Statistical analysis was carried out using ANOVA to compare between different groups and Tukey's post-hoc HSD was used to compare differences between two groups. A 'p' value less than 0.05 was considered to denote statistically significant difference.

5.3. RESULTS:

5.3.1. Complexation efficiency:

DFS was complexed at different ratios with Duolite AP 143 (1:1, 1:2 and 2:1) and agitated for 24 h. When the amount of IR used was half the amount of DFS used, only a 49.3 ± 3.9% of complexation was observed between DFS and the resin. At 1:1 and 1:2 ratio of DFS:IR a complexation efficiency of approximately 99% was observed in both cases (**Table 5.2**). Thus, all further studies using complexed DFS employed 1:1 ratio of DFS: IR.

Table 5.2: Percentage drug bound to the resin at different ratios of drug:IR.

Formulation	Free Drug concentration (mg/mL)	Amount of drug bound to resin (mg/mg)	Percentage drug bound
Drug	16.02	0	0
1:2::Drug:resin	0.15	15.87	99.04 ± 0.1
1:1::Drug:resin	0.49	15.53	99.03 ± 0.1
2:1::Drug:resin	8.11	7.91	49.34 ± 3.9

FTIR spectra shows DFS binds to Duolite™ AP143. Characteristic peak of DFS at 3430.5 cm^{-1} (N-H stretching), 1573.5 cm^{-1} (N-H bending) & 748.12 cm^{-1} (C-Cl stretching) were observed in the FTIR spectra. Duolite^{TM} AP 143 displays broad peak at about 3400 cm^{-1} corresponding to the quaternary ammonium bending vibration, peaks at 2850 t0 2900 cm^{-1} were corresponding to CH, CH$_2$ and CH$_3$ stretching vibrations and two bands at 1600 and 1500 cm^{-1} were corresponding to the aromatic ring. The N-H bending and C-Cl stretching were observed in DFS-IR complex demonstrating no covalent interaction between the drug and IR. (**Fig.5.2**).
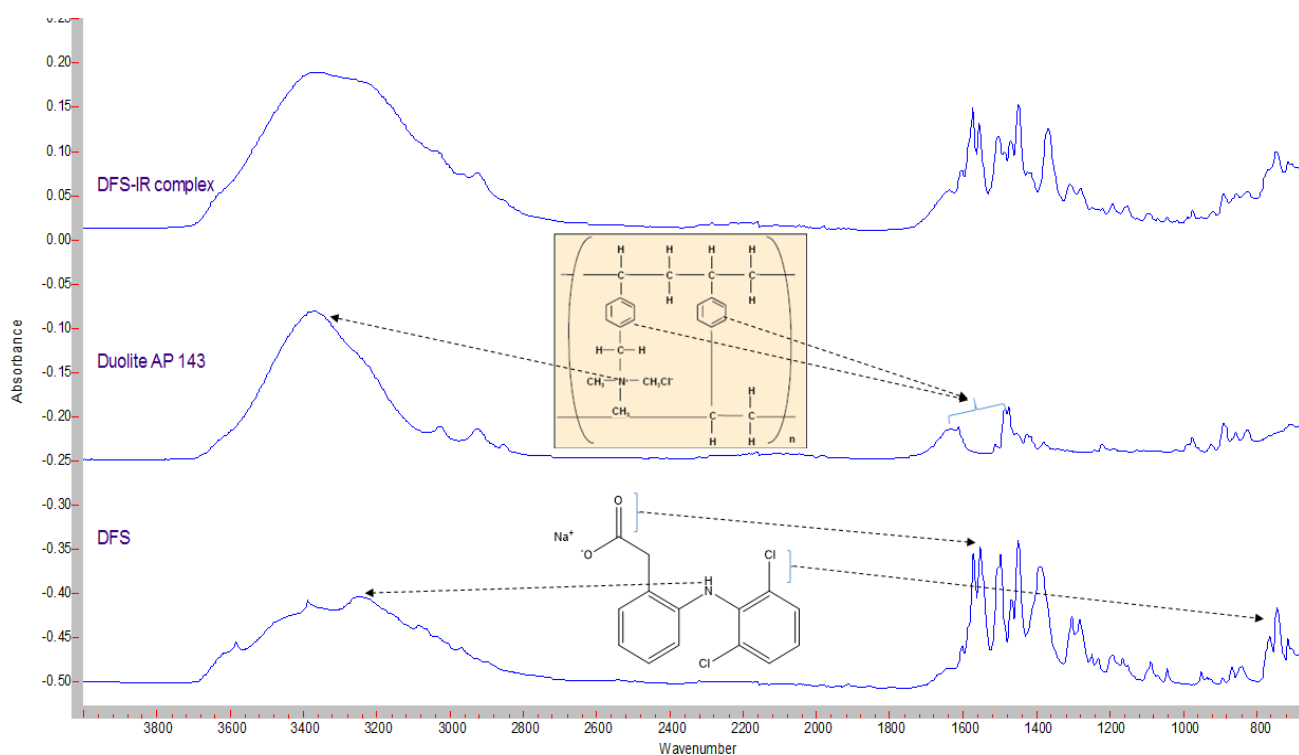
Figure 5.2: FTIR spectra of DFS, Duolite^{TM} AP 143/1083 (IR) and DFS-IR complex.

5.3.2. Assay and content uniformity studies

DFS content in all the films was observed to be approximately between 94-103 % of the theoretical values. DFS was found to be uniformly distributed within the matrix film (RSD<2.3 %).

5.3.3. *In vitro* release and corneal permeability studies

Release of DFS from 0.1% w/v ophthalmic solution was 80% within 6 h of the study. Percent release of DFS from 1:1 (100% DFS in complex form) and 1+1:1 IR-complex (1 part DFS free and 1 part bound to the IER) suspensions was 48.8 ± 2.3 and 72.4 ± 2.9, respectively. With the 1:1 and 1+1:1 DFS combination loaded in matrix films 52.7 ± 4.9 and 75.5 ± 3.8 percent of the DFS, respectively, was released in 24 h (**Fig.5.3**). Release kinetics from each formulation is presented in **table 5.3**.
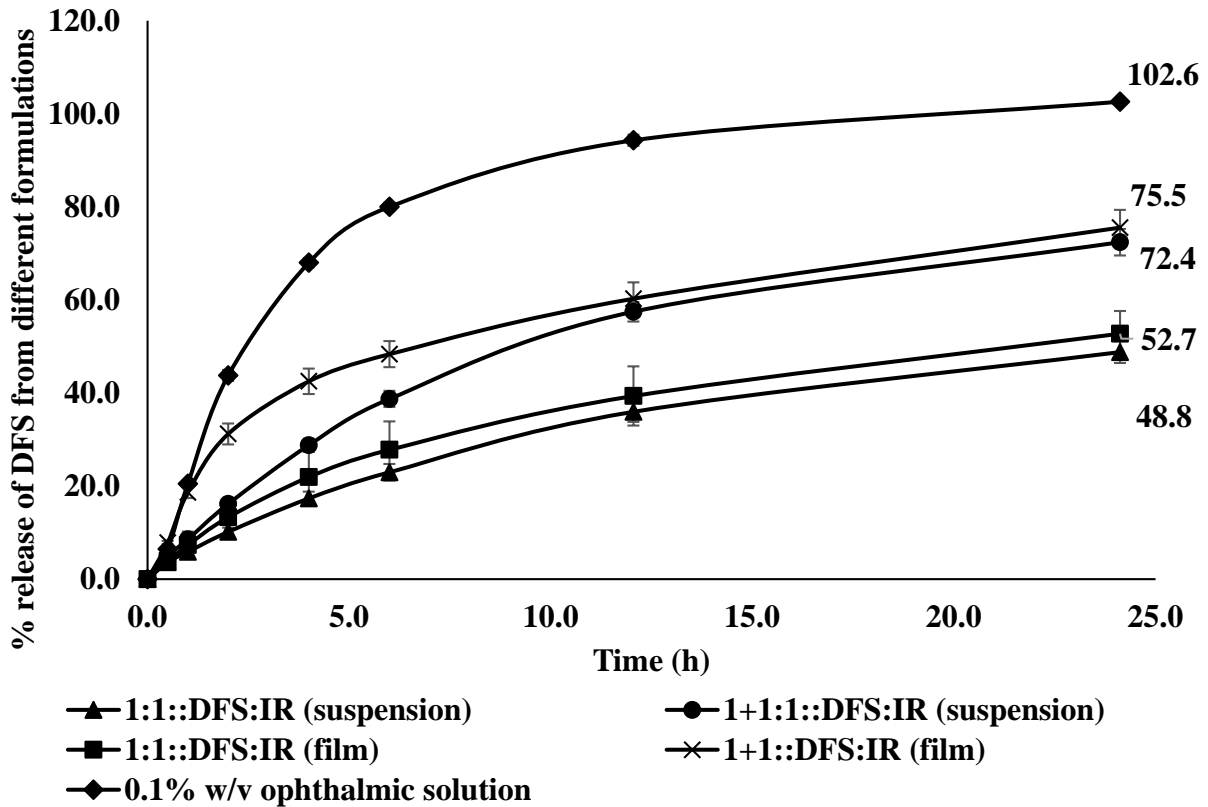
Figure 5.3: Percentage release of DFS up to 24 h form various ion exchange resin formulations and marketed ophthalmic solution.

Flux across the cornea was 10.2 ± 0.2 (0.1% w/v DFS ophthalmic solution), 2.0 ± 0.9 (DFS matrix film), 0.4 ± 0.05 (DFS:IR::1:1 film) and 0.7 ± 0.04 (DFS:IR::1+1:1 film) $\mu g/min/cm^2$.

Table 5.3: Rate constant and Coefficient of correlation of percentage release of DFS from different formulations of DFS fitted into Zero order, first order and Higuchi model.

Formulation	Rate order	Zero	First	Higuchi
Drug:Resin::1:1 (solution)	Kinetic constant	2.0547	0.012	10.891
	Coefficient correlation	0.9273	0.9688	0.9894
Drug:Resin::2:1 (solution)	Kinetic constant	3.0905	0.0237	16.681
	Coefficient correlation	0.8874	0.9671	0.9871
Drug:Resin::1:1(film)	Kinetic constant	2.1577	0.013	11.639
	Coefficient correlation	0.8973	0.9573	0.9913
Drug:Resin::2:1 (film)	Kinetic constant	2.8066	0.0227	15.879
	Coefficient correlation	0.7871	0.9424	0.9567
0.1% w/v ophthalmic solution	Kinetic constant	3.9885	0.0961	23.449
	Coefficient correlation	0.6748	0.9895	0.8857

Under the settings employed, DFS flux across the Spectra/Por® membrane (representing the precorneal loss) was 3.0 ± 0.2 and 5.5 ± 0.6 from 1:1 and 1+1:1::DFS:IR film in 6 h respectively. Rate and flux of DFS from various formulations is represented in **table 5.4**.

Table 5.4: Rate and flux of DFS across isolated rabbit cornea from various formulations.

Formulation	Flux (µg/min/cm²)	Rate (µg/min)
0.1 % w/v ophthalmic formulation	10.13 ± 0.16	6.5 ± 0.1
Pure DFS film	2.0 ± 0.1	1.3 ± 0.05
1:1::DFS:IR suspension	0.34 ± 0.04	0.24 ± 0.02
1+1:1::DFS:IR film	0.7 ± 0.05	0.46 ± 0.02
1:1::DFS:IR film	0.41 ± 0.05	0.26 ± 0.04

5.3.4. *In vivo* studies

Initially, ocular tissue concentrations were evaluated *in vivo*, 4h post topical application of the DFS formulations. Ocular tissue concentrations of DFS were analyzed only in the anterior segment of the eye (AH and IC) for the initial study. With 0.1% w/v DFS ophthalmic solution, 181.4 ± 64.8 and 932.4 ± 422.0 ng of DFS/gm of tissue were detected in AH and IC, respectively,

at the end of 4 h. Matrix film with uncomplexed/free DFS was able to deliver 2.68 ± 0.2 µg and 2.7 ± 0.06 µg of DFS/gm of tissue to AH and IC respectively. As expected, matrix film with IR complex delivered lower amounts of DFS to the anterior segment of the eye due to presence of the complexed form. Matrix film with DFS:IR complex was able to deliver 0.9 ± 0.2 and 1.02 ± 0.05 µg of DFS/gm of tissue to AH and IC respectively.

To evaluate the sustained release effect of the matrix film with DFS and IR complex, the study was carried out for 8 h. DFS free and complexed with IR's such that 3 parts of the total DFS dose was in uncomplexed form and 1 part was bound to the IER's (3+1:1) in solution was used as control. All the tissues including RC and VH were analyzed following the 8 h time point. DFS levels were below the limit of detection in VH with all the formulations tested. Matrix film loaded

Figure 5.4A: DFS concentrations form various formulations in Aqueous humor (AH) and iris ciliary bodies (IC), 4 h post topical application. Conscious animal model.
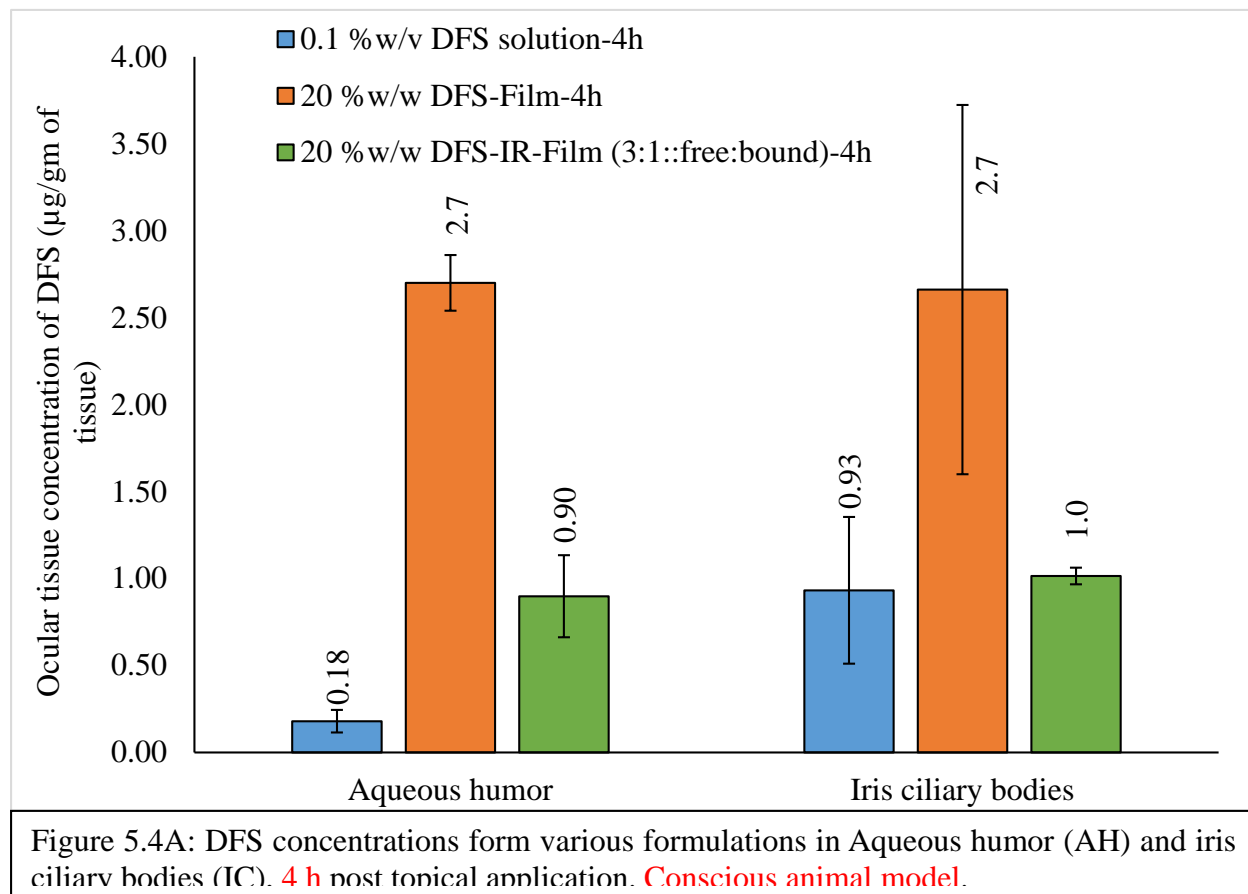
with free DFS was able to deliver 0.75 ± 0.06 µg/gm of AH, 0.78 ± 0.35 µg/gm of IC, 7.5 ± 3.4

Figure 5.4B: DFS concentrations form various formulations in Aqueous humor (AH) and iris ciliary bodies (IC), 8 h post topical application. Conscious animal model.
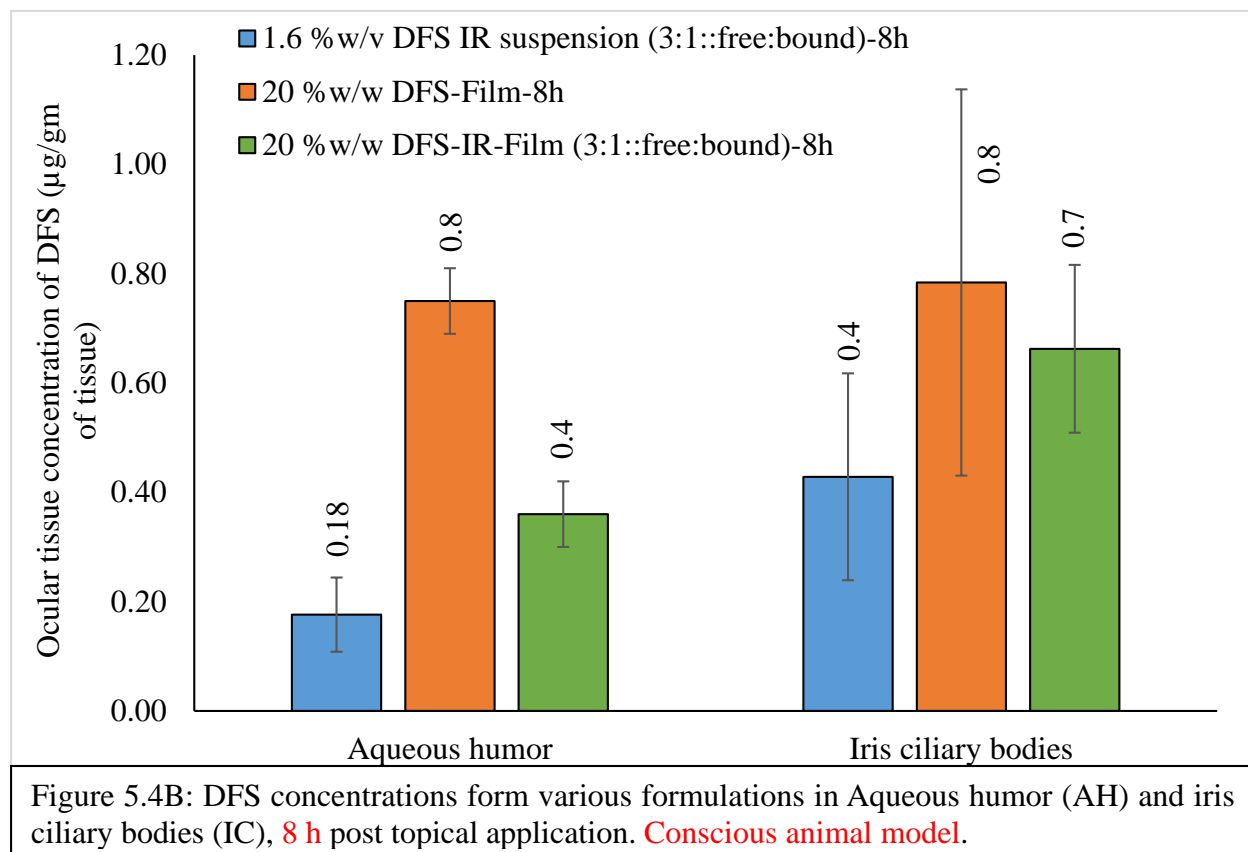
Table 5.5: Ocular tissue concentration of DFS obtained from various formulations of DFS. AH-Aqueous humor, IC-Iris ciliary bodies, RC-Retina-choroid. NA- not analyzed, ND-below detection limit.

Formulations (#)	Time (h)	Cornea	AH	IC	RC	Sclera
0.1 %w/v DFS solution (#1)	4	NA	0.18 ± 0.06	0.93 ± 0.4	NA	NA
1.6 %w/v DFS IR suspension (3+1:1::DFS:IR) (#2)	8	1.3 ± 1.0	0.18 ± 0.07	0.43 ± 0.19	ND	8.4 ± 1.7
20 %w/w DFS-Film (#3)	4	NA	2.68 ± 0.2	2.7 ± 1.1	NA	NA
20 %w/w DFS-Film (#3)	8	7.5 ± 3.4	0.76 ± 0.06	0.78 ± 0.35	ND	14.6 ± 4.8
20 %w/w DFS-IR-Film (3+1:1::DFS:IR) (#4)	4	NA	0.9 ± 0.2	1.02 ± 0.05	NA	NA
20 %w/w DFS-IR-Film (3+1:1::DFS:IR) (#4)	8	2.3 ± 1.4	0.36 ± 0.06	0.66 ± 0.15	0.09 ± 0.02	7.02 ± 4.03

µg/gm of cornea and 14.6 ± 4.8 µg/gm of sclera. DFS-IR film was able to deliver AH: 0.36 ± 0.06 µg/g of tissue, RC: 89.2 ± 24.2 ng/g of tissue, IC: 662.6 ± 153.5 ng/g of tissue, Cornea: 2.3 ± 1.4 µg/gm of tissue and Sclera: 7.02 ± 4.03 µg/gm of tissue. At an equivalent dose, DFS-IR complex in solution delivered much lower concentrations than the film. Results from *in vivo* studies are presented in **table 5.5** and **figure 5.4 A and B**.

Rates of elimination for both AH and IC for the DFS film were twice that of DFS-IR film (**Fig.5.5 A & B**). Rate of elimination of DFS in AH and IC from film were 0.2375 and 0.2347 µg/h respectively. While for the film loaded with IR complexes AH (0.0623 µg/h) and IC (0.0441 µg/h).

5.4. Discussion:

Use of IRs in the field of drug delivery as taste masking and controlled release excipients has been reported. Recently, IR's have also been used in ophthalmic dosage forms to achieve sustained release profiles and improved bioavailability. Jain et al developed a suspension formulation of betaxalol hydrochloride (Betoptic® S) by binding it to IR's Betoptic® S retards drug release in the tear, increases retention at the ocular surface and enhances drug bioavailability. As a result, Betoptic® S 0.25% is found to be bioequivalent to Betoptic Solution 0.5% in terms of lowering of intraocular pressure.

Our aim in this project was to develop a matrix film loaded with IR's for immediate and sustained release profiles, thus providing both loading and maintenance doses. This could be achieved by keeping part of drug in the free or uncomplexed state in the matrix film. In the present study, an 8 mg matrix film with a 20% w/w drug load (1.6 mg of drug) was prepared. Of this 1.6 mg, 3 part (1.2 mg) is maintained in uncomplexed for immediate release and the other 0.4 mg (1 part) is in the complexed state to provide the sustained release profile. The matrix film by itself

adds to the sustained release profile. These amounts can be modified accordingly to achieve the required drug release profiles.

Duolite™ AP143 resin is an insoluble, strongly basic, anion exchange resin supplied as a dry powder. It is suitable for use in pharmaceutical applications, both as an active ingredient (for adsorption of toxic chemicals) and as a carrier for acidic (anionic) drugs [174]. Since DFS is negatively charged in the solution, DFS forms a complex with the positively charged Duolite™ AP143. In the present study we evaluated the complexation efficiency of DFS with the resin at varying weight ratios of DFS and IR as mentioned in **table 5.1**. No significant differences were observed between 1:1 and 1:2 DFS:IR in terms of complexation efficiency. Thus, further studies were carried out using the 1:1::DFS:IR complexation ratio. Additional amounts of free DFS was added to provide immediate release.

In vitro release of DFS from IR complexed formulations show an immediate release profile followed by the sustained release profile. A 100% release was observed with the 0.1% DFS ophthalmic solution in 24 h. With 1+1:1 complex in film, unbound DFS was released in first 2 h. Due to constant equilibrium between the IR and the DFS, a sustained release of remaining DFS was observed from the complex in the later part of the release profile. The release of DFS from 1+1:1 complex in suspended state was slower compared to the film. This can be attributed to the greater concentration gradient from the film than the solution formulation. In film the 1.6 mg of DFS is concentrated in 4 mm x 2 mm surface area, where as in a solution it is distributed over a greater surface and reducing the concentration gradient. DFS:IR::1:1 film and suspension showed approximately 33% less release compared to the 1+1:1 complex. This is because of the absence of the free DFS and the total DFS was in complexed state, the release was more sustained. Similarly, 1:1 film showed slightly higher release than the suspension. All the results when fitted into into

zero order, first order and higuchi kinetics, it was observed that the 0.1% ophthalmic solution was following first order release kinetics with coefficient of relation (R^2) 0.9895. But all other formulations (1:1::DFS:IR solution, 1:1::DFS:IR film, 1+1:1::DFS:IR solution and 1+1:1::DFS:IR film) were best fitted for Higuchi model with coefficient of relations (R^2) 0.9894, 0.9913, 0.9871 and 0.9567 respectively (**Table 5.3**). This demonstrates that the release from the IR complexes is more controlled.

In vitro transcorneal permeability studies were performed over a period of 6 h. With DFS:IR::1:1 film (total 1.6 mg in complexed state) flux across the isolated cornea was approximately half of the flux obtained from 1+1:1::DFS:IR film (Of the total dose, 0.8 mg was free and 0.8 mg was in complexed state). Presence of free 1 part of DFS in the 1+1:1::DFS:IR film was aiding in the increased flux of DFS across the cornea. Similarly, flux with DFS film was higher than that of 1+1:1::DFS:IR film. With 1+1:1::DFS:IR film, flux was 1/3rd of the flux obtained from the unbound DFS film (**Table 5.4**). This was because the total dose (1.6 mg of DFS) was in unbound state. In case of ophthalmic solution, the total DFS is in solution without any rate controlling material for the permeation of DFS across the cornea resulting in high flux compared to all other formulations.

Based on *in vitro* release and permeability results, 1+1:1::DFS:IR formulations are holding DFS for longer duration. For 50% release of DFS to release from the 1+1:1::DFS:IR formulations, it is talking approximately 12 h. To improve the % drug release from the formulations, *in vivo* studies were carried out with 3 parts of unbound DFS (1.2 mg) and 1 part (0.4 mg) of IR bound DFS out of 1.6 mg dose. Conscious rabbit models were used for the study to keep the active lymphatic drainage and tear turnover rate unaffected. When 3+1::DFS:IR complexes in solution

were administered, slight increase in the eye blinking was observed in the rabbits compared to the ophthalmic solution. As per USP guidelines, any ophthalmic solution preparation containing particles greater than 10 µm would be recognized as foreign particle by the eye causing discomfort [196]. As a result 3+1::DFS:IR complexes in suspension formulation was causing discomfort to the rabbit eye. Polymeric matrix film did not cause any excessive tearing, redness or allergies to the eye as reported in our previous study [192]. When 3+1::DFS:IR film was applied to the eye, there was no excess blinking or tearing in the rabbits. This is because the particles were embedded in the film and did not cause any discomfort to the eye.

DFS ophthalmic solution was administered into the rabbits to estimate the minimal basal levels of DFS, but not as a control. As expected, with 0.1% w/v ophthalmic solution, ocular tissue concentrations in AH and IC were very less at the end of 4h compared to other formulations (181.3 ± 64.8 and 932.4 ± 422.01 ng/gm of tissue respectively). Matrix film with DFS gave very high ocular tissue concentrations in the AH and IC. These levels were much higher compared to the 3+1:1::DFS:IR matrix film. The matrix film transforms into gel and starts releasing the drug much faster than an IR film. As a result, we can see both AH and IC loaded with DFS in first the 4h post topical application of DFS film.

On the other hand, as 3+1:1::DFS:IR matrix film transforms into gel it starts releasing the free drug. Simultaneously, the bound DFS is also exchanged for the counter ions in the tear fluid and released into the tissues. IR's have the ability to form *in situ* complexes [175]. As a results some of the free DFS again starts forming complex to maintain the equilibrium. Because of this constant change in the equilibrium the ocular tissue levels obtained from the 3+1:1::DFS:IR film were less compared to the DFS film.

DFS and 3+1:1::DFS:IR films were evaluated for ocular tissue distribution, 8h post topical

Figure 5.5A: Rate of elimination of DFS concentrations form Aqueous humor (AH) at the end of 8 h post topical application. Conscious animal model.

administration. Along with the above two formulations, 3+1:1::DFS:IR in suspension (same dose) was also tested for ocular distribution to evaluate the effect of polymeric matrix film. When 3+1:1::DFS:IR was administered in suspension state, ocular tissue concentrations achieved were similar (in AH) and less (in IC). This is because the suspension formulation is getting drained off from ocular surface due to precorneal loss even before getting released and absorbed from IR. At the end of 8 h, with DFS film the levels in AH and IC were higher than the 3+1:1::DFS:IR in suspension and in film. But it is very important to note that the rate of elimination of DFS from ocular tissues at the end of 4 h and 8 h was much higher in AH and IC from DFS (3.7 and 3.3 fold respectively) compared to 3+1:1::DFS:IR film rate of elimination of DFS was less (2.5 and 1.5 fold in AH and IC respectively). Since there is a constant release of DFS from IR, ocular tissues were supplied with DFS continuously. As a result, rate of elimination in these tissues was much

less compared to the DFS film. The rate of elimination for the film without IR was very high compared to IR loaded film (**Fig.5.5 A & B**).

With 3+1:1::DFS:IR in suspension state, there was not enough concentration gradient build up and most of the DFS was restricted to cornea and sclera. At the end of 8h, posterior segment
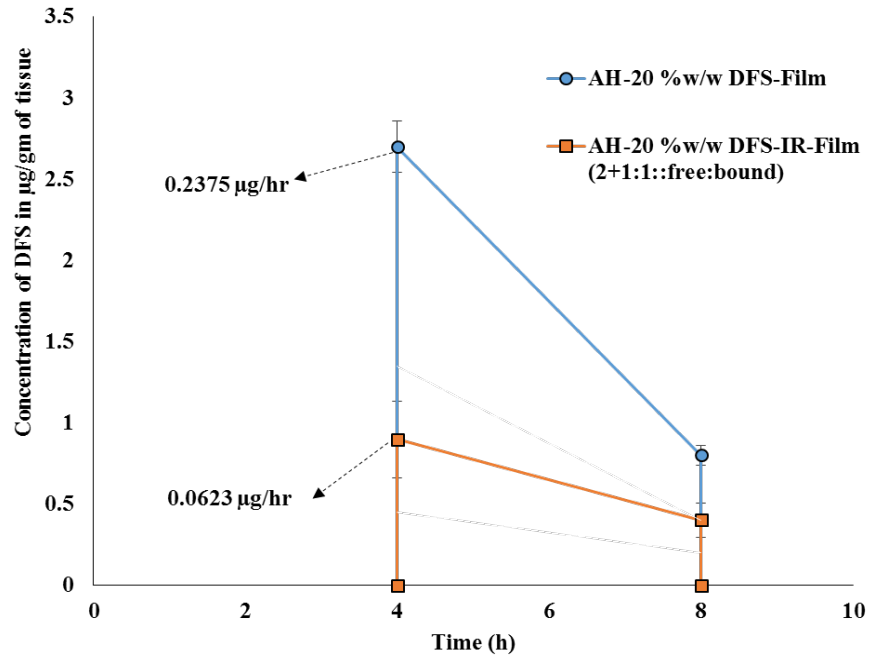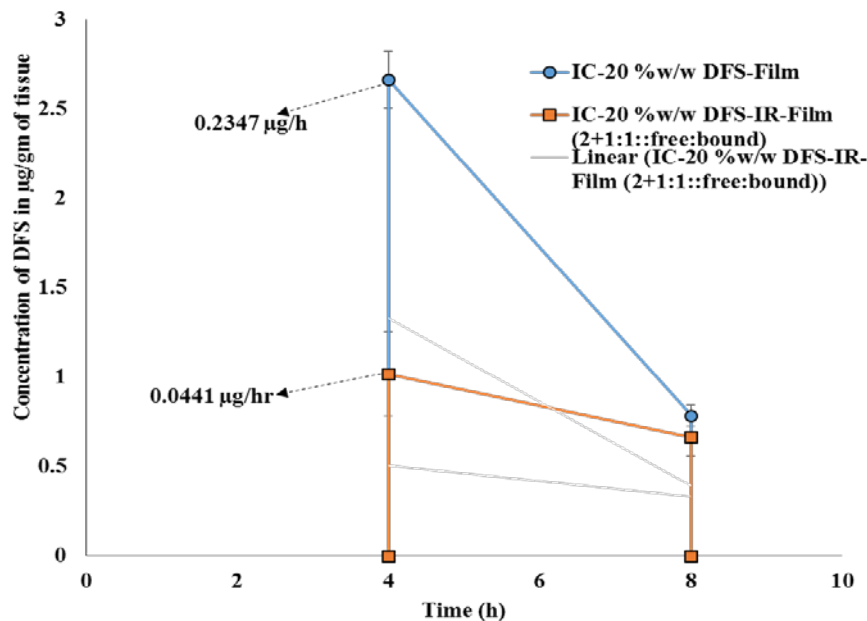

Figure 5.5B: Rate of elimination of DFS concentrations form Iris ciliary bodies (IC) at the end of 8 h post topical application. Conscious animal model.

ocular tissues were also evaluated of DFS concentrations. None of the formulations were able to deliver detectable levels of DFS in VH. Film with 3+1:1::DFS:IR was able to deliver very minimal but detectable levels of DFS to RC (89.2 ± 24.2 ng/gm of tissue).

According to Blanco et al, half-maximal inhibitory concentration (IC_{50}) values of DFS for inhibiting COX-1 and COX-2 enzymes are [197] 0.611 µM (194.4 ng/mL) and 0.63 µM (200.4 ng/mL). DFS concentrations obtained from both solution formulations in AH were below IC_{50} levels. Both films with uncomplexed DFS and with a combination of free and complexed DFS:IRs were able to maintain significant levels of DFS in the ocular tissues even at the end of 8 h post topical application. Additionally, rate of elimination from the inner ocular tissues with the DFS:IR

film was significantly lower compared to the film loaded with free DFS. Thus, DFS:IR loaded matrix films can maintain DFS levels for prolonged period of time and may provide at least a twice a day application. Moreover, the IR loaded dosage form avoids the spikes in the ocular tissues noted with the other dosage forms including the free drug loaded matrix films.

5.5. Conclusion:

Ocular tissue concentrations of DFS from film demonstrated high concentrations in aqueous humor and iris-ciliary bodies. Although, DFS film was able to load the tissues with the drug, DFS-IR film showed more controlled release across the tissues. Interestingly, only the IR film was able to deliver the drug the posterior segment of the eye (retina-choroid). Thus, drug IR complexes loaded into a matrix film can be a perfect platform for an immediate and sustained release delivery systems. Modification of the IR-film using different resins, different concentration of unbound drug and drug IR complexes can be used to meet the requirement of individual drug release profiles.

BIBILIOGRAPHY

1.   Kawanishi, K., H. Ueda, and M. Moriyasu, *Aldose reductase inhibitors from the nature.* Curr Med Chem, 2003. **10**(15): p. 1353-74.

2.   Arden, G.B., *The absence of diabetic retinopathy in patients with retinitis pigmentosa: implications for pathophysiology and possible treatment.* Br J Ophthalmol, 2001. **85**(3): p. 366-70.

3.   Kowluru, R.A. and S. Odenbach, *Role of interleukin-1beta in the development of retinopathy in rats: effect of antioxidants.* Invest Ophthalmol Vis Sci, 2004. **45**(11): p. 4161-6.

4.   Fong, D.S., et al., *Diabetic retinopathy.* Diabetes Care, 2003. **26 Suppl 1**: p. S99-S102.

5.   Lieth, E., et al., *Retinal neurodegeneration: early pathology in diabetes.* Clin Experiment Ophthalmol, 2000. **28**(1): p. 3-8.

6.   Gardner, T.W., et al., *New insights into the pathophysiology of diabetic retinopathy: potential cell-specific therapeutic targets.* Diabetes Technol Ther, 2000. **2**(4): p. 601-8.

7.   Wilkinson-Berka, J.L., *Vasoactive factors and diabetic retinopathy: vascular endothelial growth factor, cycoloxygenase-2 and nitric oxide.* Curr Pharm Des, 2004. **10**(27): p. 3331-48.

8.   Watkins, P.J., *Retinopathy.* BMJ, 2003. **326**(7395): p. 924-6.

9.   Watkins, P.J., *Diabetic complications: retinopathy.* Br Med J (Clin Res Ed), 1982. **285**(6339): p. 425-7.

10. Fong, D.S., et al., *Diabetic retinopathy.* Diabetes Care, 2003. **26**(1): p. 226-9.

11. Tout, S., et al., *The role of Muller cells in the formation of the blood-retinal barrier.* Neuroscience, 1993. **55**(1): p. 291-301.

12. Aizu, Y., et al., *Degeneration of retinal neuronal processes and pigment epithelium in the early stage of the streptozotocin-diabetic rats.* Neuropathology, 2002. **22**(3): p. 161-70.

13. Niesman, M.R., K.A. Johnson, and J.S. Penn, *Therapeutic effect of liposomal superoxide dismutase in an animal model of retinopathy of prematurity.* Neurochem Res, 1997. **22**(5): p. 597-605.

14. Flynn, J.T., et al., *Retinopathy of prematurity. A randomized, prospective trial of transcutaneous oxygen monitoring.* Ophthalmology, 1987. **94**(6): p. 630-8.

15. Penn, J.S., *Oxygen-induced retinopathy in the rat: possible contribution of peroxidation reactions.* Doc Ophthalmol, 1990. **74**(3): p. 179-86.

16. Chan, P.H., *Antioxidant-dependent amelioration of brain injury: role of CuZn-superoxide dismutase.* J Neurotrauma, 1992. **9 Suppl 2**: p. S417-23.

17. Stanimirovic, D.B., et al., *Liposome-entrapped superoxide dismutase reduces ischemia/reperfusion 'oxidative stress' in gerbil brain.* Neurochem Res, 1994. **19**(12): p. 1473-8.

18. Nielsen, J.C., M.I. Naash, and R.E. Anderson, *The regional distribution of vitamins E and C in mature and premature human retinas.* Invest Ophthalmol Vis Sci, 1988. **29**(1): p. 22-6.

19. Kowluru, R.A., et al., *Diabetes-induced activation of nuclear transcriptional factor in the retina, and its inhibition by antioxidants.* Free Radic Res, 2003. **37**(11): p. 1169-80.

20. Kowluru, R.A., *Diabetes-induced elevations in retinal oxidative stress, protein kinase C and nitric oxide are interrelated.* Acta Diabetol, 2001. **38**(4): p. 179-85.

21. Serou, M.J., M.A. DeCoster, and N.G. Bazan, *Interleukin-1 beta activates expression of cyclooxygenase-2 and inducible nitric oxide synthase in primary hippocampal neuronal*

culture: platelet-activating factor as a preferential mediator of cyclooxygenase-2 expression. J Neurosci Res, 1999. **58**(4): p. 593-8.

22. Tilton, R.G., et al., *Vascular dysfunction induced by elevated glucose levels in rats is mediated by vascular endothelial growth factor.* J Clin Invest, 1997. **99**(9): p. 2192-202.

23. Sone, H., et al., *Vascular endothelial growth factor is induced by long-term high glucose concentration and up-regulated by acute glucose deprivation in cultured bovine retinal pigmented epithelial cells.* Biochem Biophys Res Commun, 1996. **221**(1): p. 193-8.

24. Brooks, S.E., et al., *Modulation of VEGF production by pH and glucose in retinal Muller cells.* Curr Eye Res, 1998. **17**(9): p. 875-82.

25. Natarajan, R., et al., *Effects of high glucose on vascular endothelial growth factor expression in vascular smooth muscle cells.* Am J Physiol, 1997. **273**(5 Pt 2): p. H2224-31.

26. Kuroki, M., et al., *Reactive oxygen intermediates increase vascular endothelial growth factor expression in vitro and in vivo.* J Clin Invest, 1996. **98**(7): p. 1667-75.

27. Plouet, J., J. Schilling, and D. Gospodarowicz, *Isolation and characterization of a newly identified endothelial cell mitogen produced by AtT-20 cells.* Embo J, 1989. **8**(12): p. 3801-6.

28. Leung, D.W., et al., *Vascular endothelial growth factor is a secreted angiogenic mitogen.* Science, 1989. **246**(4935): p. 1306-9.

29. Williams, B., *Vascular permeability/vascular endothelial growth factors: a potential role in the pathogenesis and treatment of vascular diseases.* Vasc Med, 1996. **1**(4): p. 251-8.

30. Connolly, D.T., et al., *Tumor vascular permeability factor stimulates endothelial cell growth and angiogenesis.* J Clin Invest, 1989. **84**(5): p. 1470-8.

31. Senger, D.R., et al., *Tumor cells secrete a vascular permeability factor that promotes accumulation of ascites fluid.* Science, 1983. **219**(4587): p. 983-5.

32. Dvorak, H.F., et al., *Vascular permeability factor/vascular endothelial growth factor, microvascular hyperpermeability, and angiogenesis.* Am J Pathol, 1995. **146**(5): p. 1029-39.

33. Schmedtje, J.F., Jr., et al., *Hypoxia induces cyclooxygenase-2 via the NF-kappaB p65 transcription factor in human vascular endothelial cells.* J Biol Chem, 1997. **272**(1): p. 601-8.

34. Michiels, C., et al., *Stimulation of prostaglandin synthesis by human endothelial cells exposed to hypoxia.* Am J Physiol, 1993. **264**(4 Pt 1): p. C866-74.

35. Ji, Y.S., Q. Xu, and J.F. Schmedtje, Jr., *Hypoxia induces high-mobility-group protein I(Y) and transcription of the cyclooxygenase-2 gene in human vascular endothelium.* Circ Res, 1998. **83**(3): p. 295-304.

36. Bazan, N.G. and W.J. Lukiw, *Cyclooxygenase-2 and presenilin-1 gene expression induced by interleukin-1beta and amyloid beta 42 peptide is potentiated by hypoxia in primary human neural cells.* J Biol Chem, 2002. **277**(33): p. 30359-67.

37. Lukiw, W.J. and N.G. Bazan, *Strong nuclear factor-kappaB-DNA binding parallels cyclooxygenase-2 gene transcription in aging and in sporadic Alzheimer's disease superior temporal lobe neocortex.* J Neurosci Res, 1998. **53**(5): p. 583-92.

38. Baeuerle, P.A. and D. Baltimore, *NF-kappa B: ten years after.* Cell, 1996. **87**(1): p. 13-20.

39. Takahashi, K., et al., *Topical nepafenac inhibits ocular neovascularization.* Invest Ophthalmol Vis Sci, 2003. **44**(1): p. 409-15.

40.	Ayalasomayajula, S.P. and U.B. Kompella, *Celecoxib, a selective cyclooxygenase-2 inhibitor, inhibits retinal vascular endothelial growth factor expression and vascular leakage in a streptozotocin-induced diabetic rat model.* Eur J Pharmacol, 2003. **458**(3): p. 283-9.

41.	Dodge, A.B., H.B. Hechtman, and D. Shepro, *Microvascular endothelial-derived autacoids regulate pericyte contractility.* Cell Motil Cytoskeleton, 1991. **18**(3): p. 180-8.

42.	Murohara, T., et al., *Vascular endothelial growth factor/vascular permeability factor enhances vascular permeability via nitric oxide and prostacyclin.* Circulation, 1998. **97**(1): p. 99-107.

43.	Eakins, K.E., *Prostaglandin and non-prostaglandin mediated breeakdown of the blood-aqueous barrier.* Exp Eye Res, 1977. **25 Suppl**: p. 483-98.

44.	Hardy, P., et al., *Oxidants, nitric oxide and prostanoids in the developing ocular vasculature: a basis for ischemic retinopathy.* Cardiovasc Res, 2000. **47**(3): p. 489-509.

45.	Ziche, M., J. Jones, and P.M. Gullino, *Role of prostaglandin E1 and copper in angiogenesis.* J Natl Cancer Inst, 1982. **69**(2): p. 475-82.

46.	Form, D.M. and R. Auerbach, *PGE2 and angiogenesis.* Proc Soc Exp Biol Med, 1983. **172**(2): p. 214-8.

47.	Gately, S., *The contributions of cyclooxygenase-2 to tumor angiogenesis.* Cancer Metastasis Rev, 2000. **19**(1-2): p. 19-27.

48.	Dannenberg, A.J., et al., *Cyclo-oxygenase 2: a pharmacological target for the prevention of cancer.* Lancet Oncol, 2001. **2**(9): p. 544-51.

49.	Gasparini, G., et al., *Inhibitors of cyclo-oxygenase 2: a new class of anticancer agents?* Lancet Oncol, 2003. **4**(10): p. 605-15.

50.	Lukiw, W.J., et al., *Coordinate activation of HIF-1 and NF-kappaB DNA binding and COX-2 and VEGF expression in retinal cells by hypoxia.* Invest Ophthalmol Vis Sci, 2003. **44**(10): p. 4163-70.

51.	Salgo, M.G., et al., *Peroxynitrite causes DNA damage and oxidation of thiols in rat thymocytes [corrected].* Arch Biochem Biophys, 1995. **322**(2): p. 500-5.

52.	Salgo, M.G., G.L. Squadrito, and W.A. Pryor, *Peroxynitrite causes apoptosis in rat thymocytes.* Biochem Biophys Res Commun, 1995. **215**(3): p. 1111-8.

53.	Zhuang, S. and G. Simon, *Peroxynitrite-induced apoptosis involves activation of multiple caspases in HL-60 cells.* Am J Physiol Cell Physiol, 2000. **279**(2): p. C341-51.

54.	Halliwell, B., *What nitrates tyrosine? Is nitrotyrosine specific as a biomarker of peroxynitrite formation in vivo?* FEBS Lett, 1997. **411**(2-3): p. 157-60.

55.	Mancino, R., et al., *Lipid peroxidation and total antioxidant capacity in vitreous, aqueous humor, and blood samples from patients with diabetic retinopathy.* Mol Vis. **17**: p. 1298-304.

56.	Kansagara D, G.K., Gillingham M, Freeman M, Quiñones A., *Nutritional Supplements for Age-Related Macular Degeneration: A Systematic Review [Internet].* VA Evidence-based Synthesis Program Reports., 2012.

57.	Buschini, E., et al., *Age related macular degeneration and drusen: neuroinflammation in the retina.* Prog Neurobiol. **95**(1): p. 14-25.

58.	Khandhadia, S. and A. Lotery, *Oxidation and age-related macular degeneration: insights from molecular biology.* Expert Rev Mol Med. **12**: p. e34.

59.	Cano, M., et al., *Cigarette smoking, oxidative stress, the anti-oxidant response through Nrf2 signaling, and Age-related Macular Degeneration.* Vision Res. **50**(7): p. 652-64.

106

60.   Ding, X., M. Patel, and C.C. Chan, *Molecular pathology of age-related macular degeneration.* Prog Retin Eye Res, 2009. **28**(1): p. 1-18.

61.   Olofsson, E.M., S.L. Marklund, and A. Behndig, *Enhanced diabetes-induced cataract in copper-zinc superoxide dismutase-null mice.* Invest Ophthalmol Vis Sci, 2009. **50**(6): p. 2913-8.

62.   Tornquist, P., A. Alm, and A. Bill, *Permeability of ocular vessels and transport across the blood-retinal-barrier.* Eye, 1990. **4 (Pt 2)**: p. 303-9.

63.   Cunha-Vaz, J.G., *The blood-retinal barriers.* Doc Ophthalmol, 1976. **41**(2): p. 287-327.

64.   Cunha-Vaz, J., *The blood-ocular barriers.* Surv Ophthalmol, 1979. **23**(5): p. 279-96.

65.   Peng, S., C. Rahner, and L.J. Rizzolo, *Apical and basal regulation of the permeability of the retinal pigment epithelium.* Invest Ophthalmol Vis Sci, 2003. **44**(2): p. 808-17.

66.   Altunay, H., *Fine structure of the retinal pigment epithelium, Bruch's membrane and choriocapillaris in the horse.* Anat Histol Embryol, 2000. **29**(3): p. 135-9.

67.   Rizzolo, L.J., *Polarity and the development of the outer blood-retinal barrier.* Histol Histopathol, 1997. **12**(4): p. 1057-67.

68.   Konari, K., et al., *Development of the blood-retinal barrier in vitro: formation of tight junctions as revealed by occludin and ZO-1 correlates with the barrier function of chick retinal pigment epithelial cells.* Exp Eye Res, 1995. **61**(1): p. 99-108.

69.   Cunha-Vaz, J.G., *The blood-ocular barriers: past, present, and future.* Doc Ophthalmol, 1997. **93**(1-2): p. 149-57.

70.   Duvvuri, S., M.D. Gandhi, and A.K. Mitra, *Effect of P-glycoprotein on the ocular disposition of a model substrate, quinidine.* Curr Eye Res, 2003. **27**(6): p. 345-53.

71.   Constable, P.A., et al., *P-Glycoprotein expression in human retinal pigment epithelium cell lines.* Exp Eye Res, 2006. **83**(1): p. 24-30.

72.   Steuer, H., et al., *Functional characterization and comparison of the outer blood-retina barrier and the blood-brain barrier.* Invest Ophthalmol Vis Sci, 2005. **46**(3): p. 1047-53.

73.   Aukunuru, J.V., et al., *Expression of multidrug resistance-associated protein (MRP) in human retinal pigment epithelial cells and its interaction with BAPSG, a novel aldose reductase inhibitor.* Pharm Res, 2001. **18**(5): p. 565-72.

74.   Duvvuri, S., S. Majumdar, and A.K. Mitra, *Drug delivery to the retina: challenges and opportunities.* Expert Opin Biol Ther, 2003. **3**(1): p. 45-56.

75.   Kowluru, R.A. and P.S. Chan, *Oxidative stress and diabetic retinopathy.* Exp Diabetes Res, 2007. **2007**: p. 43603.

76.   Agrawal, S., M. Joshi, and J.B. Christoforidis, *Vitreous inflammation associated with intravitreal anti-VEGF pharmacotherapy.* Mediators Inflamm, 2013. **2013**: p. 943409.

77.   Limtrakul, P., O. Khantamat, and K. Pintha, *Inhibition of P-glycoprotein function and expression by kaempferol and quercetin.* J Chemother, 2005. **17**(1): p. 86-95.

78.   Adelli, G., R. Srirangam, and S. Majumdar, *Phytochemicals in ocular health: Therapeutic potential and delivery challenges.* World Journal of Pharmacology, 2013. **2**(1): p. 18-34.

79.   Hingorani, T., et al., *Effect of ion pairing on in vitro transcorneal permeability of a Delta(9) -tetrahydrocannabinol prodrug: potential in glaucoma therapy.* J Pharm Sci. **101**(2): p. 616-26.

80.   Choi, E.J., *Antioxidative effects of hesperetin against 7,12-dimethylbenz(a)anthracene-induced oxidative stress in mice.* Life Sci, 2008. **82**(21-22): p. 1059-64.

81.   Hwang, S.L. and G.C. Yen, *Neuroprotective effects of the citrus flavanones against H2O2-induced cytotoxicity in PC12 cells.* J Agric Food Chem, 2008. **56**(3): p. 859-64.

82. Kim, J.Y., et al., *Hesperetin: a potent antioxidant against peroxynitrite.* Free Radic Res, 2004. **38**(7): p. 761-9.

83. Miyake, Y., et al., *New potent antioxidative hydroxyflavanones produced with Aspergillus saitoi from flavanone glycoside in citrus fruit.* Biosci Biotechnol Biochem, 2003. **67**(7): p. 1443-50.

84. Jung, H.A., et al., *Inhibitory activity of flavonoids from Prunus davidiana and other flavonoids on total ROS and hydroxyl radical generation.* Arch Pharm Res, 2003. **26**(10): p. 809-15.

85. Pollard, S.E., M. Whiteman, and J.P. Spencer, *Modulation of peroxynitrite-induced fibroblast injury by hesperetin: a role for intracellular scavenging and modulation of ERK signalling.* Biochem Biophys Res Commun, 2006. **347**(4): p. 916-23.

86. Hirata, A., et al., *Kinetics of radical-scavenging activity of hesperetin and hesperidin and their inhibitory activity on COX-2 expression.* Anticancer Res, 2005. **25**(5): p. 3367-74.

87. Olszanecki, R., et al., *Flavonoids and nitric oxide synthase.* J Physiol Pharmacol, 2002. **53**(4 Pt 1): p. 571-84.

88. Dansky, K.H., et al., *Qualitative analysis of telehomecare nursing activities.* J Nurs Adm, 2003. **33**(7-8): p. 372-5.

89. Chiou, G.C. and X.R. Xu, *Effects of some natural flavonoids on retinal function recovery after ischemic insult in the rat.* J Ocul Pharmacol Ther, 2004. **20**(2): p. 107-13.

90. Ameer, B., et al., *Flavanone absorption after naringin, hesperidin, and citrus administration.* Clin Pharmacol Ther, 1996. **60**(1): p. 34-40.

91. Srirangam, R., et al., *Evaluation of the intravenous and topical routes for ocular delivery of hesperidin and hesperetin.* J Ocul Pharmacol Ther. **28**(6): p. 618-27.

92. Yanez, J.A., et al., *Pharmacokinetics of selected chiral flavonoids: hesperetin, naringenin and eriodictyol in rats and their content in fruit juices.* Biopharm Drug Dispos, 2008. **29**(2): p. 63-82.

93. Srirangam, R., K. Hippalgaonkar, and S. Majumdar, *Intravitreal kinetics of hesperidin, hesperetin, and hesperidin G: effect of dose and physicochemical properties.* J Pharm Sci. **101**(4): p. 1631-8.

94. Loftssona, T. and T. Jarvinen, *Cyclodextrins in ophthalmic drug delivery.* Adv Drug Deliv Rev, 1999. **36**(1): p. 59-79.

95. Geroski, D.H. and H.F. Edelhauser, *Drug delivery for posterior segment eye disease.* Invest Ophthalmol Vis Sci, 2000. **41**(5): p. 961-4.

96. Wu, Y., et al., *Enhanced and sustained topical ocular delivery of cyclosporine A in thermosensitive hyaluronic acid-based in situ forming microgels.* Int J Nanomedicine, 2013. **8**: p. 3587-601.

97. Fathi, M., et al., *Hesperetin-Loaded Solid Lipid Nanoparticles and Nanostructure Lipid Carriers for Food Fortification: Preparation, Characterization, and Modeling.* Food Bioprocess Technol, 2013.

98. Ficarra, R., et al., *Study of flavonoids/beta-cyclodextrins inclusion complexes by NMR, FT-IR, DSC, X-ray investigation.* J Pharm Biomed Anal, 2002. **29**(6): p. 1005-14.

99. Gaudana, R., et al., *Ocular drug delivery.* AAPS J, 2010. **12**(3): p. 348-60.

100. Maiti, K., et al., *Exploring the effect of Hesperetin-HSPC complex--a novel drug delivery system on the in vitro release, therapeutic efficacy and pharmacokinetics.* AAPS PharmSciTech, 2009. **10**(3): p. 943-50.

101.   Adelli, G.R., et al., *Evaluation of topical hesperetin matrix film for back-of-the-eye delivery.* Eur J Pharm Biopharm, 2015.

102.   Fathi., M., et al., *Hesperetin-Loaded Solid Lipid Nanoparticles and Nanostructure Lipid Carriers for Food Fortification: Preparation, Characterization, and Modeling.* Food Bioprocess Technol, 2012.

103.   Majumdar, S., et al., *Transcorneal permeation of L- and D-aspartate ester prodrugs of acyclovir: delineation of passive diffusion versus transporter involvement.* Pharm Res, 2009. **26**(5): p. 1261-9.

104.   Becker, U., et al., *A comparative evaluation of corneal epithelial cell cultures for assessing ocular permeability.* Altern Lab Anim, 2008. **36**(1): p. 33-44.

105.   Majumdar, S. and R. Srirangam, *Solubility, stability, physicochemical characteristics and in vitro ocular tissue permeability of hesperidin: a natural bioflavonoid.* Pharm Res, 2009. **26**(5): p. 1217-25.

106.   Fruijtier-Polloth, C., *Safety assessment on polyethylene glycols (PEGs) and their derivatives as used in cosmetic products.* Toxicology, 2005. **214**(1-2): p. 1-38.

107.   Law, D., et al., *Properties of rapidly dissolving eutectic mixtures of poly(ethylene glycol) and fenofibrate: the eutectic microstructure.* J Pharm Sci, 2003. **92**(3): p. 505-15.

108.   Craig, D.Q., *The mechanisms of drug release from solid dispersions in water-soluble polymers.* Int J Pharm, 2002. **231**(2): p. 131-44.

109.   Srirangam, R. and S. Majumdar, *Passive asymmetric transport of hesperetin across isolated rabbit cornea.* Int J Pharm. **394**(1-2): p. 60-7.

110.   Srirangam, R., et al., *Evaluation of the intravenous and topical routes for ocular delivery of hesperidin and hesperetin.* J Ocul Pharmacol Ther, 2012. **28**(6): p. 618-27.

111.   Rainey-Smith, S., et al., *Neuroprotective effects of hesperetin in mouse primary neurones are independent of CREB activation.* Neurosci Lett, 2008. **438**(1): p. 29-33.

112.   Yang, H.L., et al., *Antioxidant and anti-inflammatory potential of hesperetin metabolites obtained from hesperetin-administered rat serum: an ex vivo approach.* J Agric Food Chem. **60**(1): p. 522-32.

113.   Gabelt BT, K.P., *Aqueous humor hydrodynamics*, in *Adler's Physiology of the Eye*, H. WM, Editor. 2003: St. Louis.

114.   Cook, C. and P. Foster, *Epidemiology of glaucoma: what's new?* Can J Ophthalmol, 2012. **47**(3): p. 223-6.

115.   Kwon, Y.H., et al., *Primary open-angle glaucoma.* New England Journal of Medicine, 2009. **360**(11): p. 1113-1124.

116.   Gupta, N. and Y.H. Yucel, *Glaucoma as a neurodegenerative disease.* Current opinion in ophthalmology, 2007. **18**(2): p. 110-114.

117.   Schwartz, M. and E. Yoles, *Optic nerve degeneration and potential neuroprotection: implications for glaucoma.* Eur J Ophthalmol, 1999. **9 Suppl 1**: p. S9-11.

118.   Levin, L.A. and P. Peeples, *History of neuroprotection and rationale as a therapy for glaucoma.* Am J Manag Care, 2008. **14**(1 Suppl): p. S11-4.

119.   Pita-Thomas, D.W. and J.L. Goldberg, *Nanotechnology and glaucoma: little particles for a big disease.* Curr Opin Ophthalmol, 2013. **24**(2): p. 130-5.

120.   Almasieh, M., et al., *The molecular basis of retinal ganglion cell death in glaucoma.* Prog Retin Eye Res, 2012. **31**(2): p. 152-81.

121.   Nakazawa, T., *[Mechanism of N-methyl-D-aspartate-induced retinal ganglion cell death].* Nihon Ganka Gakkai Zasshi, 2009. **113**(11): p. 1060-70.

122. Qu, J., D. Wang, and C.L. Grosskreutz, *Mechanisms of retinal ganglion cell injury and defense in glaucoma.* Exp Eye Res, 2010. **91**(1): p. 48-53.

123. Crandall, J., et al., *Neuroprotective and intraocular pressure-lowering effects of (-)Delta9-tetrahydrocannabinol in a rat model of glaucoma.* Ophthalmic Res, 2007. **39**(2): p. 69-75.

124. El-Remessy, A.B., et al., *Neuroprotective effect of (-)Delta9-tetrahydrocannabinol and cannabidiol in N-methyl-D-aspartate-induced retinal neurotoxicity: involvement of peroxynitrite.* Am J Pathol, 2003. **163**(5): p. 1997-2008.

125. Hampson, A.J., et al., *Cannabidiol and (-)Delta9-tetrahydrocannabinol are neuroprotective antioxidants.* Proc Natl Acad Sci U S A, 1998. **95**(14): p. 8268-73.

126. Montero, C., et al., *Homology models of the cannabinoid CB1 and CB2 receptors. A docking analysis study.* Eur J Med Chem, 2005. **40**(1): p. 75-83.

127. Wu, Y., et al., *Enhanced and sustained topical ocular delivery of cyclosporine A in thermosensitive hyaluronic acid-based in situ forming microgels.* Int J Nanomedicine. **8**: p. 3587-601.

128. Jarho, P., et al., *Hydroxypropyl-beta-cyclodextrin and its combination with hydroxypropyl-methylcellulose increases aqueous solubility of delta9-tetrahydrocannabinol.* Life Sci, 1998. **63**(26): p. PL381-4.

129. Green, K. and M. Roth, *Ocular effects of topical administration of delta 9-tetrahydrocannabinol in man.* Arch Ophthalmol, 1982. **100**(2): p. 265-7.

130. Green, K., et al., *Cannabinoid penetration and chronic effects in the eye.* Exp Eye Res, 1977. **24**(2): p. 197-205.

131. John C. Merrit M.D.*, D.D.P.M.D., David N. Russel M.D. and Brenda F. Jones M.D., *Topical Δ9-Tetrahydrocannabinol and Aqueous Dynamics in Glaucoma.* The Journal of Clinical Pharmacology, 2013. **21**(S1): p. 467S-471S.

132. Merritt, J.C., et al., *Effect of marihuana on intraocular and blood pressure in glaucoma.* Ophthalmology, 1980. **87**(3): p. 222-8.

133. Muchtar, S., et al., *A submicron emulsion as ocular vehicle for delta-8-tetrahydrocannabinol: effect on intraocular pressure in rabbits.* Ophthalmic Res, 1992. **24**(3): p. 142-9.

134. Fischer, K.M., D.A. Ward, and D.V. Hendrix, *Effects of a topically applied 2% delta-9-tetrahydrocannabinol ophthalmic solution on intraocular pressure and aqueous humor flow rate in clinically normal dogs.* Am J Vet Res, 2013. **74**(2): p. 275-80.

135. Colasanti, B.K., C.R. Craig, and R.D. Allara, *Intraocular pressure, ocular toxicity and neurotoxicity after administration of cannabinol or cannabigerol.* Exp Eye Res, 1984. **39**(3): p. 251-9.

136. Jay, W.M. and K. Green, *Multiple-drop study of topically applied 1% delta 9-tetrahydrocannabinol in human eyes.* Arch Ophthalmol, 1983. **101**(4): p. 591-3.

137. Elsohly, M.A., et al., *Cannabinoids in glaucoma: a primary screening procedure.* J Clin Pharmacol, 1981. **21**(8-9 Suppl): p. 472S-478S.

138. *From the NIH: Reports of marihuana for glaucoma treatment are misleading; researchers will study.* JAMA, 1979. **242**(18): p. 1962.

139. Majumdar, S., T. Hingorani, and R. Srirangam, *Evaluation of active and passive transport processes in corneas extracted from preserved rabbit eyes.* J Pharm Sci, 2010. **99**(4): p. 1921-30.

140. Elsohly, M.A., et al., *Compositions containing delta-9-thc-amino acid esters and process of preparation.* Google Patents.

141. Hingorani, T., et al., *Ocular disposition of the hemiglutarate ester prodrug of (9)-Tetrahydrocannabinol from various ophthalmic formulations.* Pharm Res, 2013. **30**(8): p. 2146-56.

142. Bhagav, P., et al., *Sustained release ocular inserts of brimonidine tartrate for better treatment in open-angle glaucoma.* Drug Deliv Transl Res, 2011. **1**(2): p. 161-74.

143. Percicot, C.L., et al., *Continuous intraocular pressure measurement by telemetry in alpha-chymotrypsin-induced glaucoma model in the rabbit: effects of timolol, dorzolamide, and epinephrine.* J Pharmacol Toxicol Methods, 1996. **36**(4): p. 223-8.

144. Atta-ur-Rahman, M.I. Choudhary, and J.T. William, *Bioassay techniques for drug development.* 1 Edition ed. 2001: Harwood Academic Publisher, .

145. Majumdar, S., et al., *Dipeptide monoester ganciclovir prodrugs for treating HSV-1-induced corneal epithelial and stromal keratitis: in vitro and in vivo evaluations.* J Ocul Pharmacol Ther, 2005. **21**(6): p. 463-74.

146. Katragadda, S., et al., *Ocular pharmacokinetics of acyclovir amino acid ester prodrugs in the anterior chamber: evaluation of their utility in treating ocular HSV infections.* Int J Pharm, 2008. **359**(1-2): p. 15-24.

147. E.J.Ariens, *Modulation of pharmacokinetics by molecular manipulation*, in *Drug Design: Medicinal Chemistry: A series of Monographs*, E.J. Ariens, Editor. 2013, Elsevier. p. 109.

148. Andermann, G., G. de Burlet, and C. Cannet, *[Comparative study of the antiglaucomatous activity of Glauplex 2 and pilocarpine nitrate on alpha-chymotrypsin-induced experimental glaucoma].* J Fr Ophtalmol, 1982. **5**(8-9): p. 499-504.

149. Chiang, C.H., J.I. Ho, and J.L. Chen, *Pharmacokinetics and intraocular pressure lowering effect of timolol preparations in rabbit eyes.* J Ocul Pharmacol Ther, 1996. **12**(4): p. 471-80.

150. Skalka, H.W., *Alpha-chymotrypsin glaucoma.* Ann Ophthalmol, 1976. **8**(2): p. 149-51.

151. Vareilles, P., et al., *Comparison of the effects of timolol and other adrenergic agents on intraocular pressure in the rabbit.* Invest Ophthalmol Vis Sci, 1977. **16**(11): p. 987-96.

152. Housley, G.D., *Nucleotide and nucleoside signalling in the ciliary ganglion*, in *Purinergic and Pyrimidinergic Signalling: Molecular, Nervous and Urogenitary System Function*, M.W. Maria P. Abracchio, Editor. 2001, Springer Science & Business Media.

153. S Panchal, A.M., D Santani, *Occulohypotensive Effect Of Torasamide In Experimental Glaucoma.* The Internet Journal of Pharmacology, 2008. **5**(2).

154. Zimmerman, T.J. and H.E. Kaufman, *Timolol, dose response and duration of action.* Arch Ophthalmol, 1977. **95**(4): p. 605-7.

155. Loftsson, T. and M.E. Brewster, *Pharmaceutical applications of cyclodextrins. 1. Drug solubilization and stabilization.* J Pharm Sci, 1996. **85**(10): p. 1017-25.

156. Siefert, B. and S. Keipert, *Influence of alpha-cyclodextrin and hydroxyalkylated beta-cyclodextrin derivatives on the in vitro corneal uptake and permeation of aqueous pilocarpine-HCl solutions.* J Pharm Sci, 1997. **86**(6): p. 716-20.

157. Masson, M., et al., *Cyclodextrins as permeation enhancers: some theoretical evaluations and in vitro testing.* J Control Release, 1999. **59**(1): p. 107-18.

158. T. Higuchi, K.A.C., *Phase-solubility techniques.* Advanced analytical chemistry, 1965. **4**: p. 117-212.

159. Adelli, G.R., S.P. Balguri, and S. Majumdar, *Effect of Cyclodextrins on Morphology and Barrier Characteristics of Isolated Rabbit Corneas.* AAPS PharmSciTech, 2015.

160. Salem, L.B., et al., *Sparing methylation of beta-cyclodextrin mitigates cytotoxicity and permeability induction in respiratory epithelial cell layers in vitro.* J Control Release, 2009. **136**(2): p. 110-6.

161. D. Duchene, D.W., M.C. Poelman, *New Trends in Cyclodextrins and Derivatives.* Dermal uses of cyclodextrins and derivatives, ed. d. Santé. 1991, Paris.

162. Van Der Bijl, P., et al., *Comparative permeability of human and rabbit corneas to cyclosporin and tritiated water.* J Ocul Pharmacol Ther, 2002. **18**(5): p. 419-27.

163. Saarinen-Savolainen, P., et al., *Evaluation of cytotoxicity of various ophthalmic drugs, eye drop excipients and cyclodextrins in an immortalized human corneal epithelial cell line.* Pharm Res, 1998. **15**(8): p. 1275-80.

164. Lopez, C.A., A.H. de Vries, and S.J. Marrink, *Computational microscopy of cyclodextrin mediated cholesterol extraction from lipid model membranes.* Sci Rep. **3**: p. 2071.

165. Williams, R.O., 3rd, V. Mahaguna, and M. Sriwongjanya, *Characterization of an inclusion complex of cholesterol and hydroxypropyl-beta-cyclodextrin.* Eur J Pharm Biopharm, 1998. **46**(3): p. 355-60.

166. Lopez, C.A., A.H. de Vries, and S.J. Marrink, *Molecular mechanism of cyclodextrin mediated cholesterol extraction.* PLoS Comput Biol. **7**(3): p. e1002020.

167. Tsamaloukas, A., et al., *Interactions of cholesterol with lipid membranes and cyclodextrin characterized by calorimetry.* Biophys J, 2005. **89**(2): p. 1109-19.

168. Duncker, G. and J. Reichelt, *Effects of the pharmaceutical cosolvent hydroxypropyl-beta-cyclodextrin on porcine corneal endothelium.* Graefes Arch Clin Exp Ophthalmol, 1998. **236**(5): p. 380-9.

169. Huang, A.J., S.C. Tseng, and K.R. Kenyon, *Paracellular permeability of corneal and conjunctival epithelia.* Invest Ophthalmol Vis Sci, 1989. **30**(4): p. 684-9.

170. Bozkir, A., Z.F. Denli, and B. Basaran, *Effect of hydroxypropyl-beta-cyclodextrin on the solubility, stability and in-vitro release of ciprofloxacin for ocular drug delivery.* Acta Pol Pharm. **69**(4): p. 719-24.

171. Hippalgaonkar, K., et al., *Indomethacin-loaded solid lipid nanoparticles for ocular delivery: development, characterization, and in vitro evaluation.* J Ocul Pharmacol Ther. **29**(2): p. 216-28.

172. Reer, O., T.K. Bock, and B.W. Muller, *In vitro corneal permeability of diclofenac sodium in formulations containing cyclodextrins compared to the commercial product voltaren ophtha.* J Pharm Sci, 1994. **83**(9): p. 1345-9.

173. Tirucherai, G.S. and A.K. Mitra, *Effect of hydroxypropyl beta cyclodextrin complexation on aqueous solubility, stability, and corneal permeation of acyl ester prodrugs of ganciclovir.* AAPS PharmSciTech, 2003. **4**(3): p. E45.

174. Guo, X., R.K. Chang, and M.A. Hussain, *Ion-exchange resins as drug delivery carriers.* J Pharm Sci, 2009. **98**(11): p. 3886-902.

175. Sriwongjanya, M. and R. Bodmeier, *Effect of ion exchange resins on the drug release from matrix tablets.* Eur J Pharm Biopharm, 1998. **46**(3): p. 321-7.

176. CL, M., *Ion exchangers.* 1951: p. 185-216.

177. Company, T.D.C. *Applications for AMBERLITE™ & DUOLITE™ Ion Exchange Resins: Drug Formulation Applications of Dow Ion Exchange Resins.* Available from: http://pharmaandfood.dow.com/en/pharma-solutions/products/amberlite-and-duolite/applications.

178. Patra, S., et al., *Taste masking of Etoricoxib by using ion-exchange resin.* Pharm Dev Technol, 2010. **15**(5): p. 511-7.
179. Bhise, K., S. Shaikh, and D. Bora, *Taste mask, design and evaluation of an oral formulation using ion exchange resin as drug carrier.* AAPS PharmSciTech, 2008. **9**(2): p. 557-62.
180. Kankkunen, T., et al., *Improved stability and release control of levodopa and metaraminol using ion-exchange fibers and transdermal iontophoresis.* Eur J Pharm Sci, 2002. **16**(4-5): p. 273-80.
181. Halder, A. and B. Sa, *Sustained release of propranolol hydrochloride based on ion-exchange resin entrapped within polystyrene microcapsules.* J Microencapsul, 2006. **23**(8): p. 899-911.
182. Chaudhry, N.C. and L. Saunders, *Sustained release of drugs from ion exchange resins.* J Pharm Pharmacol, 1956. **8**(11): p. 975-83; discussion, 983-6.
183. Herbort, C.P., et al., *Diclofenac drops to treat inflammation after cataract surgery.* Acta Ophthalmol Scand, 2000. **78**(4): p. 421-4.
184. Fawzi, A.A., et al., *Drugs in Ophthalmology.* 2005: Springer Berlin Heidelberg.
185. Incorporated, B.L., *Diclofenac Sodium Ophthalmic Solution, 0.1%*, B.L. Incorporated, Editor.
186. Lee, V.H. and J.R. Robinson, *Topical ocular drug delivery: recent developments and future challenges.* J Ocul Pharmacol, 1986. **2**(1): p. 67-108.
187. Edelhauser, H.F., et al., *Ophthalmic drug delivery systems for the treatment of retinal diseases: basic research to clinical applications.* Invest Ophthalmol Vis Sci, 2010. **51**(11): p. 5403-20.
188. Kompella, U.B., et al., *Nanomedicines for back of the eye drug delivery, gene delivery, and imaging.* Prog Retin Eye Res, 2013. **36**: p. 172-98.
189. Suk, J.S., et al., *PEGylation as a strategy for improving nanoparticle-based drug and gene delivery.* Adv Drug Deliv Rev, 2015.
190. Honda, M., et al., *Liposomes and nanotechnology in drug development: focus on ocular targets.* Int J Nanomedicine, 2013. **8**: p. 495-503.
191. Swaminathan, J. and C. Ehrhardt, *Liposomal delivery of proteins and peptides.* Expert Opin Drug Deliv, 2012. **9**(12): p. 1489-503.
192. Adelli, G.R., et al., *Evaluation of topical hesperetin matrix film for back-of-the-eye delivery.* Eur J Pharm Biopharm, 2015. **92**: p. 74-82.
193. Kaur, I.P. and M. Kanwar, *Ocular preparations: the formulation approach.* Drug Dev Ind Pharm, 2002. **28**(5): p. 473-93.
194. Maichuk Iu, F. and A.M. Iuzhakov, *[Ocular therapeutic films: long-term results and perspectives of use].* Med Tekh, 1994(2): p. 34-6.
195. Company, T.D.C. *Introduction & Ion Exchange Principles.* 2013.
196. Dale S. Aldrich, C.M.B., William Brown, Wiley Chambers, Jeffrey Fleitman, Desmond Hunt, Margareth R. C. Marques, Yana Mill, Ashim K. Mitra, Stacey M. Platzer, Tom Tice, George W. Tin, *Ophthalmic Preparations.* USP, 2013. **39**(5): p. 1-21.
197. Blanco, F.J., et al., *Effect of antiinflammatory drugs on COX-1 and COX-2 activity in human articular chondrocytes.* J Rheumatol, 1999. **26**(6): p. 1366-73.

LIST OF APPENDICES

APPENDIX A: DEFINITIONS OF VARIOUS TERMS USED IN CHAPTER 5:

DICLOFENAC SODIUM AND ION EXCHANGE RESIN COMPLEX LOADED MELT

CAST FILMS FOR SUSTAINED RELEASE OCULAR DELIVERY

Ion exchange resins ↔ Water insoluble cross linked polymers with ionizable groups that can be exchanged to form complexes. Ion exchange resin (IR) in the present study represent Duolite^{TM} AP 143/1083.

1:1::DFS:IR ↔ 1 part by weight of DFS is bound to 1 part by weight of IR.

1:2::DFS:IR ↔ 1 part by weight of DFS is bound to 2 part by weight of IR.

2:1::DFS:IR ↔ 2 part by weight of DFS is bound to or used to form complexes with 1 part by weight of IR.

DFS Film ↔ Matrix film with unbound/free from of DFS without any IR.

1+1:1::DFS:IR ↔ 1 part by weight of DFS is bound to 1 part by weight of IR (for sustained release) and remaining 1 part by weight of DFS is in unbound or free state (for immediate release). For example, in a film with 1.6 mg of total DFS, 0.8 mg is bound or complexed with IR 0.8 mg of IR and remaining 0.8 mg of DFS is in free or unbound state.

3+1:1::DFS:IR ↔ 1 part by weight of DFS is bound to 1 part by weight of IR (for sustained release) and 3 parts by weight of DFS is in unbound or free state (for immediate release). For example, in a film with 1.6 mg of total DFS, 0.4 mg is bound or complexed with IR 0.4 mg of IR and remaining 1.2 mg of DFS is in free or unbound state.

APPENDIX B: GRAPHICAL ABSTRACT FOR THE DEVELOPMENT OF HT FILM AND

OVERVIEW OF IN VITRO PERMEABILITY, EX VIVO & IN VIVO OCULAR
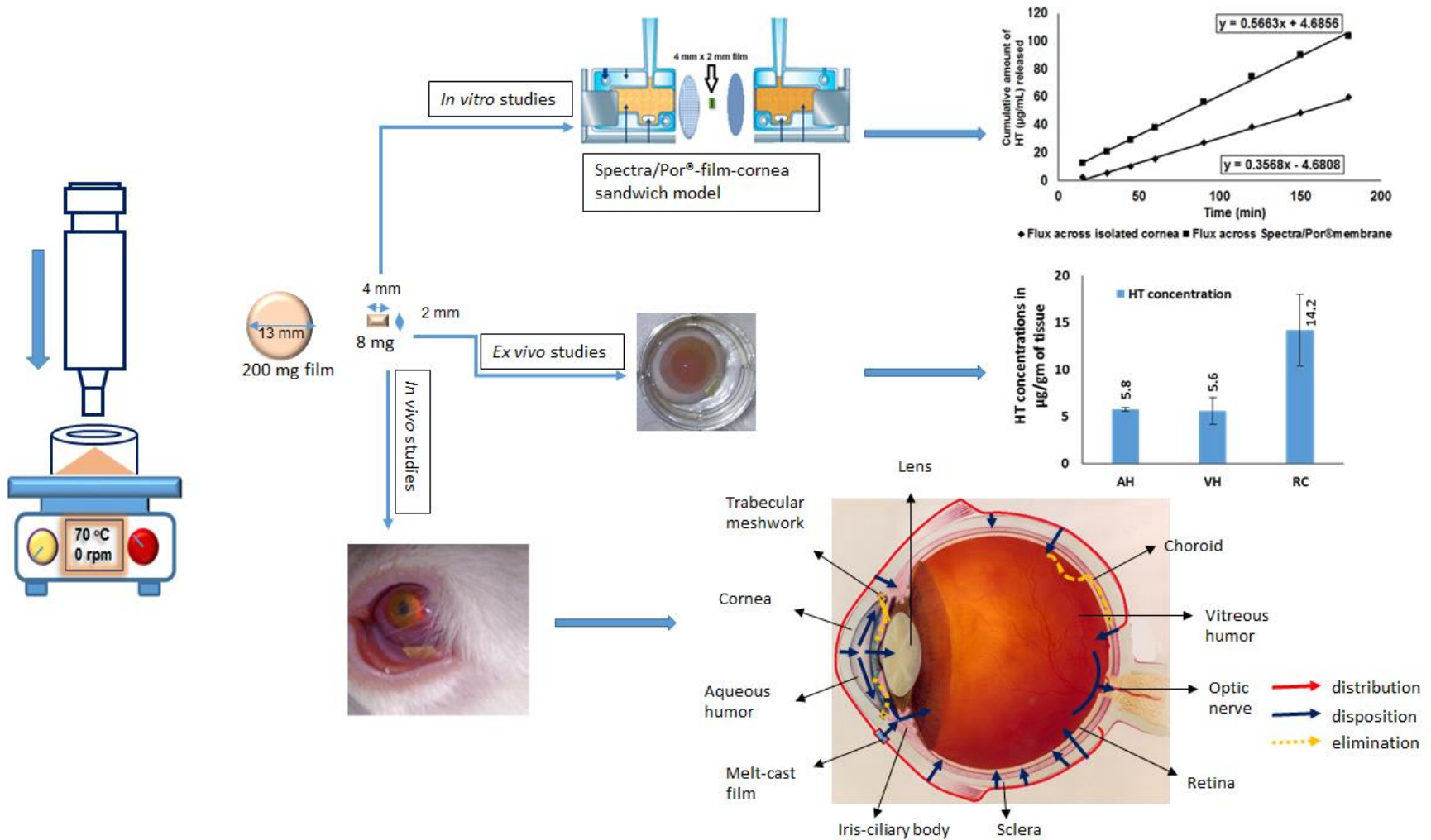
DISTRIBUTION

Graphical abstract 9.1: Development of HT film and overview of in vitro permeability, ex vivo & in vivo ocular distribution.

APPENDIX C: GRAPHICAL ABSTRACT FOR THE DEVELOPMENT OF DFS-IR-FILM

USING DUOLITE^{TM} AP 143/1089 RESIN AND MELT-CAST TECHNOLOGY
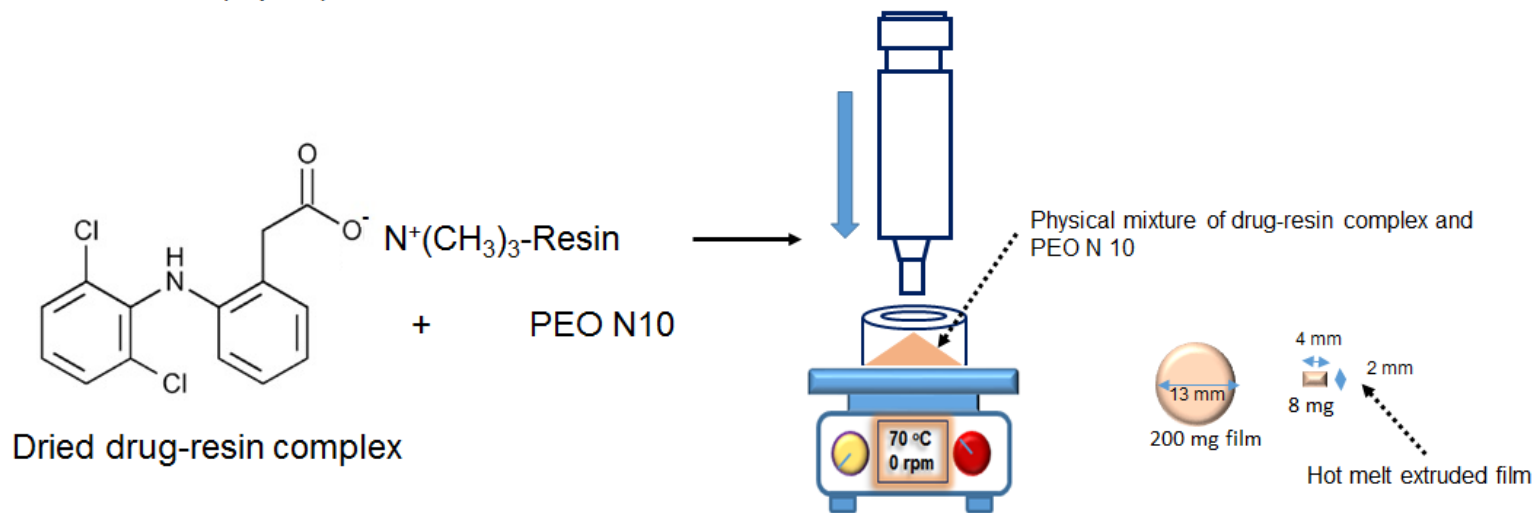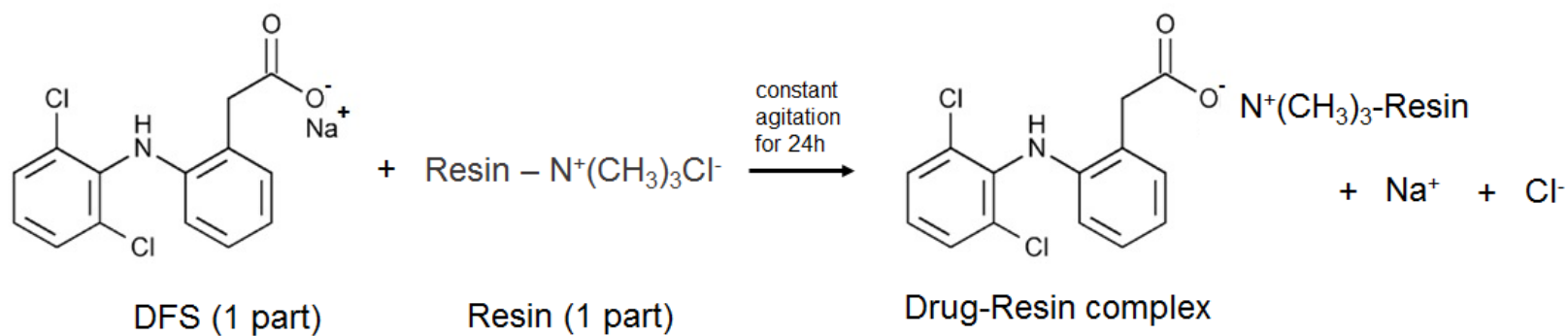
Graphical abstract 9.2: Development of DFS-IR-Film using Duolite^{TM} AP 143/1089 resin and melt-cast technology.

VITA

GOUTHAM R. ADELLI

Faser 110 **.** University, MS 38655 **.** (662) 915 7641 **.** gradelli@go.olemiss.edu

EDUCATION:

August, 2011 –May 2016	Joined Ph.D. Program, Department of Pharmaceutics and Drug Delivery, The University of Mississippi
May 2007-May 2011	B. Pharmacy, Jawaharlal Nehru Technological University, India

TEACHING EXPERIENCE:

January, 2012 –May 2015	Lab Instructor PRCT 354 Course: Formulation and compounding lab University of Mississippi
January, 2013 –May 2014	Instructor Tablet course University of Mississippi

ACHEIVEMENTS/AWARDS:

- Neuroscience Research Showcase graduate student award, April 2014, University of Mississippi, Mississippi

- NIH pre-doctoral fellowship: Center of Research Excellence in Natural Products Neuroscience (CORE-NPN) – March 2014, University of Mississippi, Mississippi

- Summer graduate research fellow award - May 2014, University of Mississippi, Mississippi

- Ocular Drug Delivery and Disposition Focus Group graduate student award-AAPS, November 2013, San Antonio, Texas

PROFESSIONAL ACITIVITES:

- Member of Rho Chi, ARVO and AAPS

- Teaching assistant: Formulation and compound lab

- Instructor/assistant : Hands-on tablet course

121

- Staff selection committee student member

- Reviewer for AAPS PharmSciTech and Pharmaceutical research Journals

PROFESSIONAL ACITIVITES:

- **Adelli GR**, Hingorani T, Punyamurthula N, Balguri S, Majumdar S. Evaluation of Topical Hesperetin Matrix film for Back-of-the-Eye Delivery. Eur J Pharm Biopharm. 2015 Feb 26.

- **Adelli GR**, Balguri S, Majumdar S. Effect of cyclodextrins on morphology and barrier characteristics of isolated rabbit corneas. AAPS PharmSciTech. 2015 Mar 13.

- Hippalgaonkar K, **Adelli GR**, Hippalgaonkar K, Repka MA, Majumdar S. Indomethacin- loaded solid lipid nanoparticles for ocular delivery: development, characterization, and in vitro evaluation. J Ocul Pharmacol Ther. 2013 Mar; 29(2):216-28. doi: 10.1089/jop.2012.0069. Epub 2013 Feb 19.

- **Adelli GR**, Bhagav P, Elsohly MA, Repka MA, Majumdar S. "Ocular Delivery of Tetrahydrocannabinol. The Handbook of Cannabis and Related Pathologies: Biology, Diagnosis, Treatment, and Pharmacology". (Accepted).

- Hingorani T, **Adelli GR**, Punyamurthula N, Gul W, Elsohly MA, Repka MA, Majumdar S. Ocular disposition of the hemiglutarate ester prodrug of Δ^9-Tetrahydrocannabinol from various ophthalmic formulations. Pharm Res. 2013 Aug; 30(8):2146-56. doi: 10.1007/s11095-013-1072-x. Epub 2013 Jun 5.

- **Goutham R Adelli**, Ramesh Srirangam, Soumyajit Majumdar. Phytochemicals in ocular health: Therapeutic potential and delivery challenges. World J Pharmacol 2013 March 9; 2(1): 18-34.